FINITE-TIME CONTROL FOR ACTIVE VEHICLE SUSPENSION SYSTEMS

ZHOU ZENGCHENG

PhD

The Hong Kong Polytechnic University

2025

The Hong Kong Polytechnic University

Department of Mechanical Engineering

Finite-Time Control for Active Vehicle Suspension Systems

Zhou Zengcheng

A thesis submitted in partial fulfillment of the requirements for the degree of Doctor of Philosophy

Jan 2025

CERTIFICATE OF ORIGINALITY

I hereby declare that this thesis is my own work and that, to the best of my knowledge and belief, it reproduces no material previously published or written, nor material that has been accepted for the award of any other degree or diploma, except where due acknowledgement has been made in the text.

_____ (Signed)

ZHOU Zengcheng (Name of student)

Abstract

With the rapid development of the vehicle industry, vehicle suspension systems, which serve as an elastic connection between the vehicle body and the wheels, have gathered increasing attention to enhance ride comfort and driving maneuverability. Sophisticated vehicle suspension systems can adapt to road imperfections and vibrations, thus maintaining safety requirements, improving ride comfort, and even avoiding physical fatigue. Compared with traditional passive suspensions and semi-active ones, active vehicle suspension systems are equipped with actuators to adjust the relative displacement between the vehicle body and the wheels, which can effectively handle the undesired vibrations generated by extremely poor road conditions. However, existing nonlinear control strategies for active suspensions may suffer from uncertain dynamics, external disturbances, slow convergence, high energy consumption, and actuator nonlinearities. To effectively address these practical issues, this thesis primarily focuses on the finite-time energy-saving control design for active vehicle suspension systems to enhance ride comfort and driving safety. Four different active suspension control algorithms are proposed in this thesis to guarantee vehicle performance under various critical conditions. Therefore, the requirements of ride comfort and driving safety for active suspensions can be sufficiently satisfied.

The main investigations and contributions of this thesis can be enumerated subsequently. (1) A novel finite-time saturated control is designed for AVSSs to handle input saturations, dead zones, and external disturbances. No exact model information is required, leading to a completely model-free control structure. Besides, the control input signal can be naturally constrained in a prior-known range without any extra anti-saturation design. The control algorithm is designed to be nonsingular and continuous to avoid singularity issues and alleviate the chattering phenomenon. (2) To deal with the high energy consumption, a bioinspired X-shaped reference model is integrated into a

fixed-time safe-by-design control scheme. Inspired by the biological motion dynamics, beneficial stiffness, and damping effects can be preserved to obtain advantageous suspension performance with potential energy conservation. The asymmetric time-varying barrier Lyapunov functions are constructed to guarantee the displacement and velocity constraints. Furthermore, the fixed-time stability of the closed-loop system is rigorously validated such that the convergence time is irrelevant to initial states to enhance the transient property and disturbance-rejection ability. (3) A predefined-time fault-tolerant control is proposed for AVSSs to deal with external disturbances and actuator faults. In addition to the reference X-dynamics with beneficial nonlinearities, a conditional disturbance cancellation design is defined to reserve beneficial disturbance characteristics, leading to enhanced energy-saving performance. Both the predefined convergence time and user-defined residual bound can be guaranteed which are independent of initial states and control parameters. Moreover, the continuous piecewise function and the quadratic fraction inequality are integrated to achieve nonsingular property and reduce chattering. (4) Different from existing active suspension control which neglected the effect of partial state estimation, this thesis proposes a predefined-time output-feedback control structure for AVSSs. A predefined-time extended state observer is developed utilizing the time-varying scaling function to approximate the unavailable velocities and disturbances. Despite the X-mechanism reference dynamics with beneficial suspension nonlinearities, the properties of both disturbances and state couplings are evaluated and preserved according to the effect characterization method, thus improving the potential energy conservation. The settling time of the whole control scheme can be user-specified with just one constant, which is free from dependence on initial states and control gains. Finally, compared with existing active suspension control designs, the proposed control algorithms are applied on a quarter-car experimental platform to present superior control performance over ride comfort, driving safety, and energy conservation.

Publications arising from the thesis

Journal Papers

[1] **Zengcheng Zhou**, Menghua Zhang, David Navarro-Alarcon and Xingjian Jing, "Predefined-time fault-tolerant control for active vehicle suspension systems with reference X-dynamics and conditional disturbance cancellation," ***IEEE Transactions on Intelligent Transportation Systems***, vol. 25, no. 11, pp. 18661-18672, 2024.

[2] **Zengcheng Zhou**, Menghua Zhang, Haiping Liu and Xingjian Jing, "Fixed-time safe-by-design control for uncertain active vehicle suspension systems with nonlinear reference dynamics," ***IEEE/ASME Transactions on Mechatronics***, vol. 29, no. 5, pp. 3348-3359, 2024.

[3] **Zengcheng Zhou**, Menghua Zhang, David Navarro-Alarcon and Xingjian Jing, "Model-free finite-time saturated control for active vehicle suspension systems with dead zones and external disturbances," ***Mechanical Systems and Signal Processing***, vol. 229, pp. 112542, 2025.

[4] **Zengcheng Zhou**, Menghua Zhang, David Navarro-Alarcon and Xingjian Jing, "Predefined-time output feedback control for active vehicle suspension systems with beneficial couplings, disturbances and nonlinearities," ***IEEE Transactions on Systems, Man, and Cybernetics: Systems***, under review, 2025.

[5] Menghua Zhang, **Zengcheng Zhou**, Ning Sun, Haokun Geng, Jing Zhao and Zhixin Yang, "Bioinspired reference model and fully actuated system approach-based neuroadaptive control for uncertain active suspension systems with input dead zones," ***IEEE Transactions on Industrial Electronics***, early access, Feb., 2025, doi: 10.1109/TIE.2025.3536552.

[6] Menghua Zhang, **Zengcheng Zhou**, Ning Sun, and Jing Zhao, "Fully actuated system approach to robust control for uncertain active suspension systems," ***Nonlinear Dynamics***, vol. 113, pp. 8757–8768, 2025.

[7] Menghua Zhang, Xingjian Jing, **Zengcheng Zhou** and Mingxu Sun, "Rapid and restricted swing control via adaptive output feedback for 5-DOF tower crane systems," ***Mechanical Systems and Signal Processing***, vol. 212, pp. 111283, 2024.

[8] Menghua Zhang, Xingjian Jing, **Zengcheng Zhou** and Weijie Huang, "Transportation for 4-DOF tower cranes: A periodic sliding mode control approach," ***IEEE Transactions on Intelligent Transportation Systems***, vol. 25, no. 11, pp. 15909-15921, 2024.

Conference Papers

[1] **Zengcheng Zhou**, Xingjian Jing, Menghua Zhang, "A novel robust finite-time control for active suspension systems with naturally bounded inputs", presented at ***The International Conference on Applied Nonlinear Dynamics, Vibration and Control – 2023***, Hong Kong, 2023.

Acknowledgements

I would like to take this opportunity to express my profound thanks and appreciation to all those who have given their continuous support and guidance during my doctoral journey in Hong Kong, as their support has been essential in realizing this thesis.

First and foremost, I want to convey my deepest gratitude to Prof. JING Xingjian, my former chief supervisor and now my co-supervisor at the City University of Hong Kong (CityU), for believing in me and for his patience and guidance over the years. This thesis would not have been possible without his support and encouragement. His mentorship and insightful advice have been instrumental in my scientific endeavors over the years and will undoubtedly continue to benefit me in my future career.

I am immensely grateful to Prof. NAVARRO-ALARCON David, my current chief supervisor at The Hong Kong Polytechnic University (PolyU), for his valuable suggestions and enough freedom during my research. His passion and patience make him a great mentor. I am profoundly thankful for his persistent direction and steadfast support throughout my research journey.

Furthermore, my genuine appreciation is extended to Prof. ZHANG Menghua at Jinan University. She has provided various pertinent suggestions and support for my research. Specifically, her scientific advice and numerous thought-provoking conversations have greatly contributed to the development of numerous ideas in this thesis.

I would like to convey my sincere appreciation to all my friends and colleagues in my research group at PolyU and CityU for their help and encouragement. I will forever value the camaraderie we have built over these unforgettable years.

Last but not least, I would like to express my heartfelt gratitude to my parents. My father, Mr. ZHOU Houping, and my mother, Ms. ZENG Feng, have been showing me unconditional love and endless support, which have been instrumental in providing me the courage to explore the world and to be who I am.

Contents

List of Figures

List of Tables

1 Introduction

1.1 Background and motivation

In recent decades, automobiles have become indispensable in contemporary daily life, playing as the backbone of modern transportation systems and significantly influencing economic, social, and environmental aspects of society. Vehicle suspensions, recognized as a vital component of automobiles, serve to transmit and mitigate the forces exerted between the road surface and the vehicle body [1]. Thanks to the utilization of vehicle suspensions, the passenger ride comfort can be greatly improved, while driving safety and maneuverability can be guaranteed simultaneously. The design of suspension systems directly affects the road handling ability and is one of the key factors in improving the quality of modern automobiles [2]. To meet the escalating demand for an enhanced driving experience, various research has been dedicated to the innovation of suspension system designs and control methods [3–5]. Therefore, more efforts should be devoted to developing suspension systems that utilize cutting-edge control strategies and advanced materials to deliver superior ride quality and vehicle performance.

Vehicle suspension systems refer to the collective term for all the force-transmitting connecting devices between the wheels and the vehicle body [6]. The forces and moments faced by vehicle suspensions mainly come from the following aspects: 1) Road surface excitation. The vibration of uneven road surfaces should be isolated and absorbed by the suspension systems, which acts as the forces on the wheels and is transmitted to the vehicle suspension systems. 2) Vertical load. The vertical load of the vehicle, including the vehicle weight, passengers, and cargo, is exerted on the suspension systems as the supporting force. 3) Vehicle braking and acceleration. During the braking and acceleration process, the vehicle generates forward or backward torques due to inertia, and the suspension systems need to resist these torques to prevent ex-

cessive pitching of the vehicle. 4) Aerodynamics: During vehicle operation, the forces generated by air flowing over the surface of the vehicle can also affect the suspension systems, especially at high speeds. Therefore, vehicle suspensions are needed to attenuate these effects to suppress vibration, improve ride comfort, and guarantee road holding capacity.

Typical vehicle suspension systems mainly comprise springs, dampers, tire components, and some other attachments [7]. The springs are one of the most critical components of suspension systems, primarily responsible for supporting the vehicle's weight and mitigating shocks and vibrations caused by uneven road surfaces. Furthermore, the dampers are utilized to dissipate vibration energy and dampen the impacts caused by irregular road surfaces, thereby reducing vehicle oscillation and enhancing driving safety. Other attachments include bolts, nuts, brackets, etc., which secure all the aforementioned components in their appropriate positions on the vehicle, ensuring the suspension system works cohesively as a whole. Tuning the parameters of springs and dampers can help increase ride comfort and mitigate vibration [8]. However, there exists a conflict in traditional vehicle suspensions to achieve ride comfort and driving safety. Thus, recent developments in the suspension system field are presented in the following sections in detail.

1.2 Classification of vehicle suspensions

Normally, vehicle suspension systems can be divided into three categories, including passive suspensions, semi-active suspensions, and active vehicle suspension systems (AVSSs) [9]. Conventional vehicles typically feature passive vehicle suspension systems which are composed of dampers and springs with invariant coefficients. Therefore, passive ones are not sufficient to guarantee ride comfort and road holding simultaneously [10]. Semi-active vehicle suspension systems integrate adjustable spring and damping components which adapt the spring rigidity or damper resistance in the presence of rough roads, thereby enhancing the capability to mitigate road disturbances [11].

However, the ride comfort improvement is limited by the suspension velocity constraint which is crucial for generating the output force [12]. AVSSs have been devoted with numerous efforts due to their great ride comfort performance. Extra actuators, such as direct-current motors, hydraulic cylinders, are equipped to produce active forces to deal with rough roads and external disturbances [13]. Given the high demands for ride comfort and driving smoothness, AVSSs have become a hot research topic in the automotive industry, which holds significant value and potential for application.

1.2.1 Passive vehicle suspension systems

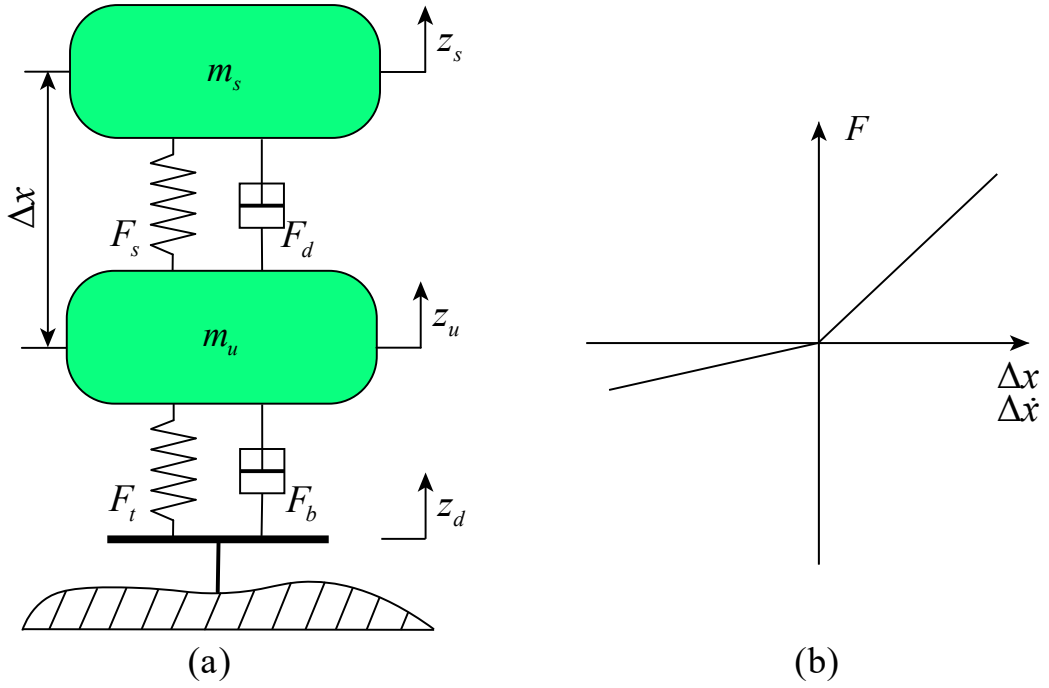

Fig. 1.1: Passive suspension system (a) System structure (b) Force range

Passive vehicle suspension systems are widely used in automobiles to support the vehicle body and suppress vibration, as shown in Fig. 1.1. The springs and dampers with fixed parameters are the main components in the passive suspensions [14]. The spring's primary roles include upholding the vehicle's structure and shielding it from the impacts of the road, thereby enhancing the overall riding comfort [15]. Meanwhile, the damper aids in the improvement of both ride comfort and driving safety [16]. The simplicity of passive vehicle suspension systems structures leads to the easiness of man-

ufacture and maintenance, which makes them widely used in economy vehicles and in situations where height adjustment capabilities are not required [17]. However, passive suspensions can not dynamically adjust according to road conditions or driving styles. To better deal with these issues, several techniques have been investigated, including suspension parameter optimization, replacing high-performance materials, suspension structure improvement, application of air springs, and so on [18]. However, the anti-vibration capability of passive vehicle suspension systems is still limited when encountering rough roads with high speed, which may lead to the deterioration of vibration isolation.

1.2.2 Semi-active vehicle suspension systems

To improve the anti-vibration performance of vehicles, semi-active vehicle suspension systems (Fig. 1.2) are developed with benefits including straightforward integration, compact design, rapid response [6]. Different variable dampers are utilized in semi-active suspensions such as electro-hydraulic dampers [19], magneto-rheological dampers [20], and electro-rheological dampers [21]. However, nonlinear behaviors including hysteresis characteristics exist in these variable dampers, which may lead to unpredictable control performance.

The generated damping forces rely on the relative suspension speed with physical constraints [22]. Different control techniques have been developed for semi-active vehicle suspension systems. The sky-hook damper technique was designed to emulate a virtual damper in the sky using an optimal control method, which constructed switching laws to generate different damper force [23]. Then the acceleration driven control method was developed using the frequency selector technique to provide benefits beyond the body resonance [24]. Furthermore, modern control designs were constructed including the model predict control [25], H_∞ control [26], sliding mode control [27], fuzzy logic control [28], and neural network control [29], etc. However, variable dampers can not generate active forces, which also limits the vibration suppression performance.

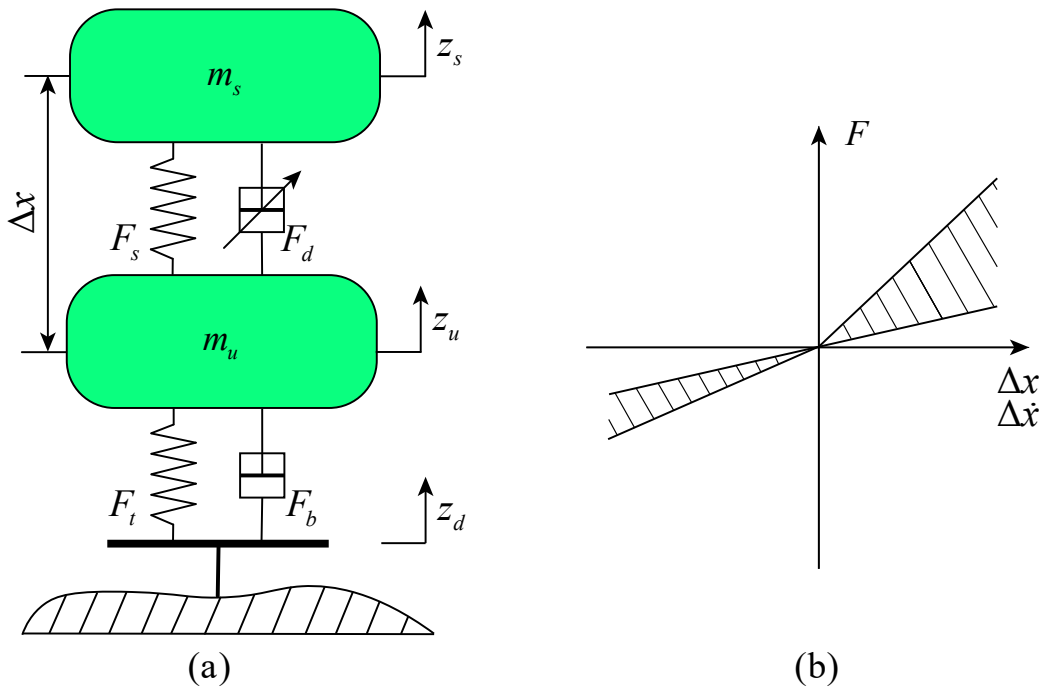

Fig. 1.2: Semi-active suspension system (a) System structure (b) Force range

1.2.3 Active vehicle suspension systems

As shown in Fig. 1.3, AVSSs represent a highly intelligent suspension technology, which are capable of dynamically adjusting the stiffness and damping of the suspension based on the vehicle's motion and road conditions [30].

Typically, key components of AVSSs include:

1) Actuators. Vertical actuators are utilized to guarantee the vehicle body to stay in good anti-vibration status, which also require external energy resources. Typical actuators are widely used such as electro-hydraulic actuators, hydraulic-cylinder actuators, and air-spring actuators [31].

2) Sensors. Vehicle states and road profiles can be collected using different sensors including accelerometers, force transducers, and so on [32].

3) Control units. Utilizing the information detected from sensors, control signals can be calculated using the control units [33].

Compared with passive and semi-active suspensions, extra actuators can provide and

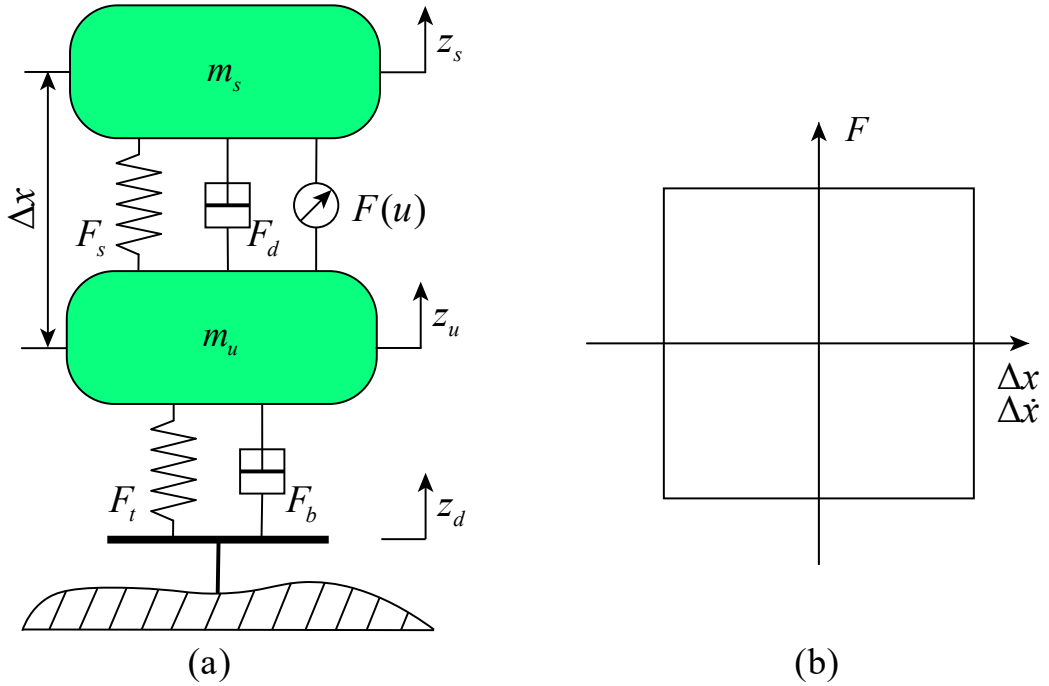

Fig. 1.3: Active suspension system (a) System structure (b) Force range

dissipate suspension energy to improve ride comfort and maneuverability [34]. Therefore, high-speed response and real-time adjustment can be achieved in the presence of various driving conditions. Considering the superior anti-vibration performance of AVSSs, both ”hard” and ”soft” suspension characteristics can be obtained to ensure ride comfort and driving stability. Therefore, the main goal of this thesis lies in the advanced finite-time control techniques and their applications to AVSSs.

1.3 Thesis scope

In this thesis, several finite-time control designs are proposed for AVSSs to ensure satisfactory anti-vibration performance with energy conservation characteristics. The finite-time control methods process better capability in rapid convergence speed and higher disturbance rejection under the conditions of system uncertainties, external disturbances, and actuator nonlinearities. Besides, energy-saving performance is critical and desirable in both theoretical analysis and practical applications. Therefore, the main scope of this thesis is to explore the finite-time energy-saving control techniques, such

that excellent suspension performance can be achieved to improve ride comfort under different road profiles. The detailed control objectives and control problems are provided in this section.

1.3.1 Control objectives

Vehicle suspensions can effectively hold the vehicle body and maintain contact with the ground. Vehicle body height can be thereby adjusted by AVSSs according to different vehicle loads, driving speeds, and uneven roads. Furthermore, the performance of vehicle suspensions can be evaluated in the following aspects.

- **Ride comfort.** As one of the most important indexes to evaluate suspension performance, ride comfort is highly related to vertical vehicle body acceleration, which reflects the impact of vibrations on human comfort and health. Normally, humans are more sensitive to vibration frequencies between 4–12.5Hz. Therefore, reducing the amplitude of vertical vehicle body acceleration becomes a major concern. The root mean square (RMS) value of the vertical acceleration $\ddot{z}_s$ is a simple but effective method to evaluate the ride comfort performance which is given as [35]

$$\text{RMS}(\ddot{z}_s) = \sqrt{\frac{1}{T}\int_0^T \ddot{z}_s^2 dt} \tag{1.1}$$

  where T is the experimental time period.

- **Suspension deflection.** The suspension deflection can be used to reflect the attitude change of the vehicle body and the adaptation capability to rough roads, which is always constrained by physical mechanisms. Extensive suspension travel may lead to a decrease in ride comfort or even system instability. The suspension deflection $z_p = z_s - z_u$ should be constrained within a specific range such that

$$\underline{z_p} \leq z_p \leq \bar{z_p} \tag{1.2}$$

  with $\underline{z_p}$ and $\bar{z_p}$ meaning the lower and upper bounds of the suspension deflection

z_p, respectively.

- **Road holding ability.** The variations in dynamic tire load will influence the contact force between the tire and the road surface, thereby affecting the road holding ability of vehicle systems. Thus, it is essential to consider the road holding ability deduced by vibrations to ensure driving safety and maneuverability. To intuitively present the road holding ability, a quantitative index is defined to maintain the dynamic tire load F_{dyn} below the static tire load F_{sta}, i.e. [36]

$$\frac{|F_{\text{dyn}}|}{F_{\text{sta}}} \leq 1 \tag{1.3}$$

where $F_{\text{dyn}} = F_t(z_u, z_r) + F_b(\dot{z}_u, \dot{z}_r)$ and $F_{\text{sta}} = (m_s + m_u)g$ are the dynamic tire load and the static tire load, respectively, $g = 9.8m/s^2$ is the gravity constant.

- **Energy consumption.** Since extra actuators are equipped for better anti-vibration performance, additional energy is required to drive the actuators. Therefore, high energy consumption is a critical problem for AVSSs. The energy consumption index is constructed as [37]

$$\text{RMS}(P^+) = \sqrt{\frac{1}{T}\int_0^T (P^+(\tau))^2 d\tau} \tag{1.4}$$

with

$$P^+(t) = \begin{cases} u(t)(\dot{z}_s - \dot{z}_u), & u(t)(\dot{z}_s - \dot{z}_u) > 0 \\ 0, & \text{else} \end{cases}$$

where $u(t)$ means the control force, $\dot{z}_s - \dot{z}_u$ represents the relative speed of the suspension.

- **Response time.** The response time of AVSSs is also a crucial performance indicator, affecting the convergence speed and ability to adapt to road surface changes and adjustments.

1.3.2 Control problems

The control problems of this thesis are listed as follows:

- To enhance the transient suspension performance, a finite-time control method is required for AVSSs such that the input signals are naturally constrained by known ranges to avoid input saturations. Furthermore, no model information should be required.
- To eliminate the settling time requirement for the initial states, fixed-time convergence is desirable for AVSSs with nonlinear reference dynamics-based energy-saving techniques. Both displacement and velocity need to be restrained within permitted asymmetric time-varying constraints, thus, safety requirements for displacement, velocity, and input saturations can be satisfied simultaneously.
- Considering the actuator fault phenomenon, the predefined-time stability of AVSSs should be deduced such that tracking errors can converge to a reassigned bound within a predefined time interval, which is irrelevant to both initial states and control gains. Moreover, beneficial disturbances and nonlinearities should be retained for better energy conservation.
- Unknown states and external disturbances should be precisely estimated using the predefined-time extended state observer technique. Besides the X-mechanism reference design, beneficial couplings and disturbances should be assessed and utilized in the control system to enhance the energy-saving characteristics. The predefined-time stability should be retained such that the settling time can be adjusted by only one parameter.

1.4 Novelties and contributions of the thesis

This thesis mainly focuses on the control designs of finite-time theories and their applications on AVSSs. Therefore, ride comfort can be enhanced with quick response and

energy-saving performance, while the requirements of suspension deflection and road holding ability can be satisfied simultaneously. The major novelties and contributions of this thesis can be summarized as follows.

1) Considering input saturations, dead zones, and external disturbances, a novel model-free finite-time saturated control is developed for AVSSs. Different from existing saturation control methods, the control signal is inherently constrained within a preassigned scope. Besides, no model information is required, leading to a sufficient model-free control method.

2) A fixed-time safe-by-design control is proposed for AVSSs to satisfy different safety requirements including input saturations and asymmetric time-varying constraints on displacement/velocity. By reserving beneficial nonlinearities of a bioinspired X-shaped reference, energy-saving performance can be ensured. Furthermore, utilizing the fixed-time stability theory, the settling time is independent of initial states.

3) To further enhance the finite-time stability, a predefined-time fault-tolerant control is constructed to address external disturbances, actuator faults, and limited transient performance. Upon the reference X-dynamics with beneficial nonlinearities, the conditional disturbance cancellation technique is introduced to assess and retain beneficial disturbances, thereby enhancing energy conservation. Besides, by constructing a novel predefined-time Lyapunov stability theorem, the preassigned bound and the predefined time period can be arbitrarily selected using simple constants, which are irrelevant to initial states and control parameters.

4) A novel predefined-time output feedback control is derived for AVSSs in the presence of partial-state measurements, uncertain dynamics, and external disturbances. Unknown velocities and external disturbances can be measured by the predefined-time extended state observer utilizing the time-varying scaling method. Expanding upon the X-mechanism reference dynamics with beneficial nonlinearities, both advantageous couplings, and disturbances are recognized and

reserved using the effect characterization method to reduce energy consumption. Moreover, the predefined-time stability of the closed-loop system can still be guaranteed to improve the transient performance.

1.5 Structure of the thesis

The structure of this thesis is organized as follows. Fundamental facts about AVSSs are presented in Chapter 2 including the dynamic model, existing control techniques, and experimental platforms. In Chapter 3, a model-free finite-time saturated control is developed for AVSSs with input saturations and dead zones. Then Chapter 4 investigates the fixed-time safe-by-design control problem for AVSSs while retaining beneficial nonlinearities of bioinspired X-shaped dynamics. A predefined-time fault-tolerant control is proposed based on the reference X-dynamics and conditional disturbance cancellation in Chapter 5. Moreover, Chapter 6 presents a predefined-time output feedback control scheme integrating a novel predefined-time extended state observer, X-mechanism reference dynamics, and coupling/disturbance effect characterization technique. Finally, the thesis concludes in Chapter 7 with future research discussions.

2 Vehicle Suspension Systems

In this chapter, fundamental facts of active suspensions are provided. Specifically, the dynamic model of a quarter-car AVSS is detailly presented in Section 2.1, which is applied in the controller designs, simulations, and experiments throughout this thesis. Different road input profiles are introduced as road disturbances in Section 2.2. Then the literature review of AVSS control design is introduced in Section 2.3. Finally, the conclusions are provided in section 2.4.

2.1 Dynamic model of a quarter-car AVSS

The dynamic model of AVSSs should be established before the design of modern control methods, which can be categorized into three different types including the quarter-car model, half-car model, and full-car model. Typically, the quarter-car model is the simplest one to describe the vertical movement of the vehicle body and wheel which can effectively verify the effectiveness and robustness of controller designs. The half-car AVSS model integrates the pitch effect of the vehicle on the basis of the quarter-car model to analyze the dynamic response of the vehicle on the rough road inputs. Furthermore, the full-car model is always the most complex one used for analyzing all degrees of freedom of the vehicle. Besides, in terms of the active suspension control designs, it is reasonable to consider a relatively simple model structure for the theoretical demonstration and primary experimental verification. Moreover, the quarter-car AVSS model can also be an effective structure for the dynamic frequency investigation within the range of 0–25Hz.

The scheme of a typical quarter-car AVSS is provided in Fig. 2.1, which is widely utilized in existing AVSS researches due to the simple structure and precise dynamic motions for practical AVSSs. This AVSS scheme can be considered as a double mass-

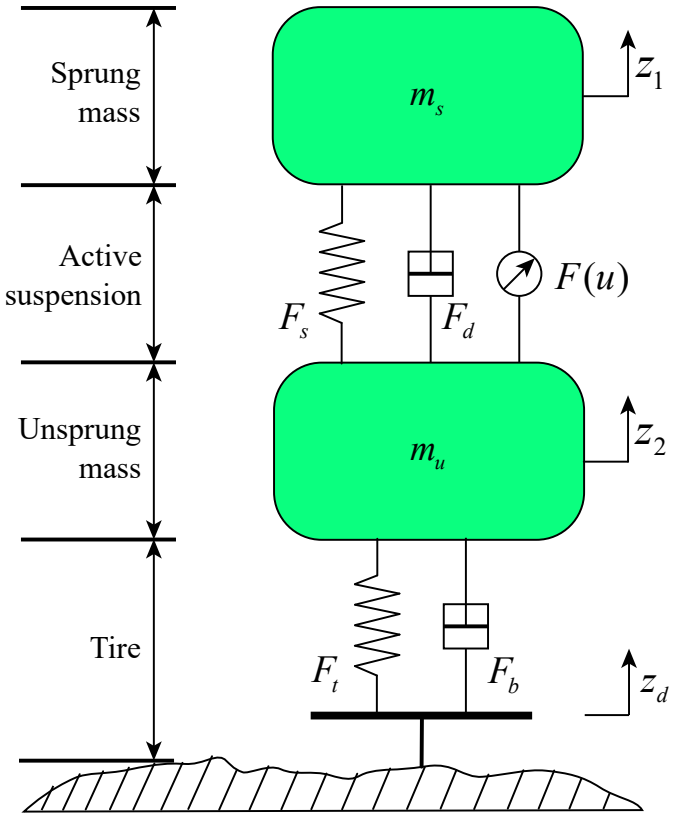

Fig. 2.1: The quarter-car AVSS structure

spring-damper platform which can be modeled using the free body diagram method.

The expressions of the spring forces and damping forces can be described as

$$\begin{aligned} F_s(z_s, z_u) &= r_s(z_s - z_u) \\ F_d(\dot{z}_s, \dot{z}_u) &= \begin{cases} r_{d1}(\dot{z}_s - \dot{z}_u), & \dot{z}_s - \dot{z}_u > 0 \\ r_{d2}(\dot{z}_s - \dot{z}_u), & \dot{z}_s - \dot{z}_u \leq 0 \end{cases} \\ F_t(z_u, z_r) &= r_t(z_u - z_r) \\ F_b(\dot{z}_u, \dot{z}_r) &= r_b(\dot{z}_u - \dot{z}_r) \end{aligned} \tag{2.1}$$

with $F_s(z_s, z_u)$ and $F_t(z_u, z_r)$ denoting the spring forces, $F_d(\dot{z}_s, \dot{z}_u)$, $F_b(\dot{z}_u, \dot{z}_r)$ representing the damping forces, r_s meaning the stiffness coefficient, r_{d1} and r_{d2} being the damping coefficients of the damper during the extension and compression motions, respectively, r_t and r_b presenting the tire stiffness and damping coefficients, respectively.

The free body diagram for the sprung and unsprung masses should be discussed re-

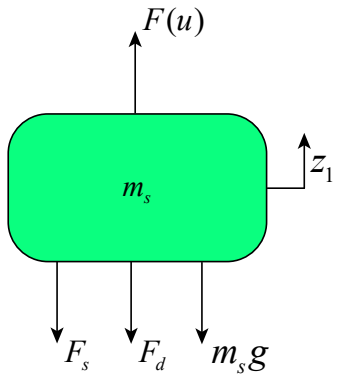

Fig. 2.2: The free body diagram of sprung mass

spectively to obtain the equations of motion for the AVSS platform [38]. The initial states are set to zero for simplicity.

As shown in Fig. 2.2, the free body diagram of the sprung mass m_s is presented including the spring force $F_s(z_s, z_u)$, damping force $F_d(\dot{z}_s, \dot{z}_u)$, control input $F(u)$, and gravity $m_s g$. A generalized reference frame is constructed with z_1 denoting the vertical vehicle body displacement (i.e. sprung mass) and z_2 representing the tire displacement (i.e. unsprung mass) with respective to the ground. The equation of motion for the sprung mass m_s becomes

$$\ddot{z}_1 = -g + m_s^{-1}(F(u) - F_s(z_s, z_u) - F_d(\dot{z}_s, \dot{z}_u)) \tag{2.2}$$

Similarly, the free body diagram of the unsprung mass m_u can be obtained in Fig. 2.3 with the spring forces $F_s(z_s, z_u)$, $F_t(z_u, z_r)$, damping forces $F_d(\dot{z}_s, \dot{z}_u)$, $F_b(\dot{z}_u, \dot{z}_r)$, control input $F(u)$, and gravity $m_u g$. The equation of motion for the unsprung mass m_u is

$$\begin{aligned} \ddot{z}_2 = -g + m_u^{-1}(&F_s(z_s, z_u) + F_d(\dot{z}_s, \dot{z}_u) - F_t(z_u, z_r) \\ &- F_b(\dot{z}_u, \dot{z}_r) - F(u)) \end{aligned} \tag{2.3}$$

One should note that gravity can only influence the equilibrium points of the AVSS rather than the dynamic model scheme, which can be further eliminated mathematically. We denote the static equilibrium points as $z_1 = z_{\text{eq1}}$ and $z_2 = z_{\text{eq2}}$ such that all orders of

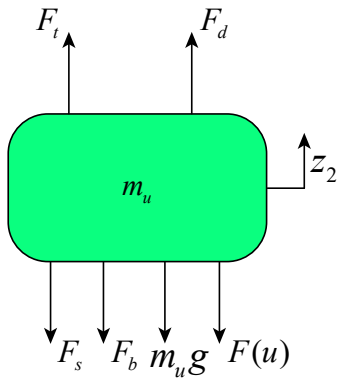

Fig. 2.3: The free body diagram of unsprung mass

the time derivatives of z_1 and z_2 are zero. Besides, the road profile z_r and control input $F(u)$ are set as zero. Then combining (2.2) and (2.3) leads to

$$\begin{aligned} m_s g + r_s z_{\text{eq1}} - r_s z_{\text{eq2}} &= 0 \\ m_u g - r_s z_{\text{eq1}} + r_s z_{\text{eq2}} + r_t z_{\text{eq2}} &= 0 \end{aligned} \tag{2.4}$$

Therefore, considering the gravity, the equilibrium points become

$$\begin{aligned} z_{\text{eq1}} &= -\frac{g(r_t m_s + r_s m_s + r_s m_u)}{r_s r_t} \\ z_{\text{eq2}} &= -\frac{g(m_s + m_u)}{r_t} \end{aligned} \tag{2.5}$$

Hence, to effectively eliminate the gravity effect, the coordinates of the AVSS structure are revised as

$$\begin{aligned} z_1 = z_s - \frac{m_s g}{r_s} - \frac{(m_s + m_u)g}{r_t}, \quad z_2 &= z_u - \frac{(m_s + m_u)g}{r_t} \\ \dot{z}_1 = \dot{z}_s, \quad \dot{z}_2 &= \dot{z}_u \\ \ddot{z}_1 = \ddot{z}_s, \quad \ddot{z}_2 &= \ddot{z}_u. \end{aligned} \tag{2.6}$$

Now the relaxed positions of the AVSS scheme, i.e. $z_s = 0$ and $z_u = 0$, can be regarded as the equilibrium points without the gravity effects. Substituting (2.6) into the equations of motion (2.2)–(2.3) leads to the dynamic model of the quarter-car AVSS

given as [39, 40]

$$\begin{aligned} m_s\ddot{z}_s &= -F_s(z_s, z_u) - F_d(\dot{z}_s, \dot{z}_u) + F(u) + d_1 \\ m_u\ddot{z}_u &= F_s(z_s, z_u) + F_d(\dot{z}_s, \dot{z}_u) - F_t(z_u, z_r) \\ &\quad - F_b(\dot{z}_u, \dot{z}_r) - F(u) + d_2 \end{aligned} \tag{2.7}$$

where the sprung mass m_s denotes the vehicle body mass and passengers; the unsprung mass m_u includes the wheel, suspension components, and brake system; z_s, z_u, z_r represent the vertical displacement of the sprung mass, unsprung mass, road profile, respectively; d_1 and d_2 are the unknown external disturbances and uncertain system dynamics in the sprung and unsprung channel, respectively; $F(u)$ is the control input signal which will be discussed later.

Considering the state transformation as $x = [x_1, x_2, x_3, x_4]^T$ with $x_1 = z_1$, $x_2 = \dot{z}_s$, $x_3 = z_3$, $x_4 = \dot{z}_u$, the dynamic model for the AVSS (2.7) can be given as

$$\begin{cases} \dot{x}_1 = x_2 \\ m_s\dot{x}_2 = f(x) + F(u) + d_1 \\ \dot{x}_3 = x_4 \\ m_u\dot{x}_4 = g(x) - F(u) + d_2 \end{cases} \tag{2.8}$$

where $f(x) = -F_s(z_s, z_u) - F_d(\dot{z}_s, \dot{z}_u)$, $g(x) = F_s(z_s, z_u) + F_d(\dot{z}_s, \dot{z}_u) - F_t(z_u, z_r) - F_b(\dot{z}_u, \dot{z}_r)$.

The control input force $F(u)$ may suffer from different actuator nonlinearities including:

1) Input saturation. The input saturation problem occurs when the control signal is constrained within a certain range due to actuator limitations and safety requirements, which also indicate the existence of maximum and minimum control input

capability. Normally, it can be represented as [41]

$$F(u) = sat(u) = \begin{cases} u_{\max}, & u \geq u_{\max} \\ u, & u_{\min} \leq u \leq u_{\max} \\ u_{\min}, & u \leq u_{\min} \end{cases} \tag{2.9}$$

where $u_{\max}$ and $u_{\min}$ are the maximum and minimum values of the control input u, respectively.

2) Dead zone. The dead zone phenomenon refers to a region within the control input signal where there is no response such that no changes will be made to the control system. Generally, the control signal becomes zero during the dead zone range until it exceeds a certain threshold. The dead zone problem can be given as [42]

$$F(u) = \begin{cases} \beta_+(u - u_r), & u > u_r \\ 0, & u_l \leq u \leq u_r \\ \beta_-(u - u_l), & u < u_l \end{cases} \tag{2.10}$$

where β_+ and β_- are the unknown slope parameters, $u_r > 0$ and $u_l < 0$ are the unknown bound constants.

3) Actuator faults. Various factors may result in actuator faults including mechanical damage, electrical issues, software problems, and external disturbances. The occurrence of actuator faults may lead to severe control performance decreases including reduced efficiency, inaccurate control, or even system corruption. A common actuator fault model can be expressed as follows [43].

$$F(u) = \Gamma u + \rho(t) \tag{2.11}$$

where $0 \leq \Gamma \leq 1$ means the loss-of-effectiveness (LOE) fault, $\rho(t)$ denotes the time-varying bias fault. Different fault modes can be represented by the fault model (2.11) including the fault-free case with $\Gamma = 1$ and $\rho(t) = 0$, the LOE fault

case with $0 < \Gamma < 1$ and $\rho(t) = 0$, the bias fault case with $\Gamma = 1$ and $\rho(t) \neq 0$, the stuck fault case with $\Gamma = 0$, and the combined case with $0 < \Gamma < 1$ and $\rho(t) \neq 0$.

2.2 Road profiles

Compared with the vehicle motion, load change, and suspension characteristics, the rough road inputs are the main source of vehicle vibration, which is thus extensively investigated in traditional active suspension control designs. The vibration-isolation performance of AVSSs is usually evaluated under different road profiles both in simulations and experiments. Common types of road excitation consist of bump road input, sinusoidal road input, and random road input. Accordingly, the bump road input is used to mimic protrusions like rocks and manhole covers. The sinusoidal road input refers to the unevenness of roads at a certain frequency, which is the common tool for examining vehicles' responses at specific frequencies. Besides, the random road input implies a random pattern of road irregularities, which is closer to the actual road conditions. The AVSSs with proper control designs are supposed to suppress the vibration induced by the rough roads. Therefore, the simplified mathematical road model should be investigated in the simulations and practical tests.

2.2.1 Bump road profile

The uneven road with abrupt changes can be described as the bump road profile, which includes potholes, speed bumps, and other similar irregularities. Usually, a continuous piecewise function $z_r(y)$ is utilized to approximate the bump road to tackle the discontinuous problem, which is given as

$$z_r(y) = \begin{cases} \frac{h_b}{2}(1 - \cos(2\pi \frac{y}{L})), & 0 \leq y \leq L \\ 0, & \text{else} \end{cases} \tag{2.12}$$

where h and L are the height and width of the bump, respectively. One should also note that the potholes can be obtained using (2.12) when $h < 0$. When the vehicle velocity is denoted by v when passing the bump, the road model can be written as

$$z_r(y) = \begin{cases} \frac{h_b}{2}(1 - \cos(\frac{2\pi v}{L}t)), & 0 \leq t \leq \frac{L}{v} \\ 0, & \text{else.} \end{cases} \tag{2.13}$$

2.2.2 Sinusoidal road profile

The sinusoidal road profile is widely utilized in the investigation of active suspension control designs, which is convenient for estimating the anti-vibration performance of the AVSSs under a certain frequency. The sinusoidal road profile, whose frequency is always selected within 0.5–15Hz, can be presented by the following mathematical model.

$$z_r(t) = A_0 \sin(2\pi f t) \tag{2.14}$$

where A_0 is the amplitude of the sinusoidal road profile, f means the road excitation frequency.

2.2.3 Random road profile

The rough road profile is an important road type in the simulations and experiments of active suspension controllers since it is considered the most effective method to approximate the practical road excitation. The road height is varying randomly with respect to a certain reference benchmark. The road roughness can be classified using the power spectral density (PSD) according to the International Organization of Standardization (ISO 8606) which is given as [44]

$$G_q(n) = G_q(n_0)(\frac{n}{n_0})^{-W} \tag{2.15}$$

where n is the spatial frequency, n_0 denotes the reference spatial frequency, $G_q(n_0)$ represents the roughness coefficient, W is a waviness index which is usually selected to be $W = 2$ in most cases.

The standard of rough roads can be classified into different categories from A to E using the PSD values, shown in Table 2.1 [45].

Table 2.1: Road Roughness Classification

Road Class	Degree of Roughness		
	$G_q(n_0) \times 10^{-6}\text{m}^3 \quad (n_0 = 0.1\text{m}^{-1})$		
	Lower Limit	Geometric Mean	Upper Limit
A (very good)	–	16	32
B (good)	32	64	128
C (average)	128	256	512
D (poor)	512	1024	2048
E (very poor)	2048	4096	8192

Then the random road profile can be generated by [45]

$$\dot{z}_r(t) = 2\pi f_0 \sqrt{(v_0 + at)G_q(n_0)}w(t) - 2\pi(v_0 + at)f_c z_r(t) \tag{2.16}$$

where f_0 and f_c are the spatial cut-off frequency for the standard and road, respectively, $w(t)$ denotes the standard white noise, v_0 and a are the initial velocity and acceleration constants, respectively.

Based on the analysis above, the random road profile can be established to meet various needs in simulations and practical experiments.

2.3 Literature review of AVSS control design

To ensure vehicle stability and enhance suspension capabilities, appropriate control designs should be investigated for AVSSs to improve ride comfort, which is still a critical problem in both theoretical analyses and practical applications. The AVSS control refers to the use of controllable actuation components to supply real-time control forces that adapt to the varying conditions of the vehicle and road profiles. Different control strategies may lead to distinct suspension performance, thereby meeting diverse demands for

ride comfort, vehicle safety, and handling stability. Hence, the investigation of AVSS control designs becomes vitally important for vehicle suspension performance improvement. In fact, extensive efforts have been made by scientists and engineers in the past few decades from the classical linear control methods (including optimal control and H_∞ control) to advanced nonlinear ones (such as sliding mode control, backstepping control, adaptive control, intelligent control, and so on). In this section, various control schemes are presented in the past few decades in the categories of linear and nonlinear control methods. As a matter of fact, numerous suspension control approaches have been developed as extensions and combinations of existing methods, accommodating uncertainties in uncertain suspension parameters, actuator nonlinearities, and external disturbances, thereby achieving a comprehensive suspension performance that balances various control requirements.

2.3.1 Linear control methods

a) Optimal control

The optimal control method, as a typical linear control technique, has been extensively integrated into traditional AVSS systems [46]. Typically, the linear quadratic Gaussian (LQG) and linear quadratic regulator (LQR) control were vastly investigated which can transform different conditions (i.e. ride comfort, suspension deflection, control force) into a quadratic-form optimization index [47]. The overall suspension performance can be improved by selecting the weight coefficients with an optimization algorithm. However, the selection of desirable weight coefficients can be a difficult task for LQG control which severely affects the vibration isolation results. A particle swarm optimization design was used in the LQR control to generate desired forces [48]. Besides, the genetic algorithm was also considered an effective way for weight coefficient tuning [49]. However, the precise dynamic AVSS model is needed for satisfactory control performance. And the variation of driving conditions, including the change of vehicle loads, different road profiles, unknown external disturbances, may lead to the degradation of suspension performance. The adaptive gain-based LQG control was constructed

for AVSS with the skyhook technique to reduce the real-time computational cost [50]. A switching control logic was designed for AVSSs which can determine the regulator coefficients with respect to tire load and suspension travel, thus, ride comfort can be satisfied within tire load constraints and suspension travel ranges [51]. Moreover, the linearized suspension dynamic model was frequently utilized in existing optimal control designs [52]. Therefore, the system robustness and stability margin are barely acceptable in these optimal control methods in the presence of unmodeled dynamics and external disturbances.

b) H_∞ control

Although traditional AVSSs can be stabilized by using optimal control methods considering several different suspension characteristics, satisfactory anti-vibration performance is still in the early stages. With the development of control theory, H_∞ control has been considered an effective technique for active suspensions to reduce the disturbance effect and balance conflict performance characteristics [53]. Considering the critical ride comfort requirements, a H_∞ control design was developed for AVSSs within a finite frequency range [54]. Based on a quarter-car model, an output-feedback H_∞ control was designed which emerged multi-objective constrained into the linear matrix inequality method [55]. Moreover, the control scheme in [55] integrated the H_∞ control with Lyapunov theory to guarantee the closed-loop system stability. An extended research was conducted for half-car AVSSs which combined sampled H_∞ control with fuzzy technique by solving an optimization problem [56]. Furthermore, a full-car AVSS model was considered in [57] to investigate the finite-frequency ride comfort which merged various constraints on system uncertainties, input saturations, and suspension deflections. Besides, the event-triggered mechanism was integrated into the H_∞ control for a full-car AVSS to ensure the minimum interevent time [58]. However, existing H_∞ research papers above mostly provide simulation results rather than experiments. The leaf spring hysteresis-based AVSS model was derived in [59], in which the H_∞ control was combined with the sliding mode technique to deal with actuator disturbances. Utilizing an improved Lyapunov function, this control design could achieve robustness

and effectiveness demonstrated through experimental results [59].

2.3.2 Nonlinear control methods

Benefiting from the simple structure and easy implementation, a variety of linear control methods have been investigated for AVSSs. However, the mathematical suspension model was often linearized to approximate the practical suspension system, which neglected the inherited nonlinearities. Specially, these nonlinear parts could become so evident that they severely affect the model structure, further impacting the control effectiveness, under some cases including the discrete-event disturbances and dry friction. The impact of the nonlinear characteristic, including the spring force and damping force, was analyzed through various simulations under different road profiles [60]. One can easily conclude that nonlinear components should be included in the theoretical model establishment and the control design. In this subsection, different nonlinear control methods are reviewed for AVSSs. Besides, more specific reviews of different finite-time energy-saving control schemes are detailed in the following chapters in this thesis.

a) Sliding mode control

In practical suspensions, robust control designs are necessary for effective suspension to deal with system uncertainties and external disturbances. The sliding mode control (SMC) can notably enhance the suspension performance in nonlinear AVSSs which processes high robustness in the presence of parameter uncertainties and external disturbances caused by road conditions. The SMC scheme mainly involves the frequent switching of control inputs, compelling the variable to slide within a predefined sliding surface. Therefore, the system stability and dynamic performance can be adjusted by the sliding mode surface and its corresponding parameters. Various SMC designs have been investigated to achieve the robust control performance. For example, a typical sliding mode surface was presented in the linear disturbance observer-based SMC [8] for AVSSs with actuator nonlinearities. Integrated with the adaptive technique and fuzzy logic system, a sliding mode filter was used to achieve finite-time convergence [61].

Based on a nonlinear disturbance observer, an adaptive SMC scheme was presented for AVSSs [33]. A second-order SMC algorithm was developed for AVSSs to achieve finite-time stability [3]. Utilizing a terminal sliding mode method, an output feedback control was proposed for AVSSs, which was verified through simulation results [62]. To guarantee the output constraints, the SMC technique was combined with the asymmetric barrier Lyapunov functions for nonlinear AVSSs [63]. However, the main drawbacks of most existing active suspension SMC approaches are the chattering phenomenon and singularity problem. The former drawback is caused by the discontinuous sliding mode scheme in the reaching phase. And the latter is due to the singular points of the sliding mode surface, especially in the finite-time SMC designs. Various efforts have been devoted to reducing the chattering and avoiding the singularity. To mention a few, an adaptive law-based SMC was constructed for AVSSs to estimate the upper bound of system uncertainties [64]. The singularity was avoided in the terminal SMC design for AVSSs with a typical signum function [65]. Besides, the integral terminal sliding mode surface can also be utilized for singularity-free active suspension designs [66]. However, the control performance still needs to compromise with the chattering phenomenon and singularity problem, leading to the deterioration of ride comfort or even system instability.

b) Adaptive control

Adaptive control is widely adopted for AVSSs to obtain high robustness, which can automatically adjust control parameters to adapt to changes in the dynamic characteristics. An additional adaptive loop is normally added in the control signal to change continuously during the control process according to certain adaptive rules. Therefore, a precise AVSS dynamic model is not required for the convenience of control design. A typical uncertain parameter of AVSSs may come from the sprung mass, including the changes in passengers and loads. A saturated adaptive control was constructed for half-car AVSSs considering unknown variable sprung mass [67]. Hua *et al.* [68] designed a robust adaptive control for half-car AVSSs to compensate for varying sprung mass, which can also compel system states to stay within restrictive constraints using the pre-

scribed performance method. Combined with a bioinspired structure and the projection mapping scheme, an adaptive control was defined for AVSSs to deal with sprung mass uncertainty and achieve energy-saving performance [69]. There are also more efforts devoted to addressing the uncertain model dynamics, external disturbances, and actuator nonlinearities. A nonlinear adaptive control was designed for AVSSs with electro-hydraulic actuators [70]. To cooperate with stochastic actuator faults, an adaptive fault-tolerant control scheme was developed for half-car AVSSs to guarantee the system stability [71]. Furthermore, different adaptive control skills were integrated into [2] to resolve AVSS system variations. More additional investigations into the adaptive control designs for AVSSs can be found in [72–75]. However, existing adaptive control methods always require extensive computational resources due to the complex online calculations, limiting the practical applications. Besides, they may process high sensitivity to disturbances, leading to degraded control performance or even instability. Thus, more adaptive control methods should be investigated for better anti-vibration results.

c) Backstepping control

Backstepping control is an ideal nonlinear control technique that can decompose the system into a series of subsystems and then design controllers subsequently to achieve control goals over the whole system. Every subsystem can be addressed separately using a virtual controller which is only designed for the next step rather than physically implemented. The closed-loop stability can be guaranteed when each step is established accordingly by selecting appropriate Lyapunov functions. Backstepping control processes a particularly attractive feature in its capability to handle systems with strong nonlinear characteristics contrasting with linearization techniques [76]. Therefore, various backstepping control designs were presented for the vibration isolation of suspension systems to enhance ride comfort and maintain road holding ability. Combined with the projection adaptive technique, Pang *et al.* proposed a backstepping control for quarter-car AVSSs with input delay [77]. A backstepping control method was designed for half-car AVSSs to improve ride comfort while meeting different constraints on suspension deflections, tire loads, and actuator saturations [78]. In [79], an extension of the backstepping con-

trol was constructed for full-car AVSSs which integrated a remote cloud for computing. However, only simulation results rather than experiments were provided for theoretical demonstration. One should also note that the time derivatives of virtual controllers in most backstepping control designs above were obtained directly, which may result in the explosion of computation. For instance, a classical low-pass filter was utilized in the backstepping control for multiple AVSSs with practical experimental verification [80]. A second-order command filtering technique was developed in the backstepping control for the pneumatic AVSSs to eliminate the derivatives of virtual signals [81]. To broaden the applicability and enhance the suspension performance, more efforts are required in the backstepping control for AVSSs with critical issues.

2.4 Conclusions

The present chapter outlines the essential concepts of AVSSs, which will serve as a foundation for the control analysis in the subsequent chapters. The dynamic model of a quarter-car AVSS is derived based on the free body diagram method considering different actuator nonlinearities. Then typical road profiles are described including the bump road, sinusoidal road, and random road. Existing active suspension control designs are summarized and analyzed including linear and nonlinear control methods. To enhance the vibration reduction performance, several finite-time control designs are proposed for AVSSs with promising energy-saving characteristics in the following chapters. These control approaches are merged with practical engineering concerns including input saturations, dead zones, actuator faults, and so on. In general, this thesis provides the detailed design process for finite-time active suspension controllers and the corresponding suspension performance, which exhibits substantial potential for practical engineering applications.

3 Finite-Time Saturated Control for AVSSs

AVSSs are important for transportation vehicles to improve ride comfort and maneuverability. However, practical AVSSs normally suffer from uncertain dynamics, unknown external disturbances, input saturations, and dead zones. To address these issues, a novel model-free finite-time saturated control with naturally constrained inputs is proposed for AVSSs to mitigate vibrations and improve ride comfort. Specifically, the hyperbolic function and the bound-based adaptive method are constructed to avoid input saturations. The finite-time convergence can be achieved by designing the nonsingular terminal sliding mode filter. Moreover, the proposed control is a completely model-free approach that does not require any prior knowledge of the exact model information. Therefore, this chapter gives the *first* model-free finite-time saturated control solution for AVSSs that can simultaneously handle input saturations, achieve finite-time convergence, reject external disturbances and uncertain dynamics, maintain model-free structures, and overcome dead zones. The results provide a much improved version of the model-free AVSS control method in which the finite-time stability could be guaranteed with the naturally constrained control input. Various experiments demonstrate the effectiveness and robustness of the proposed algorithm with satisfactory anti-vibration performance and ride comfort (up to 96.5% and 94.8% improvement respectively compared to the passive suspension).

3.1 Introduction

Background. Vehicle suspension systems have received great attention due to their important contribution to the vehicle industry of improving ride comfort and road hold-

Nomenclature			
m_s, m_u	Sprung and unsprung masses	r_{d1}, r_{d2}	Damping coefficients
z_s, z_u, z_r	Displacements of the sprung, unsprung masses and road input profile	r_t, r_b	Stiffness and damping coefficients of the tire
$\dot{z}_s$, $\dot{z}_u$, $\dot{z}_r$	Velocities of the sprung, unsprung masses and road input profile	$N(u)$	Actuator input subject to dead zones
Y_s, Y_d	Spring and damper forces	u	Control signal
Y_t, Y_b	Elasticity and damping forces of tire	d	Unknown external disturbances
r_{s1}, r_{s2}	Stiffness coefficients of the spring	x_i	Coordinate transformations

ing [12, 39]. Compared with passive suspensions and semi-active suspensions, AVSSs can provide/dissipate energy using extra actuators to enhance the anti-vibration performance when facing various road profiles [10, 69, 82, 83]. Therefore, active suspension structures and various control methods have been widely investigated in recent years by both industrial and academic communities such as optimal control [84], sliding mode control [63], adaptive control [61], H_∞ control [1] and so on.

Research challenges and gaps. Our motivation for this chapter primarily stems from the need for a model-free finite-time saturated control for AVSSs with naturally constrained inputs. Traditional AVSS controllers normally avoided the input saturations by hard-limited constraints, leading to the non-smooth sharp-corner phenomenon. Extra compensation systems were required to compensate for the saturation effect. Moreover, various actuator nonlinearities, including input saturations and dead zones, may occur simultaneously. Importantly, achieving finite-time stability usually requires higher control efforts, making it a challenging topic to constrain control inputs within prior-known ranges at the same time. Furthermore, few research studies focused on the completely model-free control for AVSSs to deal with uncertain system parameters and external disturbances. In response to these challenges, we propose a model-free finite-time saturated control for AVSSs to address these unique problems. This research is significant as it provides a simple yet effective control scheme for AVSSs to achieve model-free characteristic and finite-time convergence with naturally constrained inputs.

Literature survey. In practical applications, input saturations and dead zones should be considered due to physical limitations of actuators [7]. Sharp corners exist in traditional hard-limited saturations when the control inputs encounter the upper and lower bounds [85, 86]. Besides, the auxiliary state systems always act as the saturation com-

pensator in the AVSSs [67]. However, the constraints are directly applied to input signals after they are generated, thus, an extra anti-saturation design needs to be integrated, leading to a complex controller system. Some studies focus on exploring smooth control inputs generated by prior-known boundary functions, such as the inverse tangent function arctan and the hyperbolic tangent function tanh, which are defined as naturally constrained input techniques in this chapter. For instance, a robust saturated control was designed for AVSSs using the arctan, where the beneficial nonlinearities and disturbances were integrated to reduce energy cost [87]. An adaptive neural backstepping control was proposed for an uncertain robot while the control input was asymmetrically bounded by the tanh functions [88]. Furthermore, the dead zone phenomenon should also be investigated. For example, a disturbance observer-based sliding mode control was designed for AVSSs with dead zones and hysteresis [8]. An adaptive control strategy was proposed for half-car AVSSs with unknown dead zones [68]. Therefore, it is essential to investigate anti-vibration performance for AVSSs with both input saturations and dead zones.

Based on the aforementioned results of saturated control for AVSSs, only asymptotic convergence can be achieved [9], thus the finite-time stability should be further investigated to improve the control performance. The systems with finite-time stability process better robustness and greater disturbance rejection while higher precision and faster convergence can be achieved simultaneously [89, 90]. For example, a bounded finite-time control was designed for Euler-Lagrange systems with actuator faults [91]. A multivariable finite-time saturated control was investigated for uncertain double integrator systems [92]. Furthermore, various studies suggest that the control system guarantees finite-time stability if it can be demonstrated homogeneous of negative degree with the asymptotic stability, which plays a critical role in finite-time algorithms [93]. However, the aforementioned control designs for AVSSs may not achieve acceptable finite-time performance utilizing naturally saturated inputs, necessitating further investigations.

One should also note that exact mathematical dynamic models of AVSSs are difficult to establish due to the uncertain system parameters (including the varying sprung

mass) and unknown external disturbances. Thus, model-free control research is one of the key solutions for uncertain AVSSs, which is still at an early stage. To achieve the model-free control, some intelligent learning methods were investigated to approximate the unknown dynamical effects including the neural networks and fuzzy logic inference [45, 94]. Generally, these intelligent learning algorithms may consume a large amount of computation resources, which is a heavy burden in practical applications. The adaptive method can be an appropriate alternative to address uncertain dynamics [75, 95]. A model-free proportional-derivative sliding mode control was designed for AVSSs using the system states and the sprung/unsprung masses [96]. However, the sprung mass may change with loading conditions including variable passenger masses and payloads which was always assumed to be a constant in previous model-free control designs. The authors in [77] proposed an adaptive backstepping control for AVSSs to achieve safety constraints where the variation of the sprung mass was approximated by the adaptive method. However, the uncertain suspension parameters were not considered which may vary with different environmental conditions. Therefore, more efforts should be devoted to the model-free control designs for uncertain AVSSs.

Scope and contributions of this study. Suspension performance has become the main focus in numerous existing control studies for AVSSs. However, there still exist some practical limitations, including input saturations, dead zones, slow convergence, external disturbances, and uncertain dynamics, which have not been investigated thoroughly. To comprehensively tackle these issues, this work extends our previous study [97] to propose a novel model-free finite-time saturated control with naturally constrained inputs for the AVSSs. Compared with existing controllers for AVSSs, the main contributions of this article are summarized as follows:

1) A novel model-free finite-time saturated control is *first* proposed for AVSSs to achieve finite-time convergence with naturally constrained inputs, overcome dead zones, and reject external disturbances and uncertain system dynamics. Different from existing asymptotic controllers [8, 9], an integral terminal sliding mode filter is newly designed for AVSSs based on the geometric homogeneity theorem

such that the nonsingular characteristic and finite-time stability can be guaranteed simultaneously (refer to Remark 3.3).

2) Unlike existing AVSS controllers [75, 96], a simple yet effective model-free approach was proposed for AVSSs without any exact model information of the suspension system, which indicates superior robustness against dead zones, uncertain system parameters, and unknown external disturbances. Especially, the prior knowledge of the sprung/unsprung masses is also not required, making it more realistic and practical in the presence of changing loading conditions (refer to Remark 3.4).

3) The input signal is naturally constrained within the prior-known range. Distinguished from [19, 85], no extra anti-saturation design is needed since no input saturation will occur in the control process. Specifically, the system feedback signals are skillfully incorporated into the saturation function tanh while the bound-based adaptive method is developed in the control design (refer to Remarks 3.5 and 3.6).

4) Compared with traditional sliding mode methods [65], the structure of the whole controller is continuous to alleviate unexpected chattering problems which are usually generated by high-frequency switched inputs. Thus, better transient performance can be ensured with the smooth control inputs (refer to Remark 3.7).

Organization of the chapter. The remaining parts of this article are presented as follows. The problem formulation of the uncertain AVSSs with dead zones is described in Section 3.2. After that, the main results of this chapter are given in Section 3.3 including the design of the proposed controller and the stability analysis. In Section 3.4, comparative experimental results are utilized to verify the advantages of the proposed method. Finally, Section 3.5 contains some conclusions.

3.2 Problem Formulation

3.2.1 System description

The quarter-car suspension system contains the masses, springs, dampers, and an actuator shown in Fig. 3.1 [2]. The dynamic model of the AVSS is given as [98]

$$\begin{aligned} m_s\ddot{z}_s &= -Y_s(z_s, z_u) - Y_d(\dot{z}_s, \dot{z}_u) + N(u) + d \\ m_u\ddot{z}_u &= Y_s(z_s, z_u) + Y_d(\dot{z}_s, \dot{z}_u) \\ &\quad - Y_t(z_u, z_r) - Y_b(\dot{z}_u, \dot{z}_r) - N(u) \end{aligned} \tag{3.1}$$

with

$$\begin{aligned} Y_s &= r_{s1}(z_s - z_u) + r_{s2}(z_s - z_u)^3 \\ Y_d &= \begin{cases} r_{d1}(\dot{z}_s - \dot{z}_u), & \dot{z}_s - \dot{z}_u > 0 \\ r_{d2}(\dot{z}_s - \dot{z}_u), & \dot{z}_s - \dot{z}_u \leq 0 \end{cases} \\ Y_t &= r_t(z_u - z_r) \\ Y_b &= r_b(\dot{z}_u - \dot{z}_r). \end{aligned} \tag{3.2}$$

Considering the suspension system subjected to dead zones, the actuator input $N(u)$ is written as follows:

$$N(u) = \begin{cases} m(u - b_r), & u > b_r \\ 0, & b_l \leq u \leq b_r \\ m(u - b_l), & u < b_l \end{cases} \tag{3.3}$$

where m is the unknown slope of the dead zone characteristic, $b_r > 0$ and $b_l < 0$ are the unknown bounds. To facilitate the controller design, one can denote $N(u) = u + u_\Delta$ where u_Δ is the unknown components of the dead zone satisfying $|u_\Delta| \leq \delta_u$ with an unknown constant $\delta_u > 0$.

The states of the AVSS are constructed as $x = \begin{bmatrix} x_1 & x_2 & x_3 & x_4 \end{bmatrix}$ with $x_1 = z_s, x_2 = \dot{z}_s$,

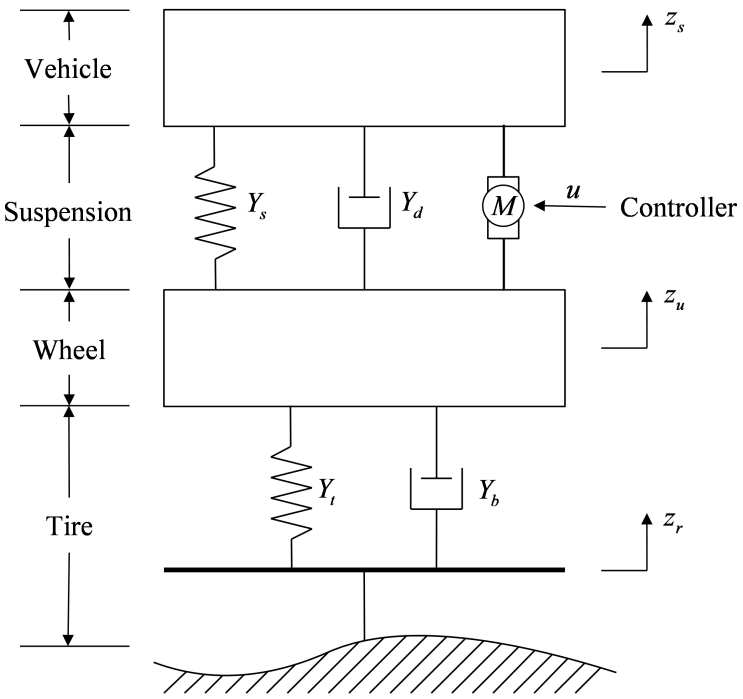

Fig. 3.1: Structure of the quarter-car AVSS

$x_3 = z_u$, $x_4 = \dot{z}_u$. Then the dynamic model of the AVSS can be written as

$$\begin{cases} \dot{x}_1 = x_2 \\ m_s \dot{x}_2 = u + \Delta \\ \dot{x}_3 = x_4 \\ m_u \dot{x}_4 = g(x) - u \end{cases} \tag{3.4}$$

where $\Delta = -Y_s - Y_d + u_\Delta + d$ is the lumped disturbance term, $g(x) = Y_s + Y_d - Y_t - Y_b - u_\Delta$.

It should be noted that the change of the passengers or the payloads may severely affect the value of the sprung mass m_s. Meanwhile, the coefficients of the stiffness and damping including r_{s1}, r_{s2}, r_{d1}, r_{d2}, r_t and r_b are hard to obtain the exact values. They may become inaccurate after a long time due to changing environmental conditions or human factors. Hence, it is worthwhile to design a model-free controller for the AVSS where the accurate values of the system are not required. That is also to say, that the whole system is uncertain with unknown model dynamics.

3.2.2 Problem formulation

Some assumptions, definitions, and lemmas are presented.

Assumption 3.1 ([96]). *The lumped disturbance term Δ and its first-time derivative $\dot{\Delta}$ are bounded by $|\Delta| \leq \delta_{\Delta 1}$, $|\dot{\Delta}| \leq \delta_{\Delta 2}$ with $\delta_{\Delta 1}$, $\delta_{\Delta 2} > 0$.*

Assumption 3.2 ([36]). *The road input profile z_r and $\dot{z}_r$ are bounded by $|z_r| \leq d_{r1}$ and $|\dot{z}_r| \leq d_{r2}$ with d_{r1} and $d_{r2} > 0$.*

One should note that the lumped disturbance term Δ includes unknown system dynamics, dead zone effects, and external disturbances, which represents all the uncertain dynamic characteristics of the AVSS control system. The assumption of the boundedness of Δ and $\dot{\Delta}$ is a common practice due to actual structure limitations and physical constraints [96]. Besides, the assumption of the road input z_r and $\dot{z}_r$ is always made for a more predictable system behavior while meeting safety requirements [36].

Definition 3.1 ([99]). *Consider a vector field $\omega(x) = \left[\omega_1(x), ..., \omega_n(x)\right]^T$. If there exists $r = \left[r_1, ..., r_n\right]^T$ with $r_i > 0$ $(i = 1, ..., n)$ such that $\omega_i(\varrho^{r_1} x_1, ..., \varrho^{r_n} x_n) = \varrho^{m+r_n}\omega_i(x)$ with $m \geq -\max\{\mathrm{r_i}\}$ for all $\varrho > 0$, then the vector field $\omega(x)$ is homogeneous of degree m with respect to r.*

Lemma 3.1 ([100]). *For a system $\dot{x} = \omega(x)$ with $\omega(0) = 0$, if the system is asymptotically stable and is homogeneous of degree $m < 0$, then the system is global finite-time stable.*

Lemma 3.2 ([101]). *For a system $\dot{x} = \omega(x)$ with $\omega(0) = 0$ and positive constants $0 < p < 1$, $\iota_1 > 0$, $0 < \iota_2 < \infty$, if there exists a positive definite Lyapunov function $V(x)$ satisfying $\dot{V}(x) \leq -\iota_1 V^p(x) + \iota_2$ and $V(0) = 0$, the whole system is practical semi-global finite-time stable and $V(x)$ satisfies $V^p(x) \leq \frac{\iota_2}{(1-\theta)\iota_1}$, $\forall t > T$, where $0 < \theta < 1$ is a constant, $T \leq [1/(\iota_1\theta(1-p))](V^{1-p}(0) - (\iota_2/(\iota_1(1-\theta)))^{(1-p)/p})$.*

Lemma 3.3 ([102]). *For a system $\dot{x} = \omega(x)$ with $\omega(0) = 0$, if there exists a Lyapunov function $V(x)$ with positive constants $0 < p < 1$, $c_1 > 0$ and $c_2 > 0$ satisfying $\dot{V}(x) \leq$*

$-c_1V^p(x) - c_2V(x)$, *then the origin of the system is finite-time stable with*

$$T \leq [c_2(1-p)]^{-1}\ln[1 + \mathrm{c}_1^{-1}\mathrm{c}_2\mathrm{V}^{1-\mathrm{p}}(0)]. \tag{3.5}$$

The main control objective is to design a model-free finite-time saturated control such that the vibration of the vehicle body can be effectively reduced or eliminated to improve the ride comfort, while the control input, the dynamic tyre load, and suspension space $z_p = z_s - z_u$ should stay within the permitted ranges expressed by $|u| < u_{\max}$, $|Y_t + Y_b| / ((m_s + m_u)g) \leq 1$, and $|z_p| \leq z_{\max}$, where $u_{\max} > 0$ is a known constant representing the maximum force provided by the actuator, g is the gravitational constant, $z_{\max}$ is the maximum suspension deflection.

3.3 Main Results

3.3.1 Model-free finite-time saturated control

The nonsingular terminal sliding mode filter σ is constructed with the integral term which is given as

$$\sigma = x_2 + \int_0^t \lambda_1[x_1]^\alpha + \lambda_2[x_2]^\beta d\tau \tag{3.6}$$

with $0 < \alpha < 1$, $\beta = 2\alpha/(1+\alpha)$, k_1, λ_1, $\lambda_2 > 0$, $[x]^* = |x|^* \,\mathrm{sgn(x)}$.

The reference velocity signal is constructed as

$$v_r = -\int_0^t \lambda_1[x_1]^\alpha + \lambda_2[x_2]^\beta d\tau - k_1\varkappa. \tag{3.7}$$

And $\varkappa$ is an auxiliary state variable denoted by

$$\dot{\varkappa} = k_2\sigma + \mathrm{sgn}(\sigma), \varkappa(0) = 0. \tag{3.8}$$

Then we define a new state variable

$$\xi = x_2 - v_r. \tag{3.9}$$

According to (3.6)-(3.8), (3.9) can be written as

$$\xi = x_2 + \int_0^t \lambda_1 [x_1]^\alpha + \lambda_2 [x_2]^\beta d\tau + k_1 \varkappa = \sigma + k_1 \varkappa. \tag{3.10}$$

The proposed model-free finite-time saturated control is

$$u = -k_3 \tanh(\xi/\gamma_1) + \phi \tag{3.11}$$

where ϕ is the adaptive parameter used to improve system robustness given as

$$\dot{\phi} = -k_4 \tanh(\xi/\gamma_2) - k_5 \phi, \quad \phi(0) \leq k_4/k_5 \tag{3.12}$$

and k_3, k_4 and k_5 are positive design parameters, γ_1, $\gamma_2 > 0$ are sharpness gains.

Remark 3.1. The proposed model-free finite-time saturated control (3.11) offers a simpler structure compared with the majority of existing model-free control for AVSSs using fuzzy logic systems or neural networks [45, 94].

Remark 3.2. Different from traditional finite-time control designs with the symbolic function sgn, the hyperbolic tangent function tanh is utilized to reduce the chattering issues. To change the rate of the control input when ξ converges to the neighborhood near zero, positive sharpness gains γ_1 and γ_2 are introduced in the denominator of the hyperbolic tangent functions. The control signal varies gentler with the signal ξ when a larger value of γ_1 is selected to suppress the chattering phenomenon [103]. However, a larger k_3 is needed for better anti-vibration performance leading to a higher saturation bandwidth. Therefore, the balance between the chattering avoidance and the saturation bandwidth should be properly considered.

Theorem 3.1. *Consider the uncertain AVSS (3.1) with the external disturbances and the*

dead zones (3.3). If the control gains satisfy $k_1 > \delta_{\xi 2}$, $k_3 > \delta_\psi$, the proposed model-free finite-time saturated control (3.11) can guarantee:

1) all the signals in the closed-loop system are bounded,

2) the sprung displacement z_s can converge in a finite time,

3) the input is naturally constrained by the prior-known range $|u| < k_3 + k_4/k_5$.

3.3.2 Stability analysis

Proof: Considering (3.4) and substituting the control design (3.11), the time derivative of (3.9) yields

$$m_s\dot{\xi} = m_s\dot{x}_2 - m_s\dot{v}_r = -k_3 \tanh(\xi/\gamma_1) + \phi + \Delta + \varsigma \tag{3.13}$$

with $\varsigma = -m_s\dot{v}_r$. The boundedness of the variable ϕ should be demonstrated first. Note that the term ϕ is generated by (3.12) satisfying

$$\dot{\phi} = -k_4 \tanh(\xi/\gamma_2) - k_5\phi < k_4 - k_5\phi. \tag{3.14}$$

Solving the inequality leads to that ϕ is bounded by $\phi < \delta_\phi = (k_4/k_5) + (\phi(0) - (k_4/k_5))e^{-k_4 t}$.

To guarantee the boundedness of ξ, we define $V_1 = \frac{1}{2}m_s\xi^2$. Considering the inequality $0 \leq |\xi| - \xi\tanh(\xi/\gamma_1) \leq 0.2785\gamma_1$ for $\forall\xi \in \Re$ and $\gamma_1 > 0$ [5]. It is possible to compute $|\varsigma| \leq \delta_\varsigma$ and $|\Delta| \leq \delta_{\Delta 1}$ by Assumptions 3.1 and 3.2 [89]. The time derivative of V_1 is

$$\dot{V}_1 = -\xi m_s\dot{\xi} \leq -\iota_1|\xi| + 0.2785\gamma_1 \leq -\iota_1 V_1^{1/2} + \iota_2 \tag{3.15}$$

where $\iota_1 = k_3 - \delta_\phi - \delta_\Delta - \delta_\varsigma$, $\iota_2 = 0.2785\gamma_1$. Thus, it is always required to tune the control gain k_3 large enough to ensure $\iota_1 > 0$. Then from Lemma 3.2, we can conclude that ξ is bounded all the time with the upper bound $|\xi| \leq \delta_{\xi 1} = \sqrt{2/m_s}(\iota_2/((1-\theta)\iota_1))$. According to (3.13), $\dot{\xi}$ is also bounded by $|\dot{\xi}| \leq \delta_{\xi 2} = (k_3 + \delta_\psi)/m_s$.

A Lyapunov function is constructed as $V_2 = (1/2)\varkappa^2$. Noting (3.10), the time derivative of $\varkappa$ can be computed as

$$\dot{\varkappa} = k_2\sigma + \mathrm{sgn}(\sigma) = \mathrm{k_2}\xi - \mathrm{k_1}\mathrm{k_2}\varkappa + \mathrm{sgn}(\sigma). \tag{3.16}$$

The time derivative of V_2 further leads to

$$\begin{aligned} \dot{V}_2 &\leq -k_1k_2\varkappa^2/2 - (k_1k_2|\varkappa|/2 - k_2\delta_{\xi 1} - 1)|\varkappa| \\ &\leq -(1/2)k_1k_2\varkappa^2 \leq 0, \quad \forall|\varkappa| \leq \varepsilon_\varkappa \end{aligned} \tag{3.17}$$

where $\varepsilon_\varkappa = 2(k_2\delta_{\xi 1} + 1)/(k_1k_2)$ is the ultimate bound of $\varkappa$ [89], then $\dot{\varkappa}$ is also bounded according to (3.16). From (3.10), σ is bounded by $|\sigma| \leq \delta_{\sigma 1}$ with $\delta_{\sigma_1} > 0$.

Next, we need to present that z_s can converge to zero in finite time. For the sliding mode filter σ, we can obtain

$$\dot{\sigma} = -k_1\dot{\varkappa} + \dot{\xi} = -k_1k_2\sigma - k_1\mathrm{sgn}(\sigma) + \xi. \tag{3.18}$$

Considering the Lyapunov function $V_3 = \frac{1}{2}\sigma^2$, we have

$$\dot{V}_3 \leq -(k_1 - \delta_{\xi 2})|\sigma| - k_1k_2\sigma^2 \leq -c_1V_3^{1/2} - c_2V_3 \tag{3.19}$$

with $c_1 = \sqrt{2}(k_1 - \delta_{\xi 2})$, $c_2 = 2k_1k_2$. According to Lemma 3.3, if k_1 is chosen to satisfy $k_1 > \delta_{\xi 2}$, then σ will converge to zero in $T_a \leq (2/c_2)\mathrm{ln}[1 + \mathrm{c_1^{-1}c_2V_3^{1/2}}(0)]$.

After the finite time T_a, there exists $\sigma = \dot{\sigma} = 0$. For the states x_1, x_2, one can design

$$V_4 = \tfrac{\lambda_1}{\alpha+1}|x_1|^{\alpha+1} + \tfrac{1}{2}x_2^2. \tag{3.20}$$

According to (3.6), the system states can be given as

$$\begin{aligned} \dot{x}_1 &= x_2 \\ \dot{x}_2 &= -\lambda_1[x_1]^\alpha - \lambda_2[x_2]^\beta. \end{aligned} \tag{3.21}$$

The time derivative of V_4 is obtained as

$$\begin{aligned}\dot{V}_4 &\leq \lambda_1|x_1|^{\alpha}x_2 + x_2(-\lambda_1[x_1]^{\alpha} - \lambda_2[x_2]^{\beta}) \\ &\leq -\lambda_2|x_2|^{\beta+1} \leq 0.\end{aligned} \tag{3.22}$$

Therefore, the system states x_1 and x_2 are bounded and asymptotically stable.

According to Definition 3.1, it is easy to verify that the system states (3.21) is homogeneous of degree $m = (\alpha - 1)/2$ with respective of $r = [1, (\alpha + 1)/2]^T$ while it is asymptotically stable obtained from (3.22). From Lemma 3.1, we can conclude that the system (3.21) is global finite-time stable with a finite time T_b.

Combining the above analysis, the state x_1 will converge to zero in a finite time T bounded by $T \leq T_a + T_b$. Hence, one can conclude that z_s can converge to zero in a finite time T.

Since $\dot{V}_4 \leq 0$, it is easy to obtain that $V_4(x) \leq V_4(0)$, where $V_4(0)$ is a bounded positive constant. One can denote $|x_1| \leq \sqrt[\alpha+1]{(\alpha+1)V_4(0)/\lambda_1}$, $|x_2| \leq \sqrt{2V_4(0)}$. Hence, x_1 and x_2 are bounded by the initial conditions.

Furthermore, from the control design (3.11), the first term of the control signal is bounded by $|k_3 \tanh(\xi/\gamma_1)| < k_3$ due to $|\tanh(*)| < 1$. Since $\phi(0) < k_4/k_5$ and according to (3.14), the term ϕ can be bounded by $|\phi| < k_4/k_5$. Therefore, the control signal u is always bounded by $|u| < k_3 + k_4/k_5$.

Therefore, the proposed controller can simultaneously stay within the permitted range without any extra anti-saturation design.

3.3.3 Zero dynamics and performance analysis

The proposed controller (3.11) is only constructed to stabilize the second-order sprung system, hence, the stability of the remained second-order unsprung system (also named as zero dynamics) should be analyzed. To obtain zero dynamics, the output signal x_1 is set as $x_1 \equiv 0$.

From (3.4), the zero dynamics can be written as [69]

$$\dot{\zeta} = P\zeta + Q \tag{3.23}$$

where $\zeta = [x_3, x_4]^T$, and

$$P = \begin{bmatrix} 0 & 1 \\ -\frac{r_t}{m_u} & -\frac{r_b}{m_u} \end{bmatrix}, Q = \begin{bmatrix} 0 \\ \frac{r_t}{m_u} z_r + \frac{r_b}{m_u} \dot{z}_r + \frac{d}{m_u} \end{bmatrix}.$$

According to Assumptions 3.1 and 3.2, the term Q is bounded.

Construct a Lyapunov function $V_\zeta = \zeta^T \zeta$ for the zero dynamics (3.23). The time derivative of V_ζ is derived as

$$\dot{V}_\zeta = \dot{\zeta}^T \zeta + \zeta^T \dot{\zeta} = \zeta^T (P^T + P)\zeta + 2\zeta^T Q. \tag{3.24}$$

Since the eigenvalues of the matrix P are negative real constants, there always exists $P^T + P < 0$. Using Young's inequality, the last term of (3.24) can be transformed as $2\zeta^T Q \leq \frac{1}{\epsilon}\zeta^T \zeta + \epsilon Q^T Q$ where ϵ is a positive constant.

Since Q is bounded, there always exists a constant $\pi_2 > 0$ such that $\epsilon Q^T Q \leq \pi_2$. Then $\dot{V}_\zeta$ can be rewritten as

$$\begin{aligned} \dot{V}_\zeta &\leq -(\lambda_{min}(P^T + P) - \frac{1}{\epsilon})\zeta^T \zeta + \pi_2 \\ &\leq -\pi_1 V + \pi_2. \end{aligned} \tag{3.25}$$

Solving the inequality (3.25) gives

$$\begin{aligned} V_\zeta(t) &\leq V_\zeta(0) e^{-\pi_1 t} + \frac{\pi_2}{\pi_1}(1 - e^{-\pi_1 t}) \\ &\leq \max\{\mathrm{V}_\zeta(0), \frac{\pi_2}{\pi_1}\} = \varpi \end{aligned} \tag{3.26}$$

which leads to $|x_i| \leq \sqrt{\varpi}$ for $i = 3, 4$. Therefore, the unsprung states x_3 and x_4 are bounded. From the above analysis, all signals are verified to be bounded. Furthermore,

performance constraints can be adjusted by

$$\begin{aligned} |z_p| = |z_s - z_u| &\leq \sqrt[\alpha+1]{(\alpha+1)V_4(0)/\lambda_1} + \sqrt{\varpi}, \\ \frac{|Y_t + Y_b|}{(m_s + m_u)g} &\leq \frac{r_t(\sqrt{\varpi} + d_{r1}) + r_b(\sqrt{\varpi} + d_{r2})}{(m_s + m_u)g}. \end{aligned} \tag{3.27}$$

Therefore, if the initial conditions and parameters are carefully selected, then the constraints on the suspension space $|z_p| \leq z_{\max}$ and dynamic tyre load $|Y_t + Y_b|/((m_s + m_u)g) \leq 1$ can be guaranteed all the time.

Remark 3.3. In the existing saturated control methods for AVSSs [8, 9], only asymptotic stability is investigated for the saturated controller design with constrained inputs. In this chapter, a novel model-free finite-time saturated controller is proposed for uncertain AVSSs *for the first time* where the integral nonsingular terminal sliding mode method (3.6) is utilized to achieve finite-time stability using the geometric homogeneity theorem. This control design can greatly improve the convergence rate and transient performance during the anti-vibration process.

Remark 3.4. In the controller design process, only the vertical displacement and velocity of the sprung mass (z_s and $\dot{z}_s$) are utilized, which can be obtained by encoders and filters, respectively [104, 105]. The whole control is model-free such that no prior information of the dynamical model is needed. Specially, compared with the existing model-free controllers [75, 96], the proposed method provides much better robustness in the presence of passenger/payload variations since no nominal sprung mass m_s or unsprung mass m_u are required in the design.

Remark 3.5. Compared with [89], a novel bound-based adaptive method (3.12) is proposed with the prior-known range, thus the robustness and anti-disturbance ability of the closed-loop system can be enhanced. More importantly, the bounded-input characteristics of the adaptive control signal can be maintained simultaneously.

Remark 3.6. Combined with the bounded function tanh and the bound-based adaptive method, this controller design should be important in the AVSS control field to achieve the finite-time stability with the naturally constrained inputs. During the tuning process,

the control gain k_3 can be initially set to a large value and gradually decrease if necessary, k_4 and k_5 can be tuned accordingly to meet the actuator requirement $k_3 + k_4/k_5 < u_{\max}$. Furthermore, the selection of larger k_4 and smaller k_5 can increase the robustness of the control system.

Remark 3.7. The designed controller (3.11) contains no discontinuous terms, whose nominal part is constrained by the tanh function, and the adaptive variable part is used for improving system robustness. Thus, the unexpected chattering issues in traditional controllers [87] can be alleviated. The designed controller (3.11) contains no discontinuous terms, whose nominal part is constrained by the tanh function, and the adaptive variable part is used for improving system robustness. Thus, the unexpected chattering issues in traditional controllers [65] can be alleviated.

3.4 Experimental Verification

Comparative experiments are conducted on the quarter-car active suspension platform (Fig. 3.2) to demonstrate the effectiveness of the proposed control method in both robustness and anti-vibration performance. The parameters of the experimental suspension platform are presented in Table 3.1.

The experimental platform mainly includes three different plates. The first one on the top acts as the vehicle body which is supported by the suspension damper and spring. The payload mass is placed on the vehicle body plate indicating the unknown passengers/loads. A DC motor is utilized as the main component of the system to provide extra energy for improving anti-vibration performance and ride comfort. The tire spring and damping system provides the connection between the middle and bottom plates. And the bottom plate servo motor can generate the road profile which is transmitted to the bottom plate by the lead screw.

The following suspension systems are investigated to investigate the effectiveness of the proposed control algorithm:

1) Passive: Passive suspension system with no control input;

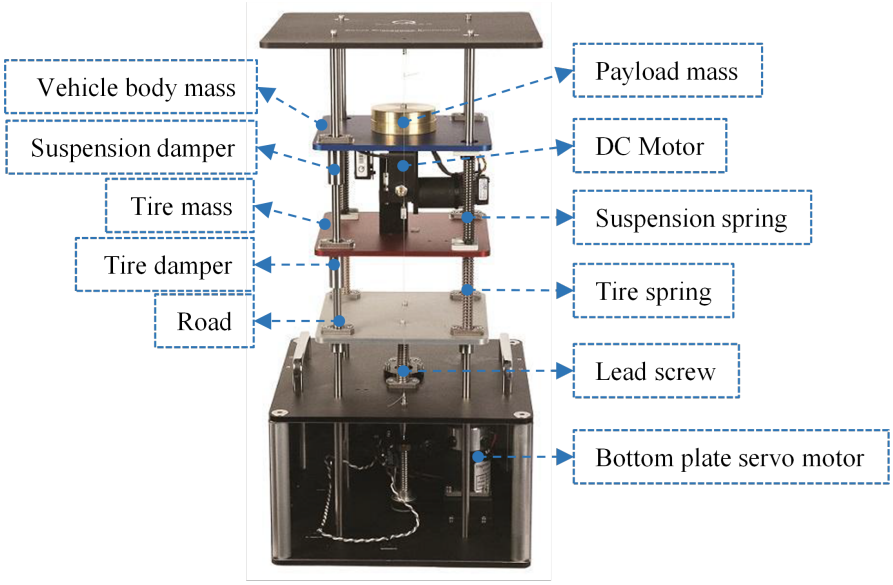

Fig. 3.2: Experimental platform of the quarter-car AVSS

Table 3.1: Parameters of the Active Suspension Setup

Symbols	Values	Symbols	Values
m_s	2.45kg	m_u	1kg
r_{s1}	900N/m	r_{s2}	10N/m^3
r_{d1}	8Ns/m	r_{d2}	7Ns/m
r_t	1250N/m	r_b	5Ns/m

2) BNRS: Beneficial nonlinearity robust saturated control, which is a model-free control with the sprung mass [87];

3) ROFB: Robust output feedback backstepping method [98];

4) Proposed: Proposed model-free finite-time control.

The sinusoidal and random road inputs are considered to further evaluate the control performance.

Case 1: A sinusoidal road is generated by a continuous sinusoidal function with frequency 3Hz and amplitude 0.5cm, namely, $z_r = 0.005 \sin 6\pi t$.

Case 2: The B-class random road profile is constructed using the filtered white noise signal [45].

The term d is selected as $d = 0.2 \sin 4\pi t$ and the system parameters fluctuate 10%.

Table 3.2: Control Gains of Comparative Suspensions

Controller	Control gains
BNRS control	$\lambda = 10$, $k_p = 50$, $k_d = 50$, $k_s = 10$, $L = 100$
ROFB control	$k_1 = 30$, $k_2 = 20$, $\lambda_0 = 3$, $\lambda_1 = 2$, $\lambda_2 = 1$, $\lambda_3 = 3$, $\lambda_4 = 1$, $L_1 = 150$, $L_2 = 20$, $\eta_1 = 5$, $\eta_2 = 5$
Proposed control	$k_1 = k_2 = 10$, $k_3 = 30$, $k_4 = 6$, $k_5 = 2$, $\lambda_1 = 10$, $\lambda_2 = 1$, $\alpha = 0.9$, $\gamma_1 = \gamma_2 = 0.1$

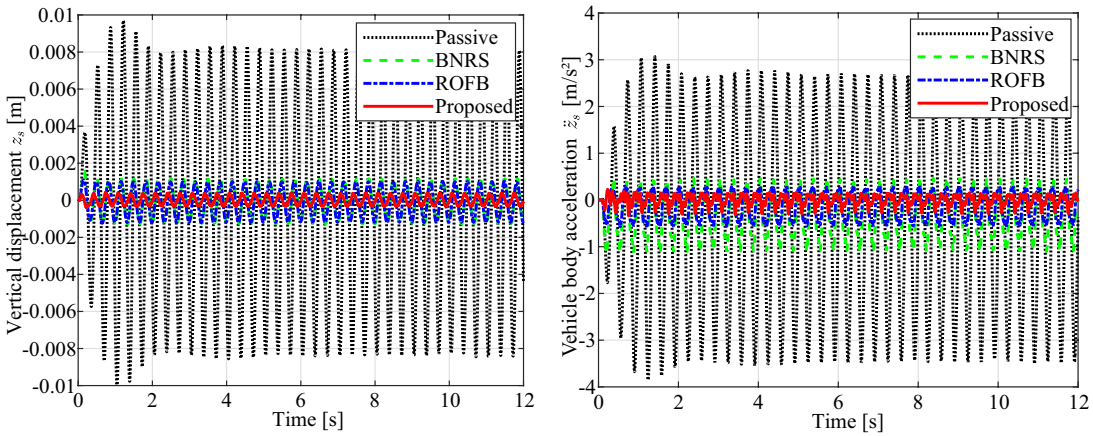

(a) (b)

Fig. 3.3: Case 1: (a) Vertical displacement z_s (b) body acceleration $\ddot{z}_s$ in the time domain.

Besides, the unknown dead zone parameters are selected as $m = 0.9$, $b_r = 1$ and $b_l = -1$. Control gains of comparative suspensions are given in Table 3.2.

It can be noticed that Figs. 3.3a and 3.7a present the vertical displacement comparison results of four suspension systems under sinusoidal and random road inputs, respectively. Besides, the maximum and the root-mean-square (RMS) values of vertical displacement and body acceleration under two cases are given in Table 3.3. According to Figs. 3.3a and 3.7a, compared with the passive one, three active controllers can obtain smaller amplitudes of the vertical displacement, indicating the effectiveness of the anti-vibration performance. The finite-time convergence of the proposed control design also ensures rapid vibration suppression. From Table 3.3, the BNRS strategy can achieve satisfactory anti-vibration control performance with 83.5%, 82.8% reduction in Case 1 and 57.9%, 54.5% reduction in Case 2 compared with the passive suspension. However, those of the proposed control are much smaller with 95.9%, 96.5% in Case 1,

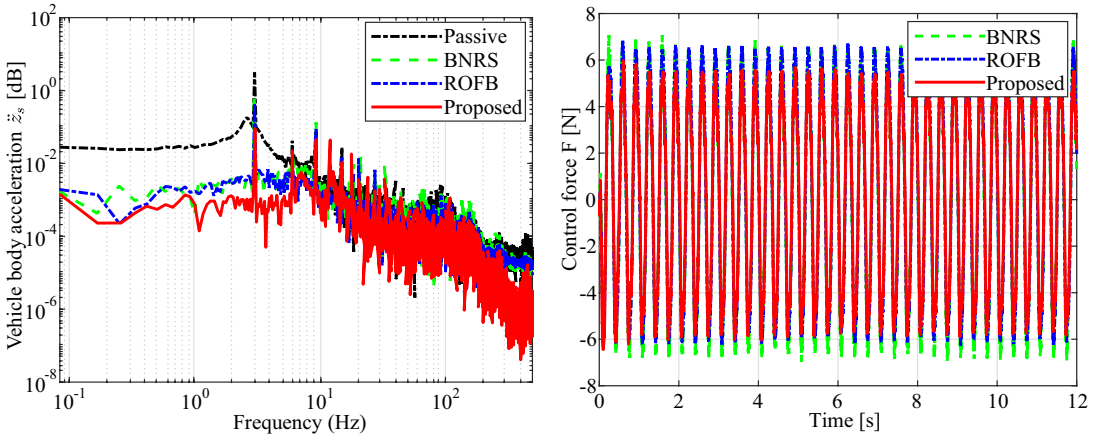

(a) (b)

Fig. 3.4: Case 1: (a) Body acceleration $\ddot{z}_s$ in the frequency domain (b) control force F.

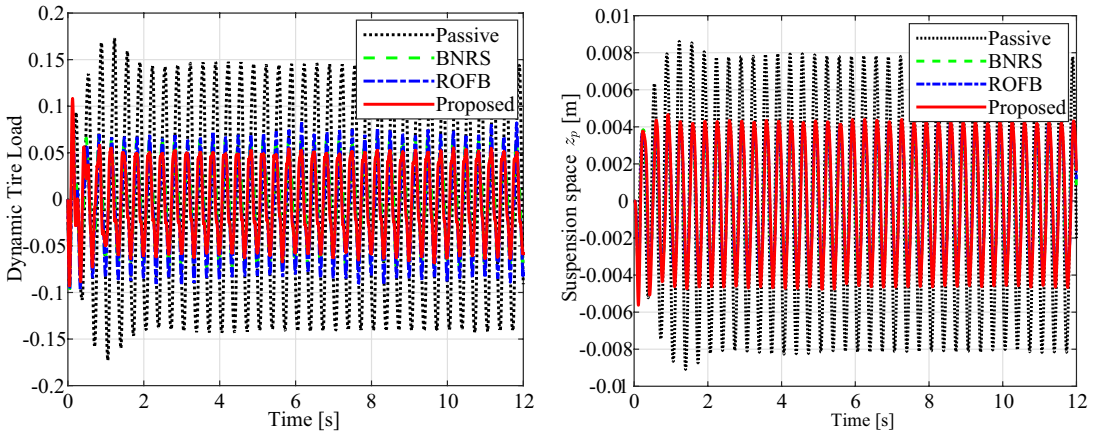

(a) (b)

Fig. 3.5: Case 1: (a) Dynamic tyre load (b) suspension space z_p.

and 94.7%, 95.3% in Case 2, respectively.

The curves in Figs. 3.3b and 3.7b record the body acceleration responses in the time domain of four suspension systems under sinusoidal and random road cases, where the corresponding frequency domain acceleration results are provided in Figs. 3.4a and 3.8a. Note that ride comfort is highly related to body acceleration [106]. From Figs. 3.3b and 3.7b, the amplitudes of the body acceleration of the proposed method are smaller, showing the better ride comfort in the presence of different rough roads. According to the International Organization of Standardization, 4–12.5 Hz oscillations exhibit a higher impact on humans [107]. From Figs. 3.4a and 3.8a, the frequency-domain body acceleration of the proposed control within the frequency spectrum is smaller than those of comparative suspensions. Quantitatively speaking, in Table 3.3, the maximum and RMS

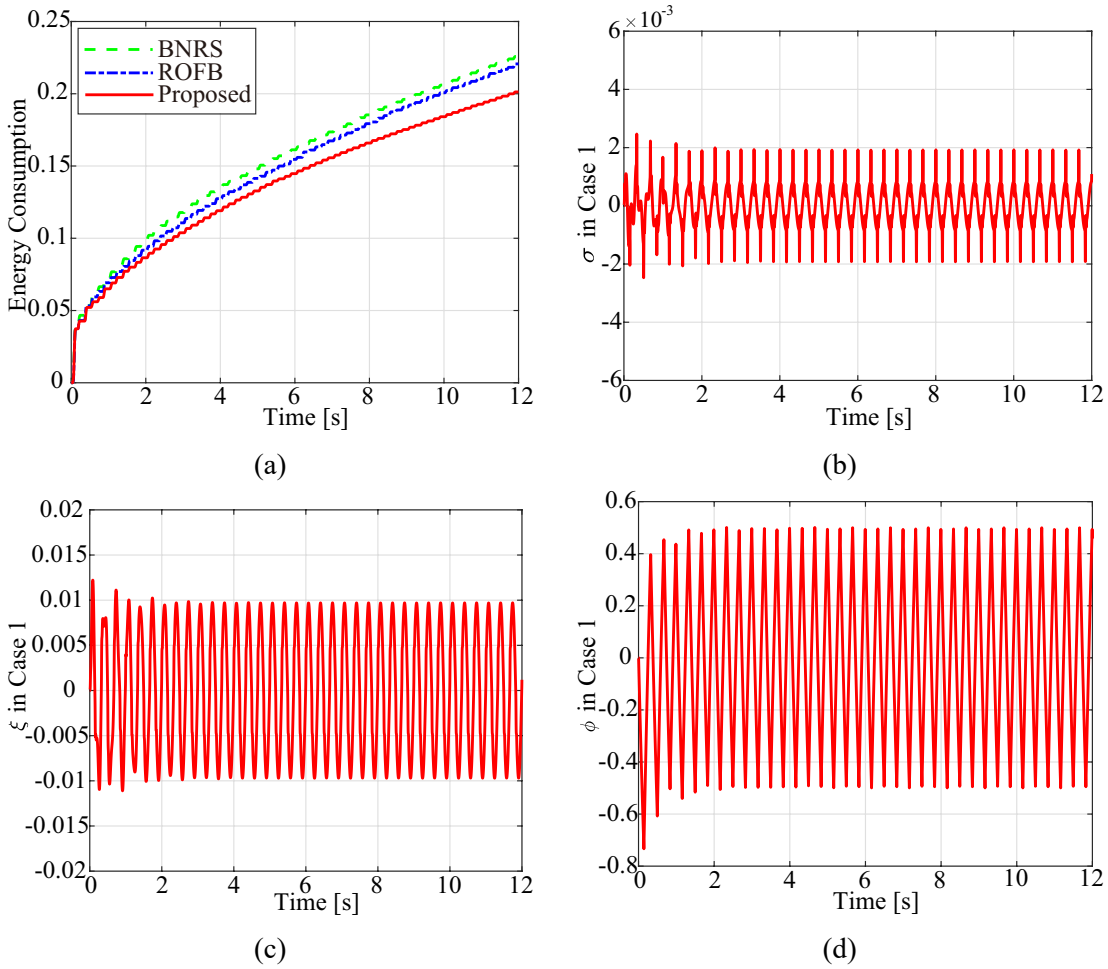

Fig. 3.6: Case 1: (a) Energy consumption (b) variable σ (c) variable ξ (d) variable ϕ.

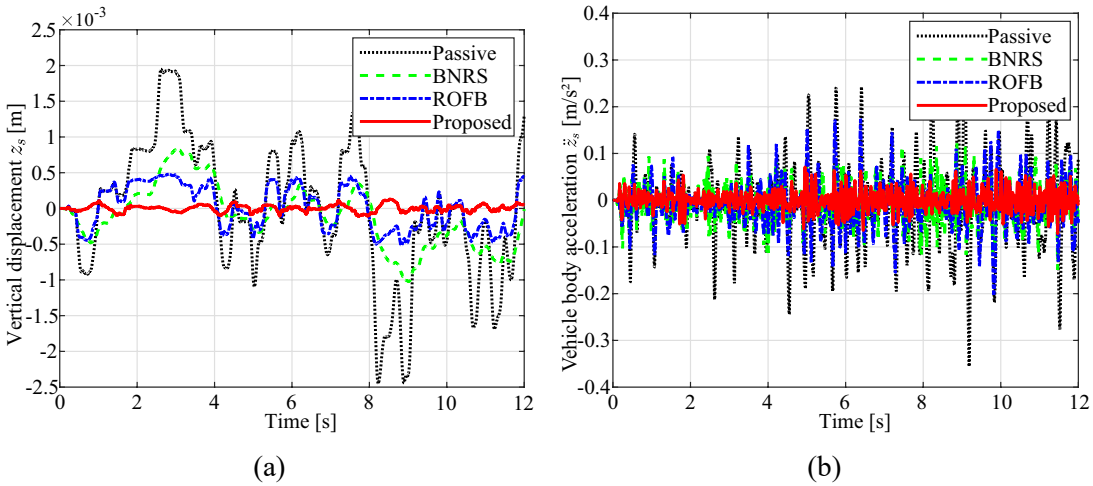

Fig. 3.7: Case 2: (a) Vertical displacement z_s (b) body acceleration $\ddot{z}_s$ in the time domain.

values for the body acceleration of the proposed control are reduced by 92.7%, 94.8% in Case 1, and 77.5%, 76.4% in Case 2, respectively, which demonstrates the ride comfort

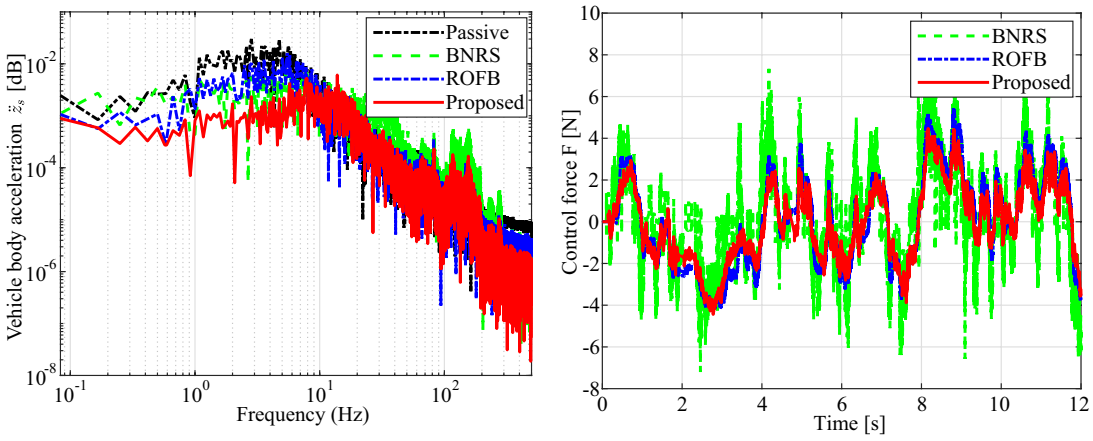

(a) (b)

Fig. 3.8: Case 2: (a) Body acceleration $\ddot{z}_s$ in the frequency domain (b) control force F.

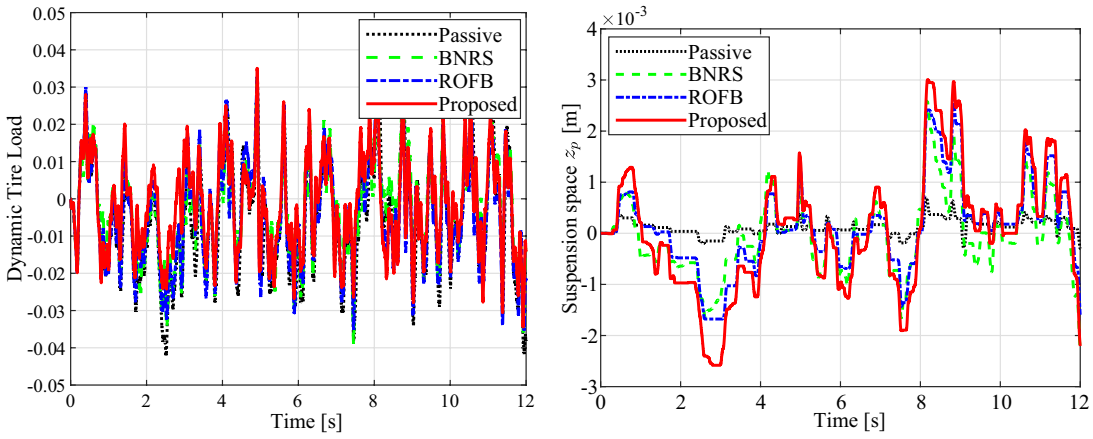

(a) (b)

Fig. 3.9: Case 2: (a) Dynamic tyre load (b) suspension space z_p.

performance of the proposed control method.

Besides, the control force results shown in Figs. 3.4b and 3.8b suggest that the proposed control can achieve better anti-vibration results and ride comfort performance with relatively lower control force inputs, which indicates the lower energy consumption. Specially, the control force of the BNRS control may suffer from severe chattering problems due to the switching logic in the controller design. The proposed control utilizes the hyperbolic tangent functions to mitigate the chattering issues and avoid the saturations simultaneously.

Furthermore, the physical limitations of the tire deflection and suspension space should be obeyed all the time. As can be depicted in Figs. 3.5a and 3.9a, four suspension systems behave with satisfactory performance in the dynamic tyre load, which present

Table 3.3: Control Performance Under Different Cases

Cases	Types	Vertical Displacement				Body Acceleration			
		MAX(m&%)		RMS(m&%)		MAX(m/s^2&%)		RMS(m/s^2&%)	
C1	Passive	0.0097	100.0%	0.0064	100.0%	3.0746	100.0%	2.3428	100.0%
	BNRS	0.0016	↓ 83.5%	0.0011	↓ 82.8%	0.4837	↓ 84.3%	0.6482	↓ 72.3%
	ROFB	0.0011	↓ 88.7%	0.0009	↓ 85.9%	0.3014	↓ 90.1%	0.3635	↓ 84.5%
	Proposed	0.0004	↓ 95.9%	0.0002	↓ 96.5%	0.2252	↓ 92.7%	0.1213	↓ 94.8%
C2	Passive	0.0019	100.0%	0.0011	100.0%	0.3158	100.0%	0.0957	100.0%
	BNRS	0.0008	↓ 57.9%	0.0005	↓ 54.5%	0.1221	↓ 61.3%	0.0401	↓ 58.1%
	ROFB	0.005	↓ 73.7%	0.0003	↓ 72.7%	0.1736	↓ 45.0%	0.0543	↓ 43.3%
	Proposed	0.0001	↓ 94.7%	0.00005	↓ 95.3%	0.0709	↓ 77.5%	0.0226	↓ 76.4%

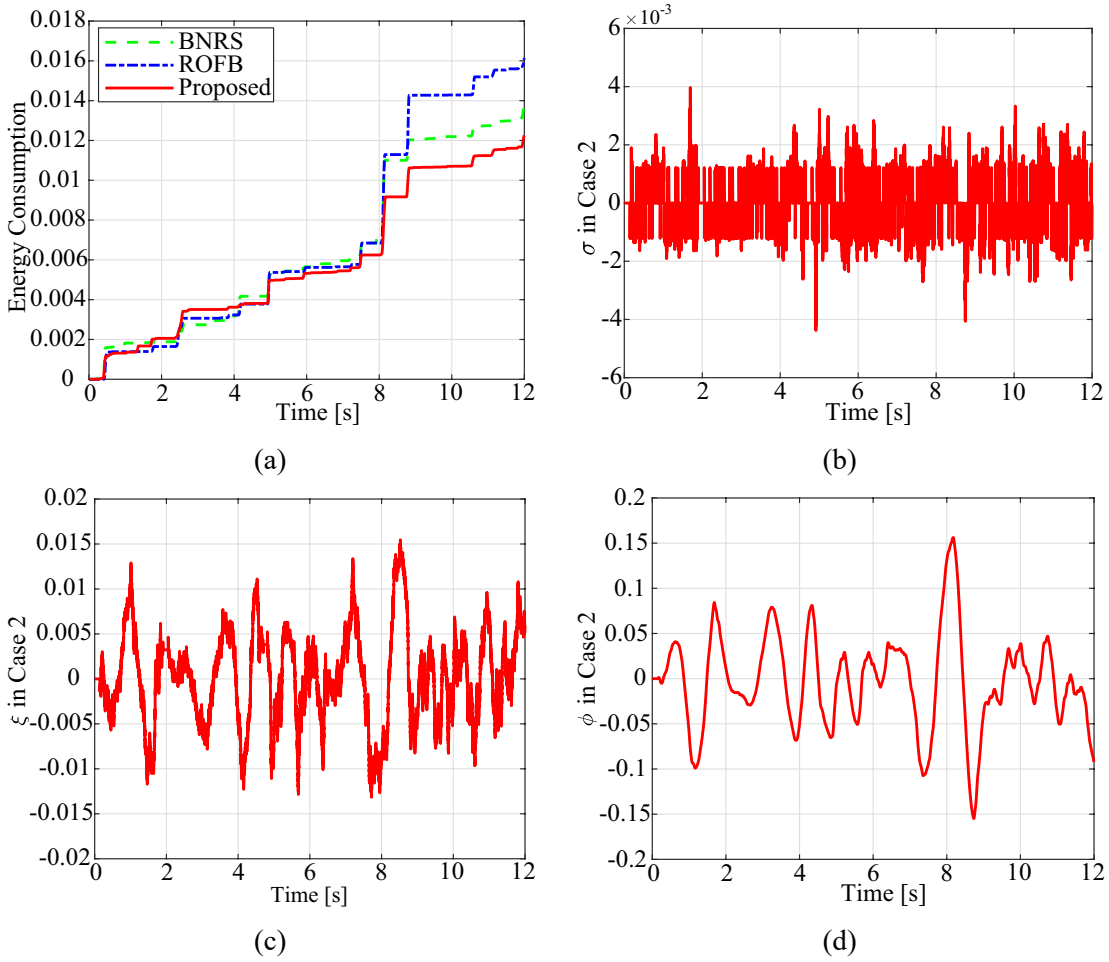

Fig. 3.10: Case 2: (a) Energy consumption (b) variable σ (c) variable ξ (d) variable ϕ.

the road holding ability. According to [96], the allowable suspension space is 3.8cm for the quarter-car AVSS. The suspension space displacements presented in Figs. 3.5b and 3.9b are all kept in the permitted set. Thus, the safety requirements during the whole process can be guaranteed for drivers and occupants. Furthermore, the energy consumption index E is evaluated by $E(R^*) = \sqrt{\frac{1}{T}\int_0^T (R^*(\tau))^2 d\tau}$ with $R^* = u(t)\dot{z}_p$ for $u(t)\dot{z}_p > 0$

and $R^* = 0$ for else, and T is the total experimental time [37, 87]. The energy consumption indexes under different cases are provided in Figs. 3.6a and 3.10a, which show the relatively lower energy cost of the proposed control compared with BNRS and ROFB control design. The figures of the sliding mode variable σ are given in Figs. 3.6b and 3.10b which can converge in finite time. Figs. 3.6c and 3.10c show the state variable ξ and the behaviors of the adaptive parameter ϕ are provided in Figs. 3.6d and 3.10d. Therefore, all internal virtual signals can remain bounded all the time.

3.5 Conclusions

In this chapter, a novel model-free finite-time saturated control is proposed to enhance the anti-vibration performance and ride comfort for the AVSSs under unknown dynamics, external disturbances, and dead zones. By incorporating the hyperbolic tangent function and the bound-based adaptive variable, the input constraint can be prior-known and adjusted by control gains, eliminating the need for additional saturation compensation designs. Furthermore, a nonsingular terminal sliding mode filter is designed for AVSSs to guarantee globally finite-time convergence. Notably, no discontinuous terms exist to alleviate unexpected chattering. Moreover, the proposed control strategy solely relies on the displacement and velocity of the sprung mass without any model information. Therefore, this controller design provides a simple yet effective version of the model-free AVSS control in which the finite-time stability could be guaranteed with naturally constrained inputs. The superior anti-vibration performance and ride comfort of the proposed control are further verified by the experimental studies.

4 Fixed-Time Safe-by-Design Control for AVSSs

This chapter presents a novel fixed-time safe-by-design control for uncertain active vehicle suspension systems with matched/unmatched disturbances, high energy consumption, input saturations, and asymmetric time-varying constraints on both displacement/velocity. Several asymmetric time-varying barrier Lyapunov functions are carefully constructed to deal with displacement/velocity constraints under the fixed-time convergence framework. Furthermore, a new fixed-time auxiliary state system is proposed to compensate for the saturation effect. It is then rigorously demonstrated that the convergence time is independent of initial state conditions and both the displacement/velocity are always restricted within the asymmetric time-varying ranges. Importantly, by employing beneficial nonlinearities of a bioinspired X-shaped reference model, the burden of high control energy cost can be relaxed compared with traditional controllers. As far as we know, this should be the first attempt to achieve a fixed-time safe-by-design control for active vehicle suspension systems which simultaneously considers practical issues including meeting the safety requirements for input saturations and displacement/velocity, achieving fixed-time convergence, maintaining energy efficiency, and rejecting matched/unmatched disturbances. Experimental testing results validate the effectiveness, advantage, and feasibility of the proposed control algorithm, compared to other existing methods.

4.1 Introduction

Vehicle suspension systems have been investigated extensively in the vehicle industry due to their significantly superior characteristics in improving ride comfort and road

handling ability [39]. There exist three kinds of vehicle suspensions including passive vehicle suspensions, semi-active vehicle suspensions, and AVSSs [108]. Unlike passive and semi-active ones, AVSSs with extra actuators can adjust the attitude of vehicles, thus eliminating the shocks from rough roads, and improving ride comfort and maneuverability [109]. Therefore, various control designs have been developed for AVSSs in the past decades, such as backstepping control [77], adaptive control [61], H_∞ control [110], and sliding mode control [65]. However, safety should be one of the key factors in the control design with various practical constraints. The control for AVSSs should satisfy the safety requirements both for mechanical devices and humans. Accordingly, constraints on displacement, velocity, and input saturations should be respected all the time, then the whole system can be considered *safe* [111].

In actual applications, the displacement constraints always exist which are inherited from physical limitations or performance requirements. To handle these constraint problems, the barrier Lyapunov function (BLF)-based constraint controllers are extensively investigated and applied to different systems [112]. To mention a few, a log-type BLF is designed for AVSSs to tackle the displacement constraints based on the event-triggered mechanism [113]. Furthermore, BLF-based backstepping control is investigated for AVSSs to maintain various motions [95]. The displacement constraints are resolved by the BLF for AVSSs that are underactuated as constraint-following [114]. An adaptive neural network control is proposed for AVSSs to address the symmetric displacement/velocity constraints [75]. Besides, an adaptive neural tracking control is developed for AVSSs where the constraints are addressed by tan-type BLFs [40]. However, only symmetric or time-invariant constraints are considered for AVSSs in the above BLF-based constraint controllers, which are the special cases of asymmetric time-varying constraints. Therefore, more efforts should be devoted in the field of constraint control for AVSSs to meet the safety requirements.

As a matter of fact, asymmetric time-varying constraints are more common and practical in real applications. To address this problem, an asymmetric time-varying BLF (ATVBLF) is utilized with neural network methods for robotic manipulators with out-

put constraints [115]. However, only displacement constraints are considered while neglecting the significant effect of velocity constraints on driving safety. The ATVBLF is constructed to tackle the displacement and velocity constraints for AVSSs with the asymptotic stability [116]. Notice that the input saturations should be considered from a practical view due to the physical limitation of the actuators. One possible way is that the input saturations are approximated by smooth functions such as [117]. Another method is the auxiliary state systems which have been widely applied to different systems [41]. However, the fixed-time convergence of the auxiliary state systems is seldom achieved which needs further discussion. Despite the rapid developments in BLF-based constraint control, no existing safe-by-design controllers have been constructed to meet the enhanced safety requirements for AVSSs. The enhanced safety requirements here refer to the input saturations and asymmetric time-varying displacement/velocity constraints.

We should also note that these control methods can achieve asymptotic or finite-time stability of AVSSs. Compared with asymptotic controllers, finite-time controllers can enforce system outputs to converge faster to the equilibrium, but the convergence time would increase dramatically when the initial states approach infinity. In [118], adaptive finite-time control is combined with neural networks for nonlinear systems with state constraints. Robust finite-time control is proposed for uncertain AVSSs aiming at disturbance attenuation [119]. However, fixed-time convergence, considered an extension of finite-time convergence, provides a fixed convergence time independent of initial conditions, which is a desirable property in practical applications. Integrated with time-varying BLF, adaptive control is constructed with fuzzy techniques for nonlinear systems to obtain fixed-time convergence [120]. To the best of our knowledge, there is still no fixed-time control method proposed for AVSSs to achieve fixed settling time and enhanced safety regulations simultaneously.

High energy consumption is always required in AVSSs to achieve ride comfort and maneuverability, which severely limits its practical application and development. In the recent decade, more and more papers have been devoted to the field of energy-

saving controller design. In [69], an X-shaped anti-vibration structure is constructed mimicking animals' legs, which processes extraordinary quasi-zero stiffness properties for vibration suppression, leading to potentially less energy consumption. Furthermore, a fuzzy adaptive control for AVSSs is proposed considering the beneficial damping [73]. A saturated PD-SMC method with an X-shaped structure is developed for AVSSs to achieve energy-saving performance [96]. One should note that regulating the system outputs into the predefined constraints may result in much higher energy consumption. However, in the above research papers, displacement/velocity constraints on the AVSSs are rarely considered in the field of energy-saving controller design.

To the best of our knowledge, for the uncertain AVSSs with matched/mismatched disturbances, there is still no proper fixed-time safe-by-design control design which can achieve energy-saving performance while attenuating the enhanced safety requirements for the input saturations and asymmetric time-varying displacement/velocity constraints. Compared with existing controllers for the AVSSs, the major contributions of this research can be summarized.

1) This is the *first* attempt to achieve fixed-time safe-by-design control for the AVSSs with input saturations, unknown matched/unmatched disturbances, and asymmetric time-varying displacement/velocity constraints. Compared with existing finite-time control for AVSSs [65, 121], the convergence time is irrelevant to the initial system states.

2) Unlike traditional symmetric constraints [122], asymmetric time-varying constraints are ensured for AVSSs by the delicately constructed ATVBLFs. Furthermore, the safety requirements for both the displacement and velocity of AVSSs are considered in the control design thus the enhanced output safety can be further guaranteed.

3) A novel adaptive law is deliberately established in the auxiliary state system to compensate for the input saturations. Different from previous auxiliary-state-system-based methods [123], fixed-time stability of the auxiliary state system can

be achieved.

4) An X-shaped anti-vibration nonlinear reference model is introduced to the proposed controller which exploits beneficial nonlinear stiffness and damping characteristics to achieve the energy-saving performance.

The rest of this chapter is organized as follows. In Section 4.2, the system description and problem statement are provided. The main results are given in Section 4.3. Various experimental results are presented in Section 4.4. Finally, the whole chapter is summarized in Section 4.5.

4.2 Problem Formulation

4.2.1 System description

The dynamical model of the quarter-car AVSS can be written as follows [121]

$$\begin{aligned} m_s\ddot{z}_s &= -F_s - F_d + F_{\Delta 1} + u(F) \\ m_u\ddot{z}_u &= F_s + F_d - F_t - F_b + F_{\Delta 2} - u(F) \end{aligned} \tag{4.1}$$

where m_s and m_u are the sprung and unsprung masses, z_s and z_u are the displacements of the sprung and unsprung masses, $F_s = p_{s1}(z_s - z_u) + p_{s2}(z_s - z_u)^3$, p_{s1} and p_{s2} represent the stiffness coefficients of the nonlinear spring, $F_d = p_{d1}(\dot{z}_s - \dot{z}_u) + p_{d2}(\dot{z}_s - \dot{z}_u)^2$, p_{d1} and p_{d2} are the damping coefficients, $F_t = p_t(z_u - z_r)$ and $F_b = p_b(\dot{z}_u - \dot{z}_r)$ with p_t and p_b standing for the coefficients of tire elasticity and tire damping, $F_{\Delta 1}$ and $F_{\Delta 2}$ denote the external disturbances and unknown system uncertainties, respectively, $u(F)$ is the control input to be defined later.

The bioinspired X-shaped reference model is utilized in the controller design for vibration suppression due to its ideal quasi-zero stiffness (Fig. 4.1).

Define the suspension space as $z_p = z_s - z_u$ and introduce the nominal masses as m_{s0} and m_{u0} such that $M = m_{s0}m_{u0}/(m_{s0} + m_{u0})$. Define $x_1 = z_p$, $x_2 = \dot{z}_p = \dot{z}_s - \dot{z}_u$,

then the whole dynamic model can be revised as

$$\begin{aligned} \dot{x}_1 &= x_2 + \Delta_1 \\ \dot{x}_2 &= M^{-1}u(F) + \Delta_2 \end{aligned} \tag{4.2}$$

where Δ_1 is the unmatched disturbance generated by the numerical differentiation, Δ_2 is the lumped disturbance

$$\begin{aligned} \Delta_2 = M^{-1}\big(&- F_s - F_d + \frac{m_s F_{\Delta 1} - m_u F_{\Delta 2}}{m_s + m_u} \\ &+ \frac{m_s}{m_s + m_u}(F_s + F_b) + (M - \frac{m_s m_u}{m_s + m_u})\ddot{z}_p\big). \end{aligned} \tag{4.3}$$

Remark 4.1. In practical applications, the velocity is often obtained by letting the displacement signal pass through the differential filter to avoid sensor estimation noises, which may cause undesired information loss. However, the information loss is always neglected by existing controllers. Hence, in the dynamic model of the AVSS (4.2), the unknown information loss deduced by the numerical operation is considered as the unmatched disturbance.

To quantitatively evaluate the control performance, the following root mean square (RMS) values are given. The RMS value of the acceleration $\ddot{z}_s$ represents the ride comfort

$$RMS(\ddot{z}_s) = \sqrt{\frac{1}{T}\int_0^T \ddot{z}_s^2 dt}$$

And energy cost is evaluated by

$$RMS(P^+) = \sqrt{\frac{1}{T}\int_0^T (P^+(\tau))^2 d\tau}$$

with $P^+ = F(t)\dot{z}_p$ for $F(t)\dot{z}_p > 0$ and $P^+(t) = 0$ for else.

The radial basis function neural networks (RBFNNs) will be used to approximate the

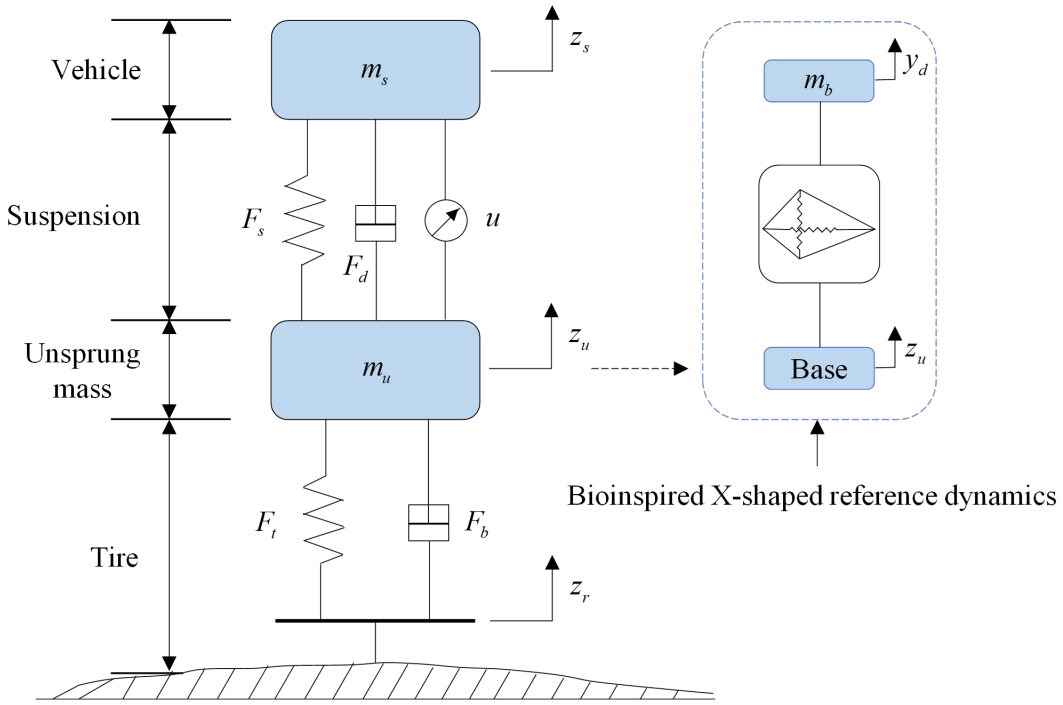

Fig. 4.1: Schematic of the AVSS

unknown functions $H(Z)$ on a compact set $\Omega_Z \subset \Re^l$ as follows [124]

$$H(Z) = \theta^T S(Z) + \varepsilon(Z) \tag{4.4}$$

where $Z \subset \Re^m$ is the input, the approximation error satisfies $|\varepsilon| \leq \bar{\varepsilon}$ with $\bar{\varepsilon} > 0$, $\theta = [\theta_1, ..., \theta_l]^T \subset \Re^l$ represents the optimal weight, $l > 1$ is the node number, $S(Z) = [S_1(Z), ..., S_l(Z)]^T$ is the radius basis function (RBF) with $S_i(Z) = \exp(-||Z-\zeta_i||^2/\nu^2)$ where $\zeta_i = [\zeta_{i1}, ..., \zeta_{im}]^T$ and ν are the center and width of the Gaussian function.

Some useful lemmas are presented for the controller design.

Lemma 4.1 ([125]). *For real numbers $x \geq 0$ and $y \geq 0$, if there exist real numbers $m > 1$ and $n > 0$ satisfying $1/m + 1/n = 1$, then the following inequality holds*

$$xy \leq x^m/m + y^n/n. \tag{4.5}$$

Lemma 4.2 ([126]). *For any $\iota > 0$ and $\zeta \in \Re$, one has*

$$0 < |\zeta| - \zeta \tanh(\zeta/\iota) \leq 0.2785\iota. \tag{4.6}$$

Lemma 4.3 ([127]). *For $x > 0$, $y > 0$ and $a > 0$, we have*

$$x^a(y - x) \leq (y^{1+a} - x^{1+a})/(1 + a). \tag{4.7}$$

Lemma 4.4 ([127]). *For $x \in \Re$ and $y \in \Re$ satisfying $x > 0$ and $y \leq x$, then if the constant $b > 1$, the inequality holds*

$$(x - y)^b \geq y^b - x^b. \tag{4.8}$$

Lemma 4.5 ([128]). *For $x \in \Re$ and $y \in \Re$, if there exists constant $p, q, r > 0$, one can obtain*

$$|x|^p|y|^q \leq pr|x|^{p+q}/(p + q) + qr^{-p/q}|y|^{p+q}/(p + q). \tag{4.9}$$

Lemma 4.6 ([128]). *For $\alpha > 0$ and x_i, $i = 1, ..., n$, there exists*

$$\big(\sum_{i=1}^{n} |x_i|\big)^{\alpha} \leq \max\{n^{\alpha-1}, 1\}(\sum_{i=1}^{n} |x_i|^{\alpha}). \tag{4.10}$$

Lemma 4.7 ([129]). *For any constants $\varkappa_1 > 0$, $\varkappa_2 > 0$, $0 < p_1 < 1$, $p_2 > 1$ and $0 \leq \Xi < \infty$, if there is a continuous positive-definite Lyapunov function $V(x)$ such that*

$$\dot{V}(x) \leq -\varkappa_1 V^{p_1} - \varkappa_2 V^{p_2} + \Xi \tag{4.11}$$

then it is fixed-time stable with

$$T \leq 1/(\varkappa_1\zeta(1 - p_1)) + 1/(\varkappa_2\zeta(p_2 - 1)) \tag{4.12}$$

with $0 < \zeta \leq 1$. The residual set of the nonlinear system is $x \in \{x|V \leq \min\{(\frac{\Xi}{(1-\zeta)\varkappa_1})^{1/p_1}, (\frac{\Xi}{(1-\zeta)\varkappa_2})^{1/p_2}\}\}$. Especially, when $\Xi = 0$, the equality holds and there exists $\zeta = 1$ such that x will converge to zero within a fixed time.

4.2.2 Problem statement

In AVSSs, the control input $u(F)$ is always subjected to the asymmetric saturation constraint

$$u(F) = \text{sat(F)} = \begin{cases} F_{\max}, & F \geq F_{\max} \\ F, & F_{\min} \leq F \leq F_{\max} \\ F_{\min}, & F < F_{\min} \end{cases} \tag{4.13}$$

where sat$(*)$ is the saturation function, $F_{\max}$ and $F_{\min}$ are the upper and lower bounds. The saturation error is $\rho_F = \text{sat(F)} - \text{F}$. We assume $|\rho_F| \leq \rho_0$ holds where $\rho_0 > 0$ is a known constant.

Different from existing literature, the displacement/velocity of the sprung mass should stay within the permitted sets with asymmetric time-varying constraints defined by

$$\begin{aligned} \Phi &= \{z_s(t) \in \Re \big| \underline{\chi}(t) < z_s < \bar{\chi}(t)\} \\ \Psi &= \{\dot{z}_s(t) \in \Re \big| \underline{\vartheta}(t) < \dot{z}_s < \bar{\vartheta}(t)\} \end{aligned} \tag{4.14}$$

where $\bar{\chi}(t) > \underline{\chi}(t)$ and $\bar{\vartheta}(t) > \underline{\vartheta}(t)$ for $\forall t > 0$.

Assumption 4.1 ([130]). *For the desired suspension space y_d, there are continuous functions $\underline{Y}(t)$, $\bar{Y}(t)$ and constant Y_1 such that $\underline{\chi}(t) < \underline{Y}(t) \leq y_d \leq \bar{Y}(t) < \bar{\chi}(t)$ and $|\dot{y}_d| \leq Y_1$.*

Assumption 4.2 ([75]). *For the time-varying constraints $\underline{\chi}(t)$, $\bar{\chi}(t)$, $\underline{\vartheta}(t)$, and $\bar{\vartheta}(t)$, there always exist constants $\underline{K}_{\chi i}$, $\bar{K}_{\chi i}$, $\underline{K}_{\vartheta i}$, $\bar{K}_{\vartheta i}$, $i = 1, 2$ with $\underline{\chi}(t) \geq \underline{K}_{\chi 1}$, $\bar{\chi}(t) \leq \bar{K}_{\chi 1}$, $\underline{\vartheta}(t) \geq \underline{K}_{\vartheta 1}$, $\bar{\vartheta}(t) \leq \bar{K}_{\vartheta 1}$ and their first derivatives $\dot{\underline{\chi}}(t) \geq \underline{K}_{\chi 2}$, $\dot{\bar{\chi}}(t) \leq \bar{K}_{\chi 2}$, $\dot{\underline{\vartheta}}(t) \geq \underline{K}_{\vartheta 2}$, $\dot{\bar{\vartheta}}(t) \leq \bar{K}_{\vartheta 2}$.*

Definition 4.1. *Considering the input saturations (4.13) and the asymmetric time-varying constraints (4.14) for the AVSS dynamics (4.2). The system is considered safe if for any initial conditions $(z_s(0), \dot{z}_s(0)) \in \Phi \times \Psi$, $(z_s(t), \dot{z}_s(t)) \in \Phi \times \Psi$ holds for $\forall t \geq 0$.*

Remark 4.2. Compared with the safety definition in [111], this definition is stronger

since the asymmetric displacement/velocity time-varying constraints and the asymmetric input constraints are required for $\forall t \geq 0$.

Hence, the target of this article is to propose a novel fixed-time control method for the AVSSs based on bioinspired X-shaped dynamics to ensure enhanced safety requirements for the input saturations and asymmetric time-varying displacement/velocity constraints, while matched/unmatched disturbances can be handled.

4.3 Main Results

The main results of the fixed-time control structure are presented in this section considering the input saturations and asymmetric time-varying displacement/velocity constraints. The dynamics of the bioinspired reference structure (also known as the X-shaped structure) are briefly introduced. Then the fixed-time safe-by-design control is proposed for the AVSSs with the ATVBLFs. Finally, a rigorous stability verification of the closed-loop system is detailly analyzed.

4.3.1 Bioinspired X-shaped reference dynamics

The bioinspired X-shaped anti-vibration model is inspired by the bird legs with the two-layer structure [131], where m_b is the object mass, l_1 and l_2 are the rod length, φ_1 and φ_2 are the initial angles, and the geometric relationship is $l_1 \sin\varphi_1 = l_2 \sin\varphi_2$. The output of the X-shaped reference model is considered as the desired suspension space denoted by y_d for energy-saving which is given by [130]

$$m_b \ddot{y}_d + \overline{h}_1 + k_v y_d / n^2 + \kappa_1 \dot{y}_d + \kappa_2 n_x \overline{h}_2 \dot{y}_d = -m_b \ddot{z}_u \tag{4.15}$$

where

$$\begin{aligned}\bar{h}_1 &= \frac{k_h\varpi}{2n}(l_1\cos\varphi_1 - \sqrt{l_1^2-\varpi^2} + l_2\cos\varphi_2 \\ &\quad - \sqrt{l_2^2-\varpi^2})\Big(1/\sqrt{l_1^2-\varpi^2} - 1/\sqrt{l_2^2-\varpi^2}\Big) \\ \bar{h}_2 &= \Big(l_1/(2n\sqrt{l_1^2-\varpi^2}) - l_2/(2n\sqrt{l_2^2-\varpi^2})\Big)^2 \\ \varpi &= l_1\sin\varphi_1 + y_d/(2n) = l_2\sin\varphi_2 + y_d/(2n)\end{aligned} \tag{4.16}$$

and $n = 2$ is the layer of the X-shaped structure, $n_x = 3n - 1$ is the joint number, k_v and k_h stand for the vertical and horizontal spring stiffness, κ_1 and κ_2 denote the air resistance coefficient and the rotating friction coefficient. The permitted range $\varsigma_1 < \ddot{y}_d < \varsigma_2$ is defined to restrict $\ddot{y}_d$ where ς_1 and ς_2 are known constants representing the bounds of $\ddot{y}_d$.

Different from existing controllers which set desired trajectories to zero, the desired trajectories in the proposed controller are considered as the output of the X-shaped structure to avoid the cancellation of beneficial nonlinearities of the AVSSs. Therefore, the advantageous characteristics of the suspension system can be remained for vibration suppression, which further enhances the energy-saving performance with satisfactory anti-vibration results. Thus, the utilization of the X-shaped structure in the control design can lead to promising energy-efficient characteristics.

The vibration suppression ability of the X-shaped structure has been analyzed and demonstrated in existing papers [69, 73, 87]. However, the enhanced safety requirements for the input saturations and the displacement/velocity constraints are seldom considered in the control designs for AVSSs with energy-saving performance, although enforcing system outputs to the predefined ranges may cost higher energy. In this chapter, the anti-vibration X-shaped structure is deliberately considered to strengthen the energy-saving performance.

4.3.2 Fixed-time safe-by-design control

For the sake of brevity, the notation $[x]^r = |x|^r\text{sgn}(x)$ is defined where $\text{sgn}(x)$ is the standard signum function.

Consider the errors as follows

$$\begin{aligned} z_1 &= x_1 - y_d \\ z_2 &= x_2 - \alpha_1 - \xi \end{aligned} \tag{4.17}$$

where y_d is generated by the X-shaped reference dynamics, α_1 is the virtual control signal, ξ is an auxiliary signal.

To ensure the asymmetric time-varying constraint on the sprung displacement, an ATVBLF function is constructed

$$V_1 = \frac{q_1}{2p}\log\frac{\Omega_{H1}^{2p}(t)}{\Omega_{H1}^{2p}(t)-z_1^{2p}} + \frac{1-q_1}{2p}\log\frac{\Omega_{L1}^{2p}(t)}{\Omega_{L1}^{2p}(t)-z_1^{2p}} \tag{4.18}$$

where $p \in \mathbb{N}_+$ with $p \geq 2$, $\Omega_{H1}(t) = \bar{\chi}(t) - z_u - y_d$, $\Omega_{L1}(t) = y_d + z_u - \underline{\chi}(t)$ and q_i is defined with $i = 1, 2$

$$q_i(z_i) = \begin{cases} 1, & \text{if} \quad z_i > 0 \\ 0, & \text{if} \quad z_i \leq 0. \end{cases} \tag{4.19}$$

Remark 4.3. Unlike [75, 120], the ATVBLF technique is adopted for the AVSSs to guarantee the asymmetric time-varying displacement constraint with $\Omega_{L1}(t) \neq -\Omega_{H1}(t)$. According to the definition of the ATVBLF (4.18), V_1 will become unbounded if $z_1 \geq \Omega_{H1}(t)$ or $z_1 \leq -\Omega_{L1}(t)$. Hence, if the boundedness of V_1 can be ensured by the design procedure of the controller, it leads to $-\Omega_{L1}(t) < z_1 < \Omega_{H1}(t)$. According to the definition of z_1, x_1, $\Omega_{L1}(t)$, and $\Omega_{H1}(t)$, it is easy to obtain that z_s will always stay in the asymmetric constraint range such that $-\underline{\chi}(t) < z_s < \bar{\chi}(t)$.

Remark 4.4. Some efforts have been taken to restrict the displacement and velocity within the permitted ranges [95]. However, only the time-invariant constraints are considered. To enhance the feasibility, time-varying displacement/velocity constraints are discussed in the proposed control, which is more practical in real applications.

The error coordinates can be further changed using $\eta_{Hi} = z_i/\Omega_{Hi}$, $\eta_{Li} = z_i/\Omega_{Li}$, $\eta_i = q_i\eta_{Hi} + (1-q_i)\eta_{Li}$ and $\lambda_i = q_i/(\Omega_{Hi}^{2p} - z_i^{2p}) + (1-q_i)/(\Omega_{Li}^{2p} - z_i^{2p})$. Then the

Lyapunov function (4.18) can be revised as:

$$V_1 = \frac{1}{2p}\log\frac{1}{1-\eta_1^{2p}}. \tag{4.20}$$

Here, V_1 is positive definite due to $|\eta_1| < 1$. Then we have

$$\begin{aligned}\dot{V}_1 &= \eta_1^{2p-1}\dot{\eta}_1/(1-\eta_1^{2p}) \\ &= \frac{\eta_1^{2p-1}}{1-\eta_1^{2p}}\big(q_1\frac{\dot{z}_1\Omega_{H1} - z_1\dot{\Omega}_{H1}}{\Omega_{H1}^2} + (1-q_1)\frac{\dot{z}_1\Omega_{L1} - z_1\dot{\Omega}_{L1}}{\Omega_{L1}^2}\big) \\ &= \lambda_1 z_1^{2p-1}\big(z_2 + \alpha_1 + \xi + \Delta_1 - \dot{y}_d + q_1 z_1\dot{\Omega}_{H1}/\Omega_{H1} \\ &\quad + (1-q_1)z_1\dot{\Omega}_{L1}/\Omega_{L1}\big).\end{aligned} \tag{4.21}$$

The virtual control signal α_1 is proposed as

$$\begin{aligned}\alpha_1 = &-k_{11}\lambda_1^{\pi_1-1}[z_1]^{2p\pi_1-2p+1} - k_{12}\lambda_1^{\pi_2-1}[z_1]^{2p\pi_2-2p+1} \\ &- \frac{\hat{\Theta}_1}{2\sigma_1^2}S_1^T S_1\lambda_1 z_1^{2p-1} - (\rho_{11}+\rho_{12})z_1 - \xi\end{aligned} \tag{4.22}$$

with $\rho_{11} = \sqrt{(\frac{\dot{\Omega}_{H1}}{\Omega_{H1}})^2 + (\frac{\dot{\Omega}_{L1}}{\Omega_{L1}})^2 + \delta_1}$, $\rho_{12} = \frac{2p-1}{2p}(\lambda_1^{\frac{1}{2p-1}} + 1)$, k_{1j}, k_{2j} are positive control gains with $j = 1, 2$, $0 < \pi_1 < 1$ and $\pi_2 > 1$ are constants to enhance the convergence rate, $\hat{\Theta}_1$ is the estimation of Θ_1 with error $\tilde{\Theta}_1 = \Theta_1 - \hat{\Theta}_1$ which will be given later, $\delta_1 > 0$ ensures the boundedness of α_1 even when $\dot{\Omega}_{H1}$ and $\dot{\Omega}_{L1}$ are zero at the same time.

Define an unknown continuous function $H_1(Z_1) = \Delta_1 - \dot{y}_d$ with $Z_1 = [x_1, \dot{y}_d]^T$. According to (4.4), $H_1(Z_1)$ can be approximated $H_1(Z_1) = \theta_1^T S_1(Z_1) + \varepsilon_1(Z_1)$ [124].

Using Young's inequality and Lemma 4.1, there exists

$$\begin{aligned}\lambda_1 z_1^{2p-1}\theta_1^T S_1 &\le \frac{\sigma_1^2}{2} + \frac{\Theta_1}{2\sigma_1^2}S_1^T S_1\lambda_1^2 z_1^{4p-2} \\ \lambda_1 z_1^{2p-1}\varepsilon_1 &\le \frac{2p-1}{2p}\lambda_1^{\frac{2p}{2p-1}}z_1^{2p} + \frac{\bar{\varepsilon}_1^{2p}}{2p} \\ \lambda_1 z_1^{2p-1}z_2 &\le \frac{2p-1}{2p}\lambda_1 z_1^{2p} + \frac{1}{2p}\lambda_1 z_2^{2p}.\end{aligned} \tag{4.23}$$

where $\Theta_1 = ||\theta_1||^2$ and $\sigma_1 > 0$ is a design constant.

Considering the virtual control signal (4.22) and noticing (4.23) with $\rho_{11}+q_1\dot{\Omega}_{H1}/\Omega_{H1}+(1-q_1)\dot{\Omega}_{L1}/\Omega_{L1} \geq 0$, we can obtain

$$\begin{aligned}\dot{V}_1 \leq & \frac{\sigma_1^2}{2} + \frac{\tilde{\Theta}_1}{2\sigma_1^2} S_1^T S_1 \lambda_1^2 z_1^{4p-2} + \frac{\bar{\varepsilon}_1^{2p}}{2p} + \lambda_1 z_1^{2p-1} z_2 \\ & - k_{11}\lambda_1^{\pi_1} z_1^{2p\pi_1} - k_{12}\lambda_1^{\pi_2} z_1^{2p\pi_2} - \frac{2p-1}{2p}\lambda_1 z_1^{2p} \\ & \leq -k_{11}(\frac{\eta_1^{2p}}{1-\eta_1^{2p}})^{\pi_1} - k_{12}(\frac{\eta_1^{2p}}{1-\eta_1^{2p}})^{\pi_2} + \frac{\sigma_1^2}{2} \\ & + \frac{\tilde{\Theta}_1}{2\sigma_1^2} S_1^T S_1 \lambda_1^2 z_1^{4p-2} + \frac{\bar{\varepsilon}_1^{2p}}{2p} + \frac{1}{2p}\lambda_1 z_2^{2p}.\end{aligned} \tag{4.24}$$

The auxiliary signal ξ is generated by

$$\dot{\xi} = -k_{\xi 1}[\xi]^{2\pi_1 - 1} - k_{\xi 2}[\xi]^{2\pi_2 - 1} - k_{\xi 3}\text{sgn}(\xi) - M^{-1}\rho_F \tag{4.25}$$

with $\rho_F = u(F) - F$ is the saturation error.

Remark 4.5. Typical auxiliary-state-system methods are widely used in the AVSSs to compensate for the input saturations [123]. The convergence time of the auxiliary signals may approach infinity in traditional controllers, which are not suitable for practical applications. However, with the carefully constructed adaptive law (4.25), the fixed-time ability of the proposed auxiliary signal system can be guaranteed.

Combining (4.2), (4.17) and (4.25) leads to

$$\begin{aligned}\dot{z}_2 = & M^{-1}F + \Delta_2 - \dot{\alpha}_1 + k_{\xi 1}[\xi]^{2\pi_1 - 1} + k_{\xi 2}[\xi]^{2\pi_2 - 1} \\ & + k_{\xi 3}\text{sgn}(\xi) + M^{-1}\rho_F.\end{aligned} \tag{4.26}$$

Here, we propose the actual control law as

$$\begin{aligned}F = M\big(& - k_{21}\lambda_2^{\pi_1 - 1}[z_2]^{2p\pi_1 - 2p + 1} - k_{22}\lambda_2^{\pi_2 - 1}[z_2]^{2p\pi_2 - 2p + 1} \\ & - \frac{\hat{\Theta}_2}{2\sigma_2^2} S_2^T S_2 \lambda_2 z_2^{2p-1} - (\rho_{21} + \rho_{22}) z_2 - k_{\xi 1}[\xi]^{2\pi_1 - 1} \\ & - k_{\xi 2}[\xi]^{2\pi_2 - 1} - k_{\xi 3}\text{sgn}(\xi) - \frac{\lambda_1 z_2}{2p\lambda_2}\big) - \rho_0 \tanh(\frac{\Psi}{\iota})\end{aligned} \tag{4.27}$$

with $\rho_{21} = \sqrt{(\frac{\dot{\Omega}_{H2}}{\Omega_{H2}})^2 + (\frac{\dot{\Omega}_{L2}}{\Omega_{L2}})^2 + \delta_2}$, $\rho_{22} = \frac{2p-1}{2p}\lambda_2^{\frac{1}{2p-1}}$, $\Psi = M^{-1}\rho_0\lambda_2 z_2^{2p-1}$, $k_{2j} > 0$, $\delta_2 > 0$, $\hat{\Theta}_2$ is the estimation of Θ_2 with the error $\tilde{\Theta}_2 = \Theta_2 - \hat{\Theta}_2$.

The following adaptive law is defined

$$\dot{\hat{\Theta}}_i = \frac{\gamma_i}{2\sigma_i^2} S_i^T S_i \lambda_i^2 z_i^{4p-2} - \varrho_{i1}\hat{\Theta}_i - \varrho_{i2}\hat{\Theta}_i^{2\pi_2 - 1} \tag{4.28}$$

where $\varrho_{ij} > 0$ are constants. With the results above, the following Theorem 4.1 can be concluded.

Theorem 4.1. *Consider the AVSSs (4.2) with matched/unmatched disturbances, input saturations (4.13) and asymmetric time-varying displacement/velocity constraints (4.14). By proposing the fixed-time safe-by-design control consisting of the virtual control law (4.22), auxiliary design signal (4.25), actual control law (4.27) and adaptive law (4.28), one can obtain:*

1. *all the closed-loop signals are bounded,*
2. *the transformed tracking errors can converge to the neighborhood of zero within a fixed time and*
3. *the asymmetric time-varying displacement/velocity constraints on z_s and $\dot{z}_s$ are satisfied all the time.*

Proof of Theorem 4.1: It is given in the next subsection.

4.3.3 Stability analysis

Similar to (4.18), the following ATVBLF is constructed

$$\begin{aligned} V_2 &= V_1 + \frac{q_2}{2p}\log\frac{\Omega_{H2}^{2p}(t)}{\Omega_{H2}^{2p}(t) - z_2^{2p}} + \frac{1-q_2}{2p}\log\frac{\Omega_{L2}^{2p}(t)}{\Omega_{L2}^{2p}(t) - z_2^{2p}} \\ &= V_1 + \frac{1}{2p}\log\frac{1}{1-\eta_2^{2p}} \end{aligned} \tag{4.29}$$

with $\Omega_{H2} = \bar{\vartheta}(t) - \dot{z}_u - \alpha_1 - \xi$, $\Omega_{L2} = \alpha_1 + \xi + \dot{z}_u - \underline{\vartheta}(t)$.

Remark 4.6. If the boundedness of V_2 can be guaranteed, it leads to $-\Omega_{L2}(t) < z_2 < \Omega_{H2}(t)$. According to the definition of z_2, x_2, $\Omega_{L2}(t)$, and $\Omega_{H2}(t)$, $\dot{z}_s$ will always stay in the range such that $-\underline{\vartheta}(t) < \dot{z}_s < \bar{\vartheta}(t)$. The velocity constraint is always neglected in previous works [95, 116]. However, driving safety and ride comfort of the passengers can also be affected by the velocity of the sprung mass. Therefore, asymmetric time-varying constraints on both displacement and velocity are considered to enhance the control performance.

The time derivative of V_2 becomes

$$\begin{aligned}\dot{V}_2 &= \dot{V}_1 + \frac{\eta_2^{2p-1}}{1-\eta_2^{2p}}\dot{\eta}_2 = \dot{V}_1 + \frac{\eta_2^{2p-1}}{1-\eta_2^{2p}}\big(q_2\frac{\dot{z}_2\Omega_{H2} - z_2\dot{\Omega}_{H2}}{\Omega_{H2}^2} \\ &\quad + (1-q_2)\frac{\dot{z}_2\Omega_{L2} - z_2\dot{\Omega}_{L2}}{\Omega_{L2}^2}\big) \\ &\leq \dot{V}_1 + \lambda_2 z_2^{2p-1}\big(M^{-1}F + k_{\xi 1}[\xi]^{2\pi_1-1} + k_{\xi 2}[\xi]^{2\pi_2-1} \\ &\quad + k_{\xi 3}\mathrm{sgn}(\xi) + M^{-1}\rho_F - q_2 z_2\frac{\dot{\Omega}_{H2}}{\Omega_{H2}} - (1-q_2)z_2\frac{\dot{\Omega}_{L2}}{\Omega_{L2}}\big) \\ &\quad + \Delta_2 - \dot{\alpha}_1.\end{aligned} \tag{4.30}$$

Define the unknown function $H_2(Z_2) = \Delta_2 - \dot{\alpha}_1$ with $Z_2 = [x_1, x_2, \dot{y}_d, \ddot{y}_d, \dot{\Omega}_{H1}, \dot{\Omega}_{H2}, \dot{\Omega}_{L1}, \dot{\Omega}_{L2}, \hat{\Theta}_1, \xi, \dot{\xi}]^T$. Similarly, according to (4.4), the unknown function $H_2(Z_2)$ can be approximated by $H_2(Z_2) = \theta_2 S_2^T(Z_2) + \varepsilon_2(Z_2)$ [124].

Using Young's inequality and Lemma 4.1, it is derived as

$$\begin{aligned}\lambda_2 z_2^{2p-1}\theta_2^T S_2 &\leq \frac{\sigma_2^2}{2} + \frac{\Theta_2}{2\sigma_2^2}S_2^T S_2 \lambda_2^2 z_2^{4p-2} \\ \lambda_2 z_2^{2p-1}\varepsilon_2 &\leq \frac{2p-1}{2p}\lambda_2^{2p/(2p-1)} z_2^{2p} + \frac{1}{2p}\bar{\varepsilon}_2^{2p}\end{aligned} \tag{4.31}$$

where $\Theta_2 = ||\theta_2||^2$ and $\sigma_2 > 0$ is a design constant.

Combining (4.27), (4.31) with Lemmas 4.2 and 4.3 and noting (4.30) with $|\rho_F| \leq \rho_0$,

Table 4.1: Parameters of the Active Vehicle Suspension Setup

Symbols	Values	Symbols	Values
m_s	2.45 kg	m_u	1 kg
p_{s1}	900 N/m	p_{s2}	10 N/m^3
p_d	8 Ns/m	p_t	1250 N/m
p_b	5 Ns/m		

Table 4.2: Parameters of the bioinspired X-shaped reference dynamics

Symbols	Values	Symbols	Values
m_b	22 kg	κ_1	5 Ns/m
φ_1	π/6 rad	κ_2	0.15 Ns/m
l_1	0.1 m	k_h	500 N/m
l_2	0.2 m	k_v	350 N/m
ς_1	-1 m/s^2	ς_2	1 m/s^2

$\rho_{21} = q_2\dot{\Omega}_{H2}/\Omega_{H2} + (1-q_2)\dot{\Omega}_{L2}/\Omega_{L2} \geq 0$ become

$$\begin{aligned}\dot{V}_2 \leq \dot{V}_1 - k_{21}(\frac{\eta_2^{2p}}{1-\eta_2^{2p}})^{\pi_2} - k_{22}(\frac{\eta_2^{2p}}{1-\eta_2^{2p}})^{\pi_2} - \frac{1}{2p}\lambda_1 z_2^{2p} \\ + \frac{\tilde{\Theta}_2}{2\sigma_2^2}S_2^T S_2 \lambda_2^2 z_2^{4p-2} + \frac{\sigma_2^2}{2} + \frac{\bar{\varepsilon}_2^{2p}}{2p} + 0.2785\iota.\end{aligned} \tag{4.32}$$

According to [74], for $|\eta_i| < 1$ and an integer $p > 0$, we have $\log(1/(1-\eta_i^{2p})) \leq \eta_i^{2p}/(1-\eta_i^{2p})$. Inserting $\dot{V}_1$ and considering Lemma 4.4 lead to

$$\begin{aligned}\dot{V}_2 \leq -c_1 \sum_{i=1}^{2} (\frac{1}{2p}\log\frac{1}{1-\eta_i^{2p}})^{\pi_1} - c_2 \sum_{i=1}^{2} (\frac{1}{2p}\log\frac{1}{1-\eta_i^{2p}})^{\pi_2} \\ + \sum_{i=1}^{2} \frac{\tilde{\Theta}_i}{2\sigma_i^2}S_i^T S_i \lambda_i^2 z_i^{4p-2} + \sum_{i=1}^{2}\frac{\sigma_i^2}{2} + \sum_{i=1}^{2}\frac{\bar{\varepsilon}_i^{2p}}{2p} + 0.2785\iota\end{aligned} \tag{4.33}$$

where $c_1 = \min\{(2p)^{\pi_1}k_{11}, (2p)^{\pi_2}k_{12}\}$, $c_2 = \min\{(2p)^{\pi_2}k_{21}, (2p)^{\pi_2}k_{22}\}$.

For $\tilde{\Theta}_i$, we construct another Lyapunov function

$$V_3 = V_2 + \sum_{i=1}^{2}\tilde{\Theta}_i^2/(2\gamma_i). \tag{4.34}$$

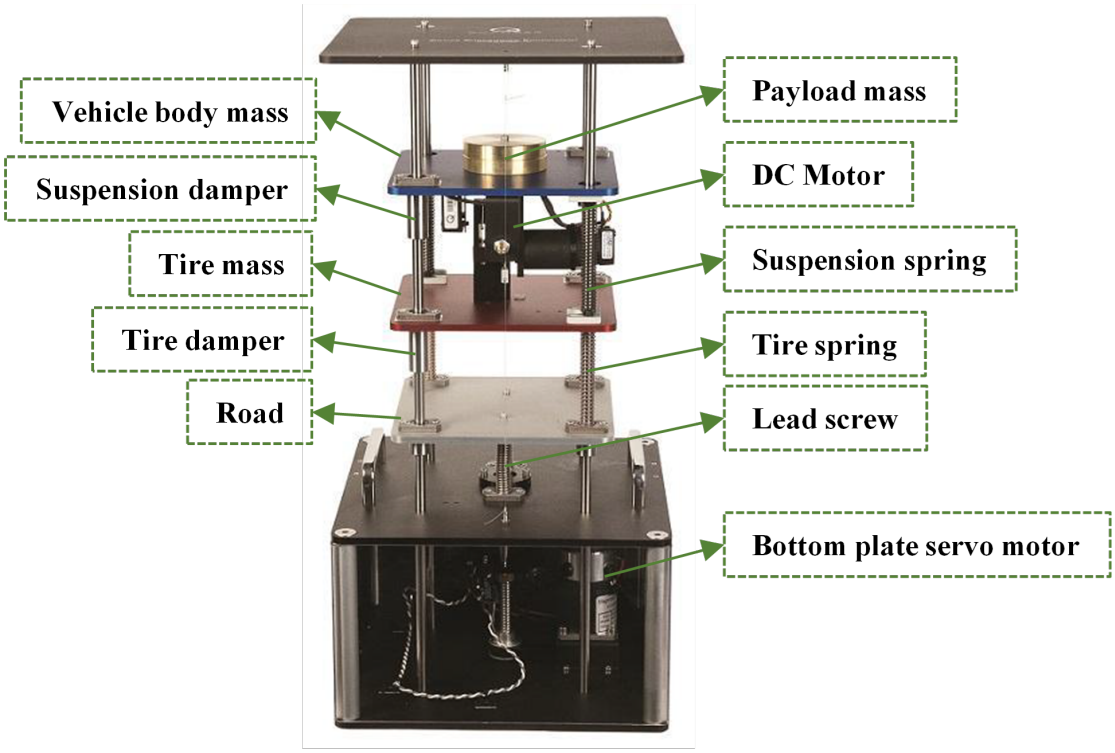

Fig. 4.2: Active suspension setup

Considering the adaptive law (4.28), we have

$$\begin{aligned}\dot{V}_3 &= \dot{V}_2 - \sum_{i=1}^{2} \tilde{\Theta}_i \dot{\hat{\Theta}}_i / \gamma_i \\ &\leq -c_1 \sum_{i=1}^{2} \left(\frac{1}{2p} \log \frac{1}{1-\eta_i^{2p}}\right)^{\pi_1} - c_2 \sum_{i=1}^{2} \left(\frac{1}{2p} \log \frac{1}{1-\eta_i^{2p}}\right)^{\pi_2} \\ &+ \sum_{i=1}^{2} \frac{\sigma_i^2}{2} + \sum_{i=1}^{2} \frac{\bar{\varepsilon}_i^{2p}}{2p} + \sum_{i=1}^{2} \frac{\varrho_{i1}}{\gamma_i} \tilde{\Theta}_i \hat{\Theta}_i + \sum_{i=1}^{2} \frac{\varrho_{i2}}{\gamma_i} \tilde{\Theta}_i \hat{\Theta}_i^{2\pi_2 - 1} \\ &+ 0.2785\iota.\end{aligned} \tag{4.35}$$

According to Young's inequality, it can be rearranged

$$\sum_{i=1}^{2} \frac{\varrho_{i1}}{\gamma_i} \tilde{\Theta}_i \hat{\Theta}_i \leq -\sum_{i=1}^{2} \frac{\varrho_{i1}(2-\Lambda_i)}{2\gamma_i} \tilde{\Theta}_i^2 + \sum_{i=1}^{2} \frac{\varrho_{i1}}{2\gamma_i \Lambda_i} \Theta_i^2 \tag{4.36}$$

where $\Lambda_i \in (0, 2)$.

Table 4.3: Settling Time (s)

Controllers	Settling time
NOFC	0.618
RBC	0.453 (↓26.7%)
TSMC	0.405 (↓34.5%)
PDSMC	0.372 (↓39.8%)
Proposed	0.304 (↓50.8%)

Table 4.4: RMS of Vehicle Body Acceleration ($\mathrm{m/s^2}$)

Controllers	Sinusoidal road input	Bump road input
Passive	0.4813	0.2987
NOFC	0.1661 (↓65.5%)	0.1488 (↓50.2%)
RBC	0.1222 (↓74.6%)	0.1215 (↓59.3%)
TSMC	0.1347 (↓72.0%)	0.1187 (↓60.3%)
PDSMC	0.1150 (↓76.1%)	0.1198 (↓59.9%)
Proposed	0.1073 (↓78.5%)	0.1147 (↓61.6%)

Using Lemmas 4.3–4.4, one can obtain

$$\begin{aligned}\sum_{i=1}^{2}\frac{\varrho_{i2}}{\gamma_i}\tilde{\Theta}_i\hat{\Theta}_i^{2\pi_2-1} &\leq \sum_{i=1}^{2}\frac{\varrho_{i2}\Theta_i^{2\pi_2}}{2\pi_2\gamma_i}-\sum_{i=1}^{2}\frac{\varrho_{i2}(\Theta_i-\tilde{\Theta}_i)^{2\pi_2}}{2\pi_2\gamma_i}\\ &\leq \sum_{i=1}^{2}\frac{\varrho_{i2}\Theta_i^{2\pi_2}}{\pi_2\gamma_i}-\sum_{i=1}^{2}\frac{\varrho_{i2}\tilde{\Theta}_i^{2\pi_2}}{2\pi_2\gamma_i}.\end{aligned} \tag{4.37}$$

Furthermore, applying Lemma 4.5 with $p=1-\pi_1$, $q=\pi_1$, $r=\pi_1^{\pi_1/(1-\pi_1)}$, $x=1$, and $y=\sum_{i=1}^{2}\tilde{\Theta}_i^2/(2\gamma_i)$, the term becomes

$$\textstyle\sum_{i=1}^{2}\left(\frac{\tilde{\Theta}_i^2}{2\gamma_i}\right)^{\pi_1}\leq(1-\pi_1)\pi_1^{\pi_1/(1-\pi_1)}+\sum_{i=1}^{2}\frac{\tilde{\Theta}_i^2}{2\gamma_i}. \tag{4.38}$$

Table 4.5: Energy Consumption (W)

Controllers	Sinusoidal road input	Bump road input
NOFC	0.0773	0.0121
RBC	0.0621 (↓19.7%)	0.0084 (↓30.6%)
TSMC	0.0415 (↓46.3%)	0.0080 (↓33.9%)
PDSMC	0.0351 (↓54.6%)	0.0079 (↓34.7%)
Proposed	0.0249 (↓67.8%)	0.0062 (↓48.8%)

Combing (4.35)–(4.38), one can obtain

$$\begin{aligned}\dot{V}_3 \leq & -c_1\sum_{i=1}^{2}\big(\frac{1}{2p}\log\frac{1}{1-\eta_i^{2p}}\big)^{\pi_1} - c_2\sum_{i=1}^{2}\big(\frac{1}{2p}\log\frac{1}{1-\eta_i^{2p}}\big)^{\pi_2} \\ & - c_3\sum_{i=1}^{2}\big(\frac{\tilde{\Theta}_i^2}{2\gamma_i}\big)^{\pi_1} - c_4\sum_{i=1}^{2}\big(\frac{\tilde{\Theta}_i}{2\gamma_i}\big)^{\pi_2} + \sum_{i=1}^{2}\frac{\varrho_{i1}\Theta_i^2}{2\gamma_i\Lambda_i} \\ & - (c_0-c_3)\sum_{i=1}^{2}\frac{\tilde{\Theta}_i^2}{2\gamma_i} + c_3(1-\pi_1)\pi_1^{\pi_1/(1-\pi_1)} \\ & + \sum_{i=1}^{2}\frac{\varrho_{i2}\Theta_i^{2\pi_2}}{\pi_2\gamma_i} + \sum_{i=1}^{2}\frac{\sigma_i^2}{2} + \sum_{i=1}^{2}\frac{\bar{\varepsilon}_i^{2p}}{2p} + 0.2785\iota\end{aligned} \tag{4.39}$$

where $c_0 = \min\{\varrho_{11}(2-\Lambda_1), \varrho_{12}(2-\Lambda_2)\}$, $c_3 > 0$ is a constant, $c_4 = \min\{(2\gamma_1)^{\pi_2}\varrho_{21}/(2\pi_2\gamma_1), (2\gamma_2)^{\pi_2}\varrho_{22}/(2\pi_2\gamma_2)\}$.

Considering Lemma 4.6, if $c_0 > c_3$ is satisfied, we have

$$\dot{V}_3 \leq -\varkappa_1 V_3^{\pi_1} - \varkappa_2 V_3^{\pi_2} + \Xi \tag{4.40}$$

where $\varkappa_1 = \min\{c_1, c_3\}$, $\varkappa_2 = 2^{1-\pi_2}\min\{c_2, c_4\}$ and

$$\begin{aligned}\Xi = & \, c_3(1-\pi_1)\pi_1^{\pi_1/(1-\pi_1)} + \sum_{i=1}^{2}\frac{\sigma_i^2}{2} + \sum_{i=1}^{2}\frac{\bar{\varepsilon}_i^{2p}}{2p} \\ & + \sum_{i=1}^{2}\frac{\varrho_{i1}\Theta_i^2}{2\gamma_i\Lambda_i} + \sum_{i=1}^{2}\frac{\varrho_{i2}\Theta_i^{2\pi_2}}{\pi_2\gamma_i} + 0.2785\iota.\end{aligned} \tag{4.41}$$

According to Lemma 4.7, the system is fixed-time stable with $0 < \zeta < 1$ such that

$$T_1 \leq 1/(\varkappa_1\zeta(1-\pi_1)) + 1/(\varkappa_2\zeta(\pi_2-1)). \tag{4.42}$$

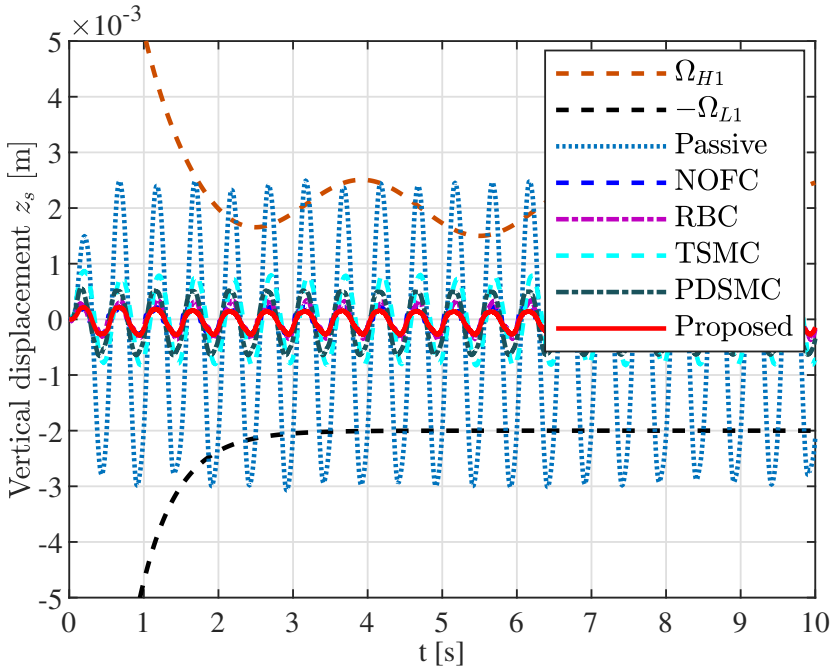

Fig. 4.3: Case 1: Vertical displacement z_s under the sinusoidal road

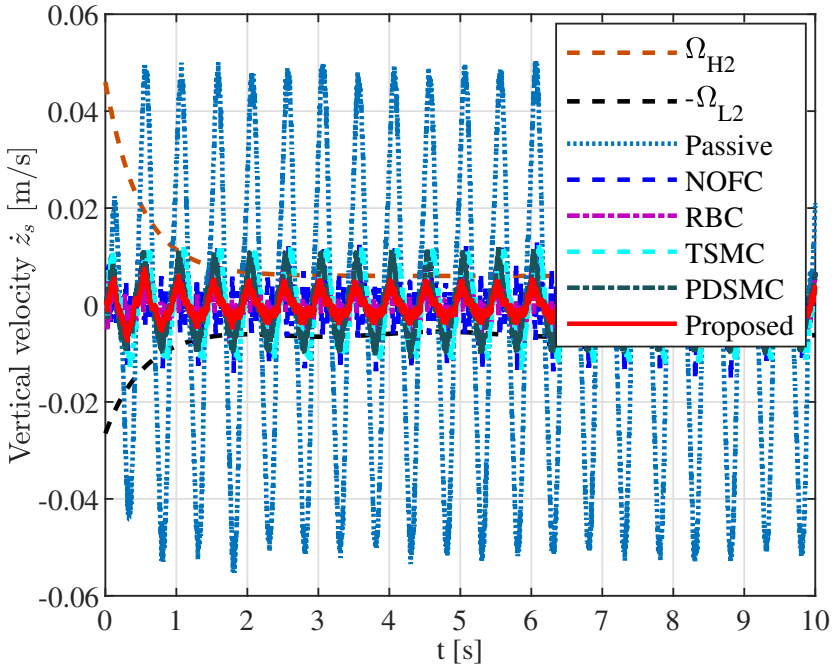

Fig. 4.4: Case 1: Vertical velocity $\dot{z}_s$ under the sinusoidal road

The fixed-time stability of the auxiliary signal ξ is further discussed. The Lyapunov function is $V_0 = (1/2)\xi^2$ such that

$$\begin{aligned}\dot{V}_0 = \xi\dot{\xi} &\leq -k_{\xi 1}|\xi|^{2\pi_1} - k_{\xi 2}|\xi|^{2\pi_2} - k_{\xi 3}|\xi| + M^{-1}|\rho_F||\xi| \\ &\leq -k_{\xi 1}|\xi|^{2\pi_1} - k_{\xi 2}|\xi|^{2\pi_2} - (k_{\xi 3} - M^{-1}\rho_0)|\xi|.\end{aligned} \tag{4.43}$$

If $k_{\xi 3} > M^{-1}\rho_0$ is satisfied all the time, we have

$$\begin{aligned}\dot{V}_0 &\leq -k_{\xi 1}|\xi|^{2\pi_1} - k_{\xi 2}|\xi|^{2\pi_2} \\ &\leq -2^{\pi_1}k_{\xi 1}V_0^{\pi_1} - 2^{\pi_2}k_{\xi 2}V_0^{\pi_2}.\end{aligned} \tag{4.44}$$

According to Lemma 4.7, the auxiliary signal system (4.25) is fixed-time stable within the time

$$T_2 \leq 1/(2^{\pi_1}k_{\xi 1}(1-\pi_1)) + 1/(2^{\pi_2}k_{\xi 2}(\pi_2 - 1)). \tag{4.45}$$

Considering the above analysis, all signals in the AVSS are bounded and the closed-loop system is fixed-time stable with $T \leq \max\{T_1, T_2\}$, which is independent of the initial system states. According to Remarks 4.3 and 4.6, we can conclude that $\underline{\chi}(t) < z_s < \bar{\chi}(t)$ and $\underline{\vartheta}(t) < \dot{z}_s < \bar{\vartheta}(t)$ hold for $\forall t \geq 0$. Hence, asymmetric time-varying displacement/velocity constraints are satisfied all the time. This completes the proof of Theorem 4.1.■

Remark 4.7. The convergence time is clearly independent of the initial states leading to the fixed-time convergence property. There exist two different cases:

1. If $T_1 \geq T_2$ such that $T = T_1$, the settling time T is affected by the parameters $\varkappa_i$, and π_i. When k_{ij} play the main role in $\varkappa_i$, the increment of k_{ij} will decrease the convergence time but enlarge the control gains in (4.22) and (4.27). When ϱ_{ij} are dominated in $\varkappa_i$, the control performance is mainly affected by the adaptive law (4.28).

2. If $T_1 < T_2$ such that $T = T_2$, the settling time T is only affected by $k_{\xi i}$ and π_2.

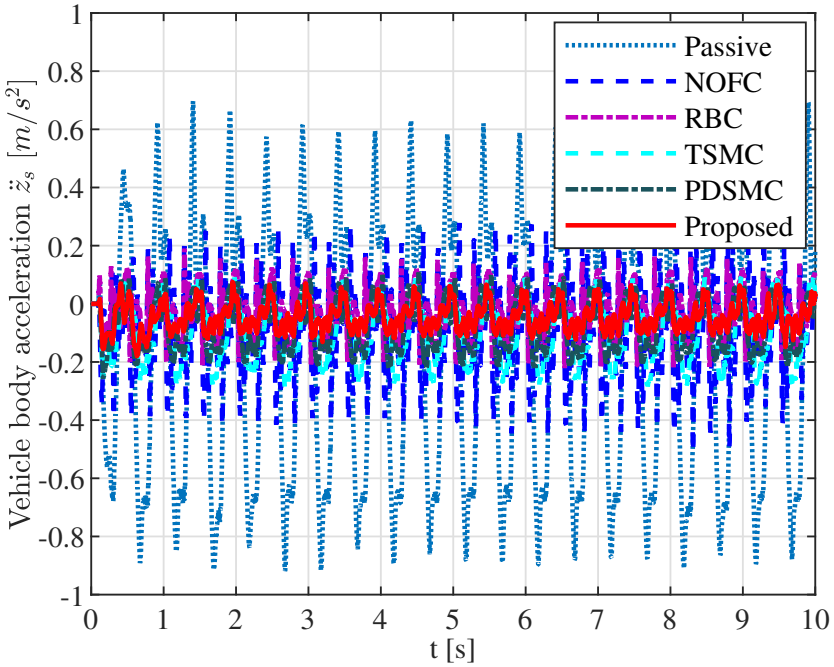

Fig. 4.5: Case 1: Vehicle body acceleration $\ddot{z}_s$ under the sinusoidal road

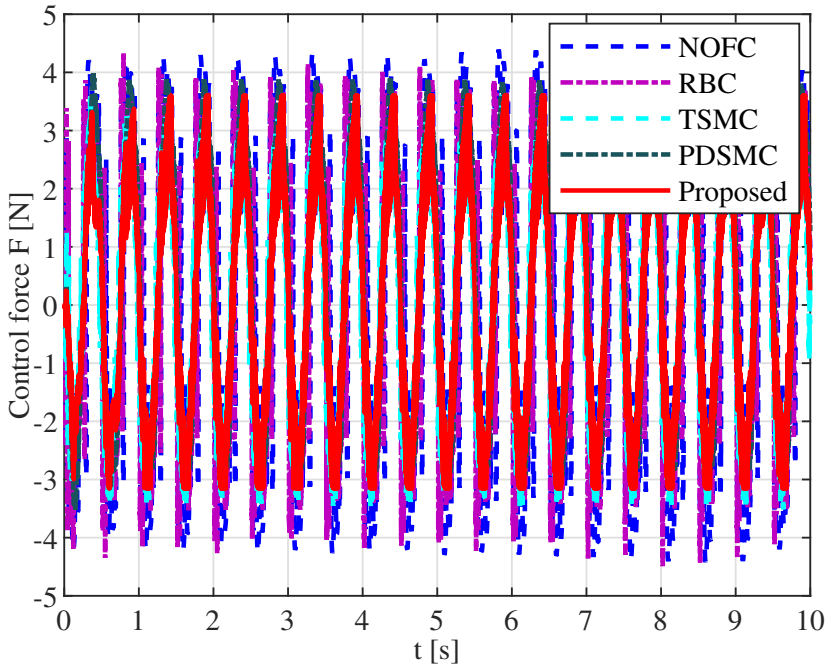

Fig. 4.6: Case 1: Control force F under the sinusoidal road

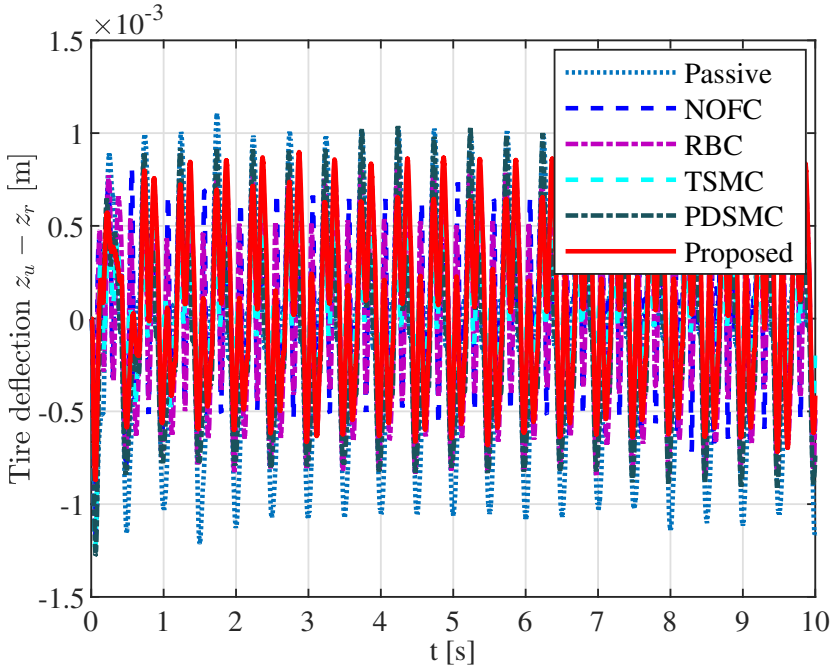

Fig. 4.7: Case 1: Tire deflection $z_s - z_u$ under the sinusoidal road

Larger $k_{\xi i}$ lead to smaller convergence time but higher gains in the auxiliary signal system (4.25). For $0 < \pi_1 < 1$, when π_1 approaches 0, there exist smaller convergence time and stronger robustness, however, it may cause chattering. When π_1 approaches 1, the smoother control input can be obtained with higher convergence time. For $\pi_2 > 1$, a large value of π_2 can reduce the convergence time but result in a high control input. Therefore, parameters should be carefully selected to balance the convergence time and control performance.

4.4 Comparative Experiments

In this section, to further present the control performance, some comparative experimental studies for a quarter-car AVSS are implemented (Fig. 4.2). The parameters of the AVSS are presented in Table 4.1.

The active vehicle suspension setup mainly consists of three independent plates/floors which are connected by springs and dampers but also move independently. The top plate refers to the vehicle body with the payload supported by the suspension damper and spring. A high-quality direct current motor is used as the active actuator for the sus-

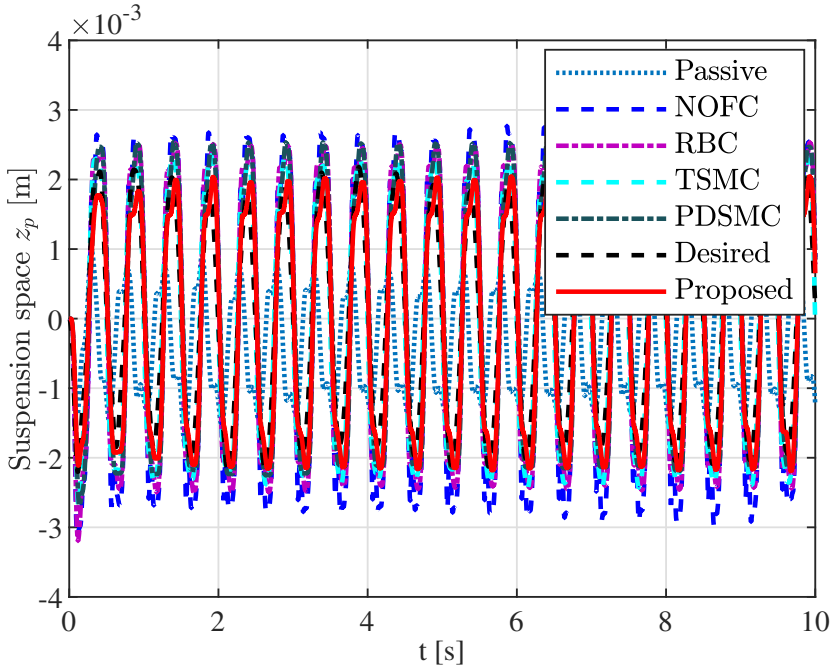

Fig. 4.8: Case 1: Suspension space z_p under the sinusoidal road

pension system to suppress the vibration and improve the ride comfort for passengers. The middle plate is connected to the bottom one by the tire spring damping system. The bottom plate represents the road providing the road inputs, which are generated by the bottom plate servo motor with the lead screw. More information of the experimental setup and procedure can be referred to [121]. Based on the hardware setup and the computer software, the sampling time is defined as 1ms.

The constraints on the displacement/velocity are selected as $\bar{\chi} = 0.002 + 0.04e^{-2t} + 0.0005\sin(2t)$, $\underline{\chi} = 0.002 + 0.03e^{-2t}$, $\underline{\vartheta} = 0.006 + 0.02e^{-2t} + 0.0005\cos(2t)$, $\bar{\vartheta} = 0.006 + 0.04e^{-2t}$.

Two types of road input profiles are considered in this section to verify the effectiveness of the proposed control.

Case 1: The sinusoidal road input is $z_r = 0.003\sin(4\pi t)$.

Case 2: The bump road input is given as

$$z_r = \begin{cases} h_b(1-\cos(8\pi t))/2, & 0 \le t \le t_b \\ 0, & t > t_b. \end{cases}$$

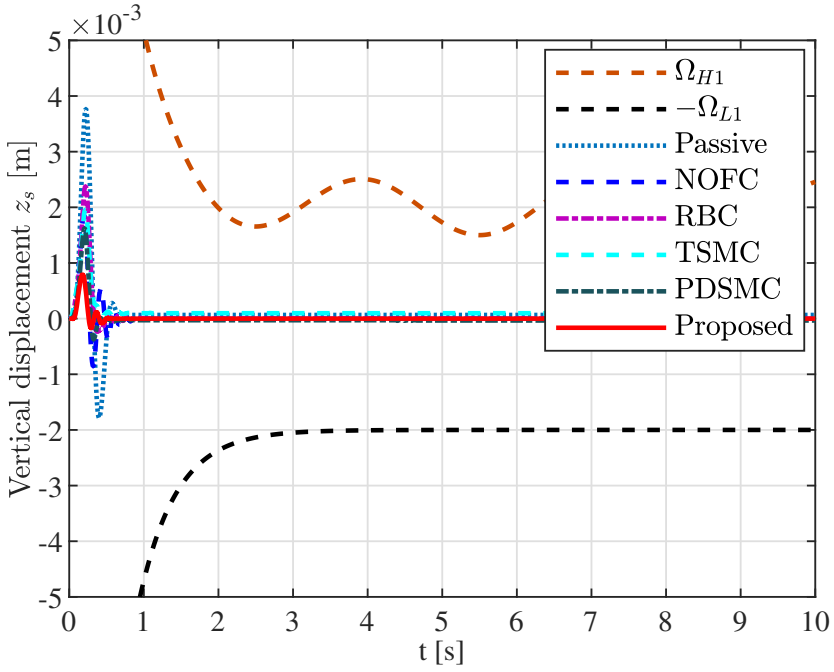

Fig. 4.9: Case 2: Vertical displacement z_s under the bump road

where $h_b = 0.004$m is the height of the bump.

The following six suspension systems are adopted.

1) Passive suspension system;

2) RBC: This abbreviation stands for the robust backstepping control adapted from [77];

3) NOFC: This abbreviation denotes the nonlinear output finite-time control from [121];

4) TSMC: This abbreviation is the terminal sliding mode control from [65];

5) PDSMC: This abbreviation is the proportional derivative sliding mode control from [96];

6) Proposed fixed-time safe-by-design controller.

Initial values of the AVSS are defined as zero for simplicity.

The RBC parameters are $k_1 = 100$, $k_2 = 20$, $k_3 = 2$. The NOFC parameters are $p = 1.5, q = 1, c_6 = 6, c_7 = 4, \alpha_1 = 0.2$. The TSMC parameters are $\alpha = 0.95, \lambda_1 = 12,$

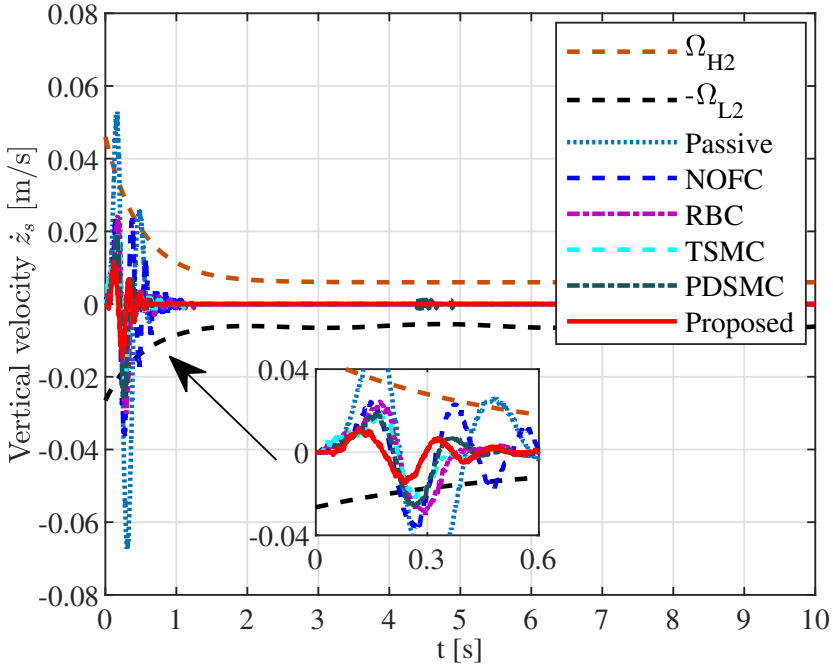

Fig. 4.10: Case 2: Vertical velocity $\dot{z}_s$ under the bump road

$\lambda_2 = 10$, $\alpha_1 = 7/9$, $\alpha_2 = 2$, $\alpha_3 = 0.5$, $k_1 = 1$, $k_2 = 8$. The PDSMC parameters are $\lambda = 30$, $k_p = 500$, $k_d = 500$, $k_s = 40$. Besides, the gains for the proposed control are $\pi_1 = 0.8$, $\pi_2 = 2$, $p = 2$, $k_{11} = 8$, $k_{12} = 5$, $k_{21} = 14$, $k_{22} = 20$, $\delta_i = 0.001$, $\rho_0 = 0.001$ and $\iota = 20$. In addition, the gains for the RBFNNs and the auxiliary state system are $\gamma_i = 10$, $\varrho_{i1} = 5$, $\varrho_{i2} = 8$, $\nu_i = 1$, $k_{\xi 1} = 5$, $k_{\xi 2} = 20$, $k_{\xi 3} = 20$.

The experimental results of six suspension systems are given in Figs. 4.3–4.8 for the sinusoidal road input and Figs. 4.9–4.14 for the bump road input. And the control gains for the bioinspired X-shaped structure are listed in Table 4.2. The RMS values of the settling time, vehicle body acceleration and energy consumption are given in Tables 4.3–4.5.

The performance in Figs. 4.3 and 4.9 depicts that the vertical displacement of the proposed control can always remain in the permitted range with the smallest steady-state error compared with other systems, while the passive system may exceed the constraints under the sinusoidal road input. Importantly, shown in Figs. 4.4 and 4.10, the asymmetric time-varying constraints on the vertical velocity are all violated in both cases for other systems. However, the vertical velocity of the proposed control stays strictly within the predefined range, which further ensures the enhanced safety requirements.

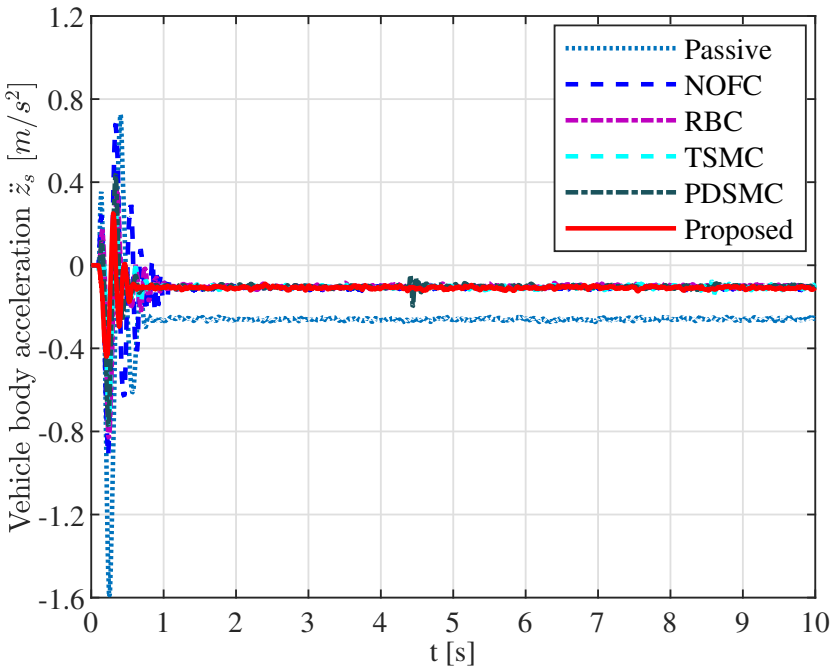

Fig. 4.11: Case 2: Vehicle body acceleration $\ddot{z}_s$ under the bump road

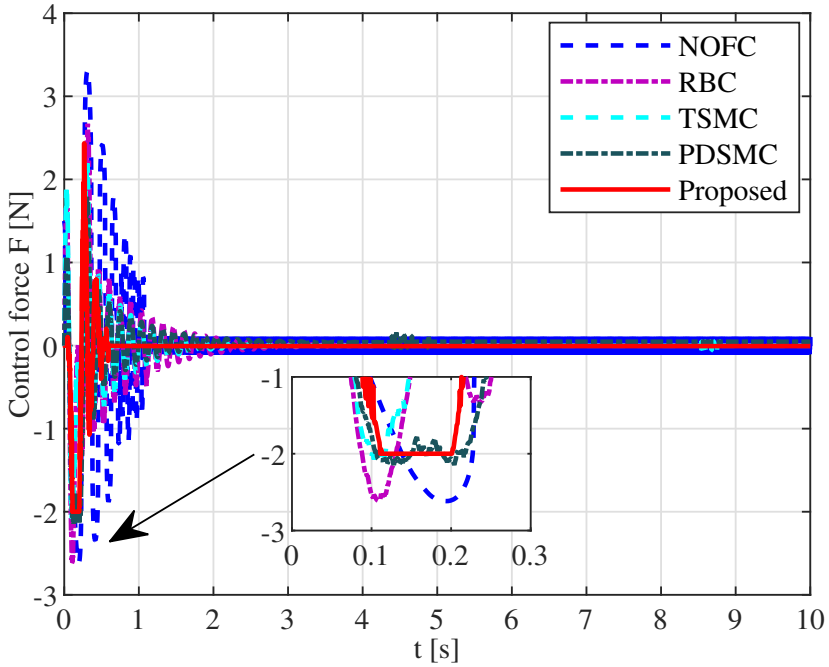

Fig. 4.12: Case 2: Control force F under the bump road

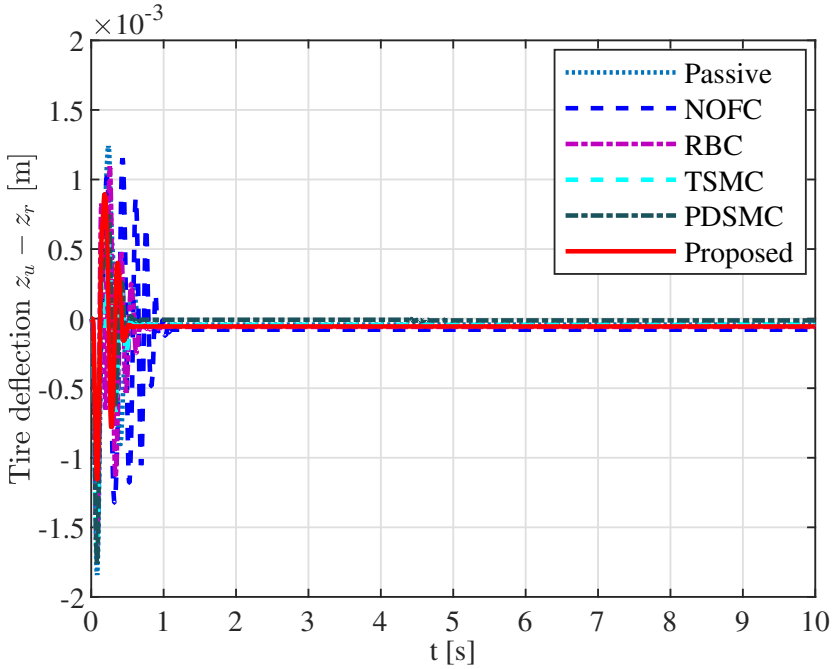

Fig. 4.13: Case 2: Tire deflection $z_u - z_r$ under the bump road

One can also easily observe that the convergence speed of the proposed control is higher than those of other controllers, which is demonstrated by the settling time under the bump road profile given in Table 4.3. The proposed control needs about 0.304s for the convergence which is only 50.8% of that for the NOFC while RBC, TSMC and PDSMC take about 0.453s, 0.405s and 0.372s, respectively. These results prove the advantages of driving safety and fixed-time convergence for the proposed control scheme.

The ride comfort is considered as an important factor in evaluating the performance of the AVSS, which is related to the vehicle body acceleration. One can conclude from Figs. 4.5 and 4.11 that the magnitude of the vehicle body acceleration of the proposed controller is considerably reduced compared with those of the passive system, RBC, NOFC, TSMC, and PDSMC. In fact, as observed from Table 4.4, the RMS values of the vehicle body acceleration drop dramatically by 78.5% under the sinusoidal road input and 61.6% under the bump road input, respectively, compared with those of the passive one. Hence, the ride comfort of the proposed controller is significantly improved for the AVSS.

The control forces for two cases are presented in Figs. 4.6 and 4.12, while the rel-

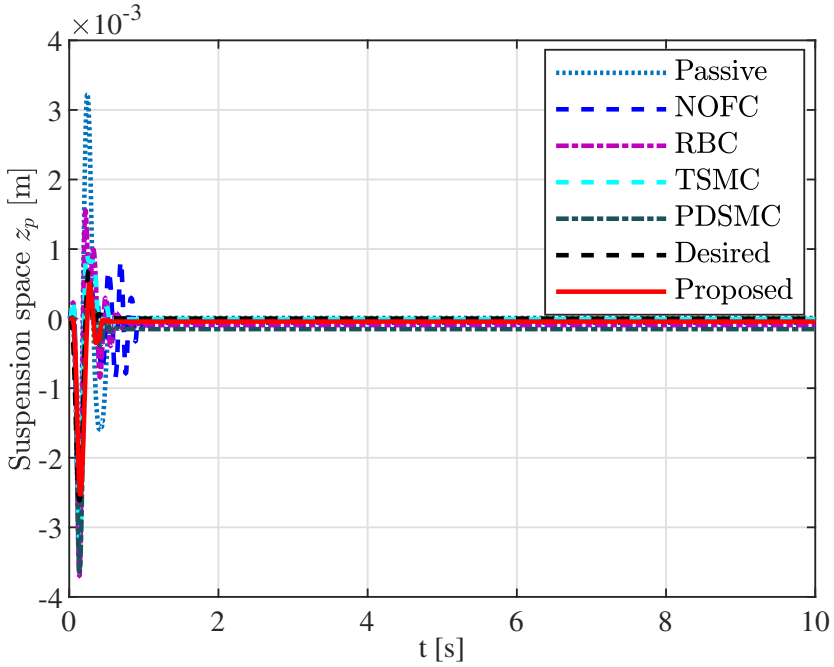

Fig. 4.14: Case 2: Suspension space z_p under the bump road

ative energy consumption is given in Table 4.5. And Fig. 4.12 indicates that the input saturation problem in Case 2 can be resolved when the saturation constraints are $F_{\max} = 3\text{N}$ and $F_{\min} = -2\text{N}$. Furthermore, the energy consumption of the proposed control (0.0249W and 0.0062W respectively) is less than that of the NOFC with a significant decrease by 67.8% and 48.8% for the sinusoidal and bump road inputs, respectively, while others consume more energy under two different road inputs. Therefore, compared with the RBC, NOFC, TSMC, and PDSMC, better ride comfort and enhanced safety requirements can be obtained by the proposed controller with less energy consumption.

The hardware limitations of the AVSS should be satisfied all the time including the tire deflection $z_u - z_r$ and suspension space z_p. As revealed in Figs. 4.7 and 4.13, the tire deflections of six suspension systems under two cases are within acceptable ranges. According to [96], the maximum suspension space is $z_{p,\max} = 3.8\text{cm}$. The maximum values of the suspension space in Figs. 4.8 and 4.14 are less than 3.8cm all the time. Therefore, driving safety can be further guaranteed.

4.5 Conclusion

A novel fixed-time safe-by-design control is proposed for the AVSSs with matched/unmatched disturbances, input saturations, and asymmetric time-varying displacement/velocity constraints. To ensure system safety, ATVBLFs are constructed to enforce both the vertical displacement/velocity to remain in the permitted ranges all the time. Furthermore, a novel fixed-time auxiliary state system is proposed to compensate for the input saturations. Compared with existing active suspension control techniques, fixed-time stability can be achieved in the proposed control with a significant improvement in ride comfort and energy consumption. Verified by the experimental results, the proposed control can guarantee fixed-time convergence, enhanced safety requirements, ride comfort, and energy-saving performance at the same time, with obvious advantages over other existing ones.

5 Predefined-Time Fault-Tolerant Control for AVSSs

Active vehicle suspension systems exhibit substantial vibration isolation capabilities, however, suffer from external disturbances, high energy consumption, risks of fault signals, limited transient performance, etc. In this chapter, a predefined-time fault-tolerant control scheme is proposed for active suspensions to improve ride comfort and reliability, and enhance energy conservation. The reference X-dynamics together with a conditional disturbance cancellation scheme are developed to avoid the cancellation of beneficial nonlinearities and beneficial disturbances, respectively, which can reduce energy consumption without any optimization calculation or hardware alteration. Importantly, the error signals can converge to a predefined bound within the predefined time interval. Both the settling time and the residual bound can be arbitrarily user-defined, which are independent of initial states and control gains. Especially, to avoid singularity and alleviate chattering, a continuous piecewise function and a quadratic fraction inequality are constructed. The utilization of the proposed predefined-time fault-tolerant control facilitates satisfactory ride comfort with low energy cost. Experimental results are presented to validate the superior control performance of the designed control scheme.

5.1 Introduction

Over the past few decades, vehicle suspension systems have been a hot research topic due to their critical roles in enhancing ride comfort and road holding of transportation vehicles [39]. Suspension systems can be categorized as passive, semi-active, and active vehicle suspension systems (AVSSs) [109]. Different from passive and semi-active suspensions, AVSSs provide higher effectiveness in improving ride comfort when vehicles

suffer from rough roads since extra actuators are equipped to generate eligible forces for providing/dissipating energy [132]. Thus, great efforts have been made on control designs for AVSSs, including sliding mode control [66], H-infinity control [110], adaptive control [40, 133], and so on. Certainly, AVSSs still need further improvement in both theoretical investigations and practical applications.

Finite-time control has been widely investigated on AVSSs with superior characteristics such as rapid convergence speed and high tracking accuracy [134–136]. An output-feedback finite-time control was proposed for AVSSs to compensate for external disturbances [121]. A terminal sliding mode control was designed for AVSSs with an adaptive disturbance observer [65]. However, the settling time of finite-time control is influenced by initial state conditions which are difficult to obtain in practice. Fixed-time control can effectively address the problem above which has also been applied to AVSSs. Considering the time-varying displacement constraints, a fixed-time fuzzy control was studied for AVSSs using an event-triggered mechanism [113]. Although remarkable advantages can be obtained with fixed-time control, the settling time estimation, calculated by control gains, is always vastly overestimated. Thus, it is not convenient to design and adjust the settling time to meet the requirements of practical applications. Recently, a predefined-time control method in [137, 138] can ensure the settling time to be arbitrarily user-defined in advance, which is completely independent of initial states and control gains. A predefined-time control was developed for AVSSs where the prescribed performance function was used to ensure the tracking errors converge to a neighborhood of zero [37]. However, the initial value of the prescribed performance function was assumed to be infinite which is not feasible in actual implementations, and the ultimate tracking accuracy can not be prior specified after the predefined settling time. Therefore, few research papers are involved in the predefined-time fault-tolerant control field for AVSSs in which the errors can converge to a prior-known residual bound during the user-defined settling time.

The high energy consumption becomes one of the main drawbacks of AVSSs compared with passive/semi-active suspensions, which limits the application in the trans-

portation industry [139, 140]. The reference X-dynamics, inspired by animals' legs, have been demonstrated to have beneficial stiffness and damping, which could be utilized in AVSS control to reduce energy consumption [30, 39, 69]. Using the reference X-dynamics, a fuzzy sliding mode method was constructed for AVSSs with dead zones and saturations [130]. It is noted that disturbances were considered as negative components in [130], which were canceled directly to ensure system stability. However, for external disturbances acting on the AVSSs, disturbance characteristics have not been well studied, nor the relationship with the expected motion. Although detrimental disturbances should be canceled out when the direction is inconsistent with expectation, beneficial ones should be retained for energy conservation. Based on the nonlinear disturbance observer, the disturbance classification was established in the conditional disturbance cancellation (CDC) method for AVSSs [141]. However, the finite-time stability of the AVSS scheme was not provided. More importantly, the chattering phenomenon could be severe due to the frequent switching between beneficial and detrimental disturbances when tracking errors oscillate around zero.

Furthermore, there always exist following difficulties in practical AVSS applications, which require more consideration to enhance the robustness and anti-vibration performance.

- *Actuator faults.* The actuators of AVSSs are sensitive to faults caused by the changing environment and aging, which may lead to the deterioration of the control results or even system instability [98, 142]. Therefore, various fault estimation and compensation methods were investigated for AVSSs to mitigate the effects of actuator faults [71, 143].

- *External disturbances.* External disturbances are also an important factor to affect the control performance and system robustness. Different methods, including the disturbance observers [144] and the adaptive compensation [95], can be applied to resolve external disturbances while keeping the system stability.

- *Singularity.* The singularity represents the inability to calculate control signals

when tracking errors equal zero, which often exists in previous control schemes [145, 146]. Discontinuous piecewise functions [147] and signum functions [148] are usually utilized to avoid the singularity problem.

- *Chattering.* The utilization of signum functions could improve system robustness which is common in disturbance observers [149], filters [150], CDC methods [35], and predefined-time controllers [151]. However, the rapid direction change may result in the chattering phenomenon when the tracking errors converge to the neighborhood of zero.

Motivated by the analysis above, the improvement of anti-vibration suspension performance has become a vital research topic. However, to the best of our knowledge, there is still no proper active suspension control scheme that can simultaneously attack these practical issues such as predefined-time/bound stability, actuator faults, external disturbances, singularity, chattering, and energy consumption problems. Therefore, a novel predefined-time fault-tolerant control is constructed in this chapter for AVSSs utilizing the reference X-dynamics and the CDC method. The key contributions of this article can be summarized in the following aspects:

1) To the best of our knowledge, this study should be the *first* endeavor to design a predefined-time fault-tolerant control for AVSSs to achieve predefined-time/bound stability, reduce energy consumption, address actuator faults, avoid singularity, alleviate chattering, and reject external disturbances. Different from existing finite/fixed-time control schemes [113, 134], both the settling time and the residual bound can be arbitrarily user-defined within physical ranges, which are independent of initial states and control gains.

2) A novel CDC method is designed including the predefined-time disturbance observer (PTDO), disturbance characteristic indicator (DCI), and switching logic function (SLF), which can cancel the detrimental disturbances and remain the beneficial ones simultaneously. Besides, beneficial stiffness/damping nonlinearities

are employed in the control design using the reference X-dynamics. The integration of the CDC method and reference X-dynamics can reduce energy consumption. No optimization calculation or hardware alteration [139, 140] is required in the control design to attain energy conservation while ensuring satisfactory vibration resistance.

3) Distinguished from existing predefined-time controllers [145, 146], the proposed control design is nonsingular due to the continuous piecewise function and the quadratic fraction inequality. The nonsingular PTDO and the nonsingular predefined-time filter are proposed to estimate the lumped disturbances (external disturbances and actuator faults) and to avoid the explosion of computational complexity, respectively. Moreover, the discontinuous signum functions can be avoided compared with previous control techniques [35, 149–151], thus, the chattering phenomenon is alleviated.

The outline of this chapter is presented as follows. Section 5.2 provides the problem statement. The main results are given in Section 5.3, including the reference X-dynamics, PTDO design, CDC method design, and predefined-time fault-tolerant control. Section 5.4 presents a variety of experimental results to showcase the superior control performance of the proposed controller. Finally, the chapter concludes in Section 5.5.

5.2 Problem statement

The dynamical model of a quarter-car AVSS can be presented as [87]

$$\begin{aligned} m_s\ddot{z}_s &= -R_s(z_s, z_u) - R_d(\dot{z}_s, \dot{z}_u) + d_1 + F(u) \\ m_u\ddot{z}_u &= R_s(z_s, z_u) + R_d(\dot{z}_s, \dot{z}_u) - R_t(z_u, z_r) \\ &\quad - R_b(\dot{z}_u, \dot{z}_r) + d_2 - F(u) \end{aligned} \tag{5.1}$$

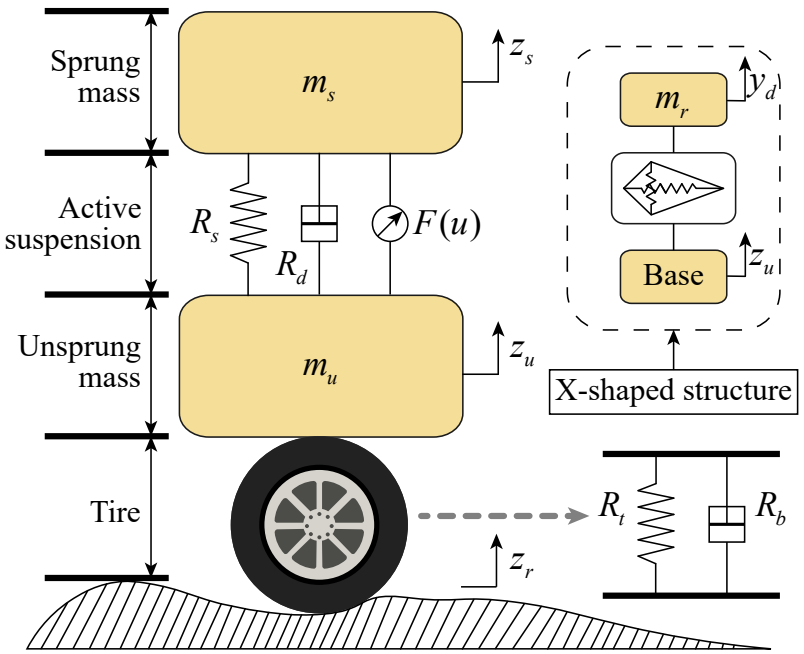

Fig. 5.1: The AVSS scheme

where m_s and m_u stand for the sprung and unsprung masses, respectively; z_s, z_u, and z_r denote the vertical displacement of the sprung mass, unsprung mass, and road excitation, respectively; d_1 and d_2 are the unknown external disturbances; $F(u)$ is the control input with actuator faults which will be defined later; $R_s(z_s, z_u)$ and $R_d(\dot{z}_s, \dot{z}_u)$ are the spring force and damper force of the suspension components, respectively; $R_t(z_u, z_r)$ and $R_b(\dot{z}_u, \dot{z}_r)$ represent the elasticity force and the damping force of the tire, respectively. The detailed expressions of $R_s(z_s, z_u)$, $R_d(\dot{z}_s, \dot{z}_u)$, $R_t(z_u, z_r)$, and $R_b(\dot{z}_u, \dot{z}_r)$ are given as [87]

$$\begin{aligned} R_s(z_s, z_u) &= w_{s1}(z_s - z_u) + w_{s2}(z_s - z_u)^3 \\ R_d(\dot{z}_s, \dot{z}_u) &= \begin{cases} w_{d1}(\dot{z}_s - \dot{z}_u) & \text{if} \quad \dot{z}_s - \dot{z}_u > 0 \\ w_{d2}(\dot{z}_s - \dot{z}_u) & \text{if} \quad \dot{z}_s - \dot{z}_u \leq 0 \end{cases} \\ R_t(z_u, z_r) &= w_t(z_u - z_r) \\ R_b(\dot{z}_u, \dot{z}_r) &= w_b(\dot{z}_u - \dot{z}_r) \end{aligned} \tag{5.2}$$

where w_{s1} and w_{s2} denote linear and nonlinear stiffness coefficients, respectively; w_{d1} and w_{d2} are damping coefficients of elongation and compression, respectively; w_t and w_b are stiffness and damping coefficients of the tire, respectively.

The reference X-dynamics [39] are integrated into this control scheme with optimal nonlinear stiffness and damping for vibration reduction (refer to Fig. 5.1). The suspension space and its time derivative are defined as $z_p = z_s - z_u$, $\dot{z}_p = \dot{z}_s - \dot{z}_u$. The energy consumption can be reduced when letting the suspension space z_p track the output of the reference X-dynamics y_d, which will be defined later.

With the coordinate transformation $x_1 = z_p$ and $x_2 = \dot{z}_p$, the AVSS model can be rewritten as

$$\begin{cases} \dot{x}_1 = x_2 \\ M\dot{x}_2 = G(\bar{x}) + F(u) + d \end{cases} \tag{5.3}$$

where $M = m_s m_u/(m_s + m_u)$ is a mass-related constant, $G(\bar{x}) = -R_s(z_s, z_u) - R_d(\dot{z}_s, \dot{z}_u) + \frac{m_s}{m_s+m_u}(R_t(z_u, z_r) + R_b(\dot{z}_u, \dot{z}_r))$ represents the known system dynamics with the state vector $\bar{x} = [z_s, \dot{z}_s, z_u, \dot{z}_u]^T$, and $d = \frac{m_s}{m_s+m_u}d_1 - \frac{m_s}{m_s+m_u}d_2$.

The actuator fault model is considered as

$$F(u) = \rho u + u_0(t) \tag{5.4}$$

where $0 < \rho \leq 1$ denotes the loss-of-effectiveness (LOE) factor, $u_0(t) \geq 0$ is the time-varying bias fault. Several cases can be represented by the actuator fault model (5.4): 1) fault-free case for $\rho = 1$ and $u_0(t) = 0$; 2) only bias fault exists for $\rho = 1$ and $u_0(t) \neq 0$; 3) only LOE fault exists for $0 < \rho < 1$ and $u_0(t) = 0$; 4) and both LOE fault and bias fault exist for $0 < \rho < 1$ and $u_0(t) \neq 0$. One should note that the stuck fault for $\rho = 0$ is not included due to only one actuator.

Then the AVSS model can be represented as follows

$$\begin{cases} \dot{x}_1 = x_2 \\ M\dot{x}_2 = G(\bar{x}) + u + D \end{cases} \tag{5.5}$$

where $D = (\rho - 1)u + u_0 + d$ denotes the lumped disturbance variable including the unknown external disturbances and actuator faults.

Assumption 5.1. *The lumped disturbance D is bounded by $|D| \leq \bar{D}$ with an unknown*

constant $\bar{D} > 0$.

Remark 5.1. The boundedness of the lumped disturbance D is adopted in existing fault-tolerant controllers [98, 142]. Specifically, when the AVSSs encounter unbounded external disturbances or actuator faults, the AVSS dynamics (5.1) may be uncontrollable. Thus, Assumption 5.1 is reasonable.

Lemma 5.1 ([152]). *For* $\varepsilon > 0$ *and* $x \in \Re$*, we have* $0 \leq |x| - \frac{x^2}{\sqrt{x^2+\varepsilon^2}} \leq \varepsilon$.

Lemma 5.2 ([153]). *For* $\forall x \in \Re$ *and* $\iota > 0$*, the inequality* $0 \leq |x| - x\tanh(x/\iota) \leq \kappa\iota$ *holds with* $\kappa = 0.2785$.

Lemma 5.3 ([148]). *Consider* $z_1, z_2, ..., z_n > 0$, $0 < \alpha \leq 1$, *and* $\beta > 1$. *Then the following inequalities hold*

$$\begin{aligned} (\sum_{i=1}^{n} z_i)^{\alpha} &\leq \sum_{i=1}^{n} z_i^{\alpha} \\ (\sum_{i=1}^{n} z_i)^{\beta} &\leq n^{\beta-1} \sum_{i=1}^{n} z_i^{\beta}. \end{aligned} \tag{5.6}$$

Lemma 5.4 ([154]). *Consider the nonlinear system* $\dot{x} = f(t, x)$. *If there exists a positive definite Lyapunov function* V *satisfying*

$$\dot{V} \leq -\frac{\pi}{\gamma T_c}(V^{1-\frac{\gamma}{2}} + V^{1+\frac{\gamma}{2}}) + \Xi \tag{5.7}$$

where $0 < \gamma < 1$, $T_c > 0$ *and* $0 < \Xi < \infty$*, then* V *is globally practical predefined-time stable (GPPTS) with the convergence region*

$$\left\{ \lim_{t \to T_p} x \middle| V \leq \min\left\{ \left(\frac{2\gamma T_c \Xi}{\pi}\right)^{\frac{2}{2-\gamma}}, \left(\frac{2\gamma T_c \Xi}{\pi}\right)^{\frac{2}{2+\gamma}} \right\} \right\} \tag{5.8}$$

and T_p *is the settling time satisfying* $T_p = \sqrt{2}T_c$.

Lemma 5.5. *Consider the nonlinear system* $\dot{x} = f(t, x)$. *If there exists a positive definite Lyapunov function* V *satisfying*

$$\dot{V} \leq -\frac{\pi}{\gamma T_c \sqrt{k_1 k_2}}(k_1 V^{1-\frac{\gamma}{2}} + k_2 V^{1+\frac{\gamma}{2}}) - cV + \Xi \tag{5.9}$$

where $0 < \gamma < 1$, $T_c > 0$, $k_1 > 0$, $k_2 > 0$ *and* $0 < \Xi < \infty$, *then* V *is semi-globally practical predefined-time stable (SGPPTS) with the convergence region* $\Omega = \{\lim_{t\to T_p} x | V \leq \Xi/c\}$ *and* T_p *is the settling time satisfying* $T_p = T_c$.

Proof: Two cases are considered in the proof process.

Case 1: If $x \notin \Omega$ which means $V > \Xi/c$, it becomes

$$\dot{V} \leq -\frac{\pi}{\gamma T_c \sqrt{k_1 k_2}}(k_1 V^{1-\frac{\gamma}{2}} + k_2 V^{1+\frac{\gamma}{2}}), \forall x \notin \Omega. \tag{5.10}$$

The settling time is

$$\begin{aligned} T_p &\leq -\int_{V(x_0)}^{0} \frac{dV}{\frac{\pi}{\gamma T_c \sqrt{k_1 k_2}}(k_1 V^{1-\frac{\gamma}{2}} + k_2 V^{1+\frac{\gamma}{2}})} \\ &= \frac{\gamma T_c \sqrt{k_1 k_2}}{k_1 \pi} \int_{0}^{V(x_0)} \frac{dV}{V^{1-\frac{\gamma}{2}}(1 + (\sqrt{\frac{k_2}{k_1}})^2 (V^{\frac{\gamma}{2}})^2)} \\ &= T_c \frac{2}{\pi} \text{arctan}(\sqrt{\frac{k_2}{k_1}} V^{\frac{\gamma}{2}}(x_0)). \end{aligned} \tag{5.11}$$

Since the initial state x_0 is bounded, then $0 < \text{arctan}(\sqrt{\frac{k_2}{k_1}} V^{\frac{\gamma}{2}}(x_0)) < \frac{\pi}{2}$. Thus, the settling time is given by $T_p = T_c$.

Case 2: If $x \in \Omega$, the trajectory of x will stay in the region Ω once it reaches the boundary of Ω since $\dot{V} \leq 0$.

From the two cases above, one can obtain $x \in \Omega$ for $\forall t \geq T_p$. Therefore, there always exists a bounded constant $\delta_1 > 0$ such that $|x| \leq \delta_1$ for $\forall t \geq T_p$, indicating that the origin of the system is SGPPTS. The proof is thus completed. ■

Remark 5.2. One should note that Lemma 5.4 is only the special case of Lemma 5.5 with $k_1 = k_2 = 1$ and $c = 0$, which extends the predefined-time stability in [154]. The parameters k_1 and k_2 are used to adjust the transient performance during the convergence process while the predefined-time stability remains. Compared with existing predefined-time designs [154], the convergence region Ω, which can be adjusted by the parameter c, is independent of the settling time $T_p = T_c$ due to the reliance of different parameters. Besides, the settling time T_p of the SGPPTS system (5.9) can be character-

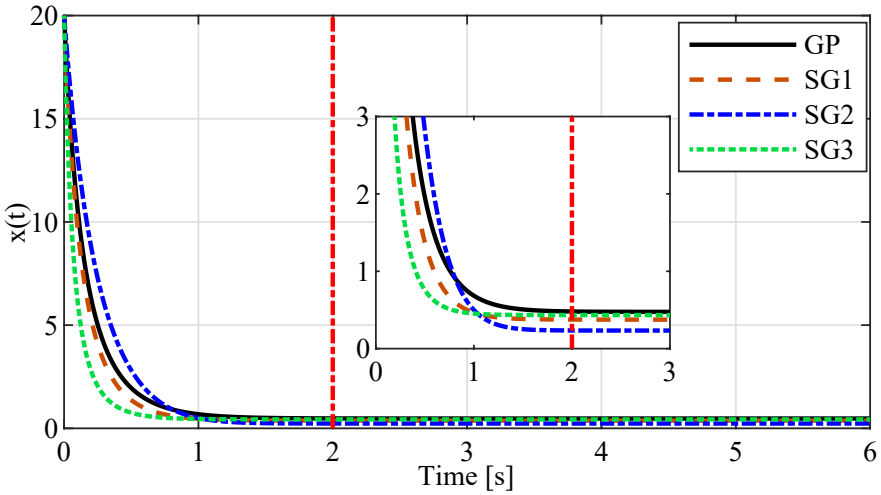

Fig. 5.2: Response of $x(t)$ under different parameters

ized with the only parameter T_c rather than initial states or control gains, which is easy and intuitive for tuning compared with existing finite/fixed-time controllers [113, 134]. Therefore, the proposed SGPPTS system (5.9) provides more beneficial features for practical applications.

To further illustrate the predefined-time performance, we take $V = |x|$ as an example. For comparison, $T_c = 2$, $\gamma = 7/9$, $\Xi = 2$ are selected for GPPTS in Lemma 5.4 (Line GP). Besides, the responses of $x(t)$ under three parameter sets for SGPPTS in Lemma 5.5 are given in Fig. 5.2, including 1) Line SG1: $k_1 = 1$, $k_2 = 1$, $c = 1$, 2) Line SG2: $k_1 = 5$, $k_2 = 1$, $c = 0.01$, 3) Line SG3: $k_1 = 1$, $k_2 = 5$, $c = 0.01$. Compared with GPPTS, Line SG1 indicates that the convergence region Ω can be adjusted by c. Line SG2 shows that higher k_1 obtains a slower convergence rate at the initial stage, leading to potentially less initial actuator torque. Line SG3 presents that higher k_2 accelerates the convergence speed. Thus, although the system state $x(t)$ can all converge within predefined time $T_c = 2s$ under GPPTS and SGPPTS, higher flexibility can be obtained utilizing the proposed SGPPTS.

5.3 Main results

5.3.1 Model of the reference X-dynamics

A two-layer X-dynamical structure inspired by animals' legs is developed with springs, rotating joints, and connecting rods [39, 131]. The geometric relationship $\ell_1 \sin\phi_1 = \ell_2 \sin\phi_2$ holds, where ℓ_1 and ℓ_2 are the rod length, ϕ_1 and ϕ_2 are the initial angles. According to [73], the outcome of the reference X-dynamics is used as the desired suspension space y_d, and then beneficial nonlinear stiffness/damping effects can be integrated into the controller to achieve satisfactory anti-vibration results with energy-saving performance. The model of the reference X-dynamics is given as [96]

$$m_r \ddot{y}_d + \varsigma_1 + \sigma_v y_d / n^2 + \varrho_1 \dot{y}_d + \varrho_2 n_x \varsigma_2 \dot{y}_d = -m_r \ddot{z}_u \tag{5.12}$$

where

$$\begin{aligned} \varsigma_1 &= \frac{\sigma_h \Theta}{2n}\big(\ell_1 \cos\phi_1 - \sqrt{\ell_1^2 - \Theta^2} + \ell_2 \cos\phi_2 \\ &\quad - \sqrt{\ell_2^2 - \Theta^2}\big)\big(1/\sqrt{\ell_1^2 - \Theta^2} - 1/\sqrt{\ell_2^2 - \Theta^2}\big) \\ \varsigma_2 &= \big(\ell_1/(2n\sqrt{\ell_1^2 - \Theta^2}) - \ell_2/(2n\sqrt{\ell_2^2 - \Theta^2})\big)^2 \\ \Theta &= \ell_1 \sin\phi_1 + y_d/(2n) = \ell_2 \sin\phi_2 + y_d/(2n) \end{aligned} \tag{5.13}$$

and m_r is the object mass, $n = 2$ means the layer, $n_x = 3n - 1$ is the joint number, σ_v and σ_h represent the vertical/horizontal spring stiffness, ϱ_1 and ϱ_2 are the air resistance/rotating friction coefficients.

Assumption 5.2 ([96]). *To ensure the output boundedness, we denote $\varpi_1 < \ddot{y}_d < \varpi_2$ with known bounds ϖ_1 and ϖ_2.*

Unlike existing anti-vibration control designs for AVSSs to set the desired trajectories as zero directly, the dynamic outcome of the reference X-dynamics is regarded as the reference suspension space, which could avoid canceling beneficial stiffness/damping nonlinearities. Advantageous AVSS characteristics are thus retained in the proposed controller design, which would lead to satisfactory anti-vibration performance with less

control effort. Therefore, thanks to the reference X-dynamics together with the following CDC method, far less energy consumption is required for the proposed control method leading to energy-saving performance.

5.3.2 Design of the PTDO

Define a new state variable $\vartheta = \psi - x_2$. The variable ψ is obtained by

$$\dot{\psi} = M^{-1}(G(\bar{x}) + u + \hat{D}) \tag{5.14}$$

where u is the control input which will be given later, $\hat{D}$ is the estimation of the lumped disturbance D expressed as

$$\begin{aligned} \hat{D} &= -\frac{\vartheta \xi_0^2}{\sqrt{\vartheta^2 \xi_0^2 + \varepsilon_0^2}} \\ \xi_0 &= \frac{\Gamma_{10} \pi \vartheta^{1-\gamma_0}}{\gamma_0 T_d \Lambda_{10}} + \frac{\Gamma_{20} \pi \vartheta^{1+\gamma_0}}{\gamma_0 T_d \Lambda_{20}} + \lambda_0 \tanh(\frac{\vartheta}{\iota_0}) \end{aligned} \tag{5.15}$$

where $\gamma_0 = p_0/q_0$, p_0 and q_0 are positive odd integers satisfying $0 < p_0 < q_0$, $\varepsilon_0 > 0$ and $\iota_0 > 0$ are small constants, $T_d > 0$, $\lambda_0 > 0$, $\Gamma_{10} = M^{1-\gamma_0/2}$, $\Gamma_{20} = M^{1+\gamma_0/2}$, $\Lambda_{10} = 2^{1-\gamma_0/2}$, $\Lambda_{20} = 2^{1+\gamma_0/2}$, and $V_0 = \frac{1}{2} M \vartheta^2$ denotes the Lyapunov function.

Theorem 5.1. *Considering the suspension dynamic model (5.5) with Assumption 5.1, a continuous PTDO is proposed as (5.14)-(5.15) where the lumped disturbance can be estimated within a predefined time* $T_{p1} = \sqrt{2} T_d$.

Proof: The time derivative of the Lyapunov function V_0 is

$$\begin{aligned} \dot{V}_0 &= \vartheta M \dot{\vartheta} = \vartheta (M\dot{\psi} - M\dot{x}_2) \\ &= -\frac{\vartheta^2 \xi_0^2}{\sqrt{\vartheta^2 \xi_0^2 + \varepsilon_0^2}} - \vartheta D. \end{aligned} \tag{5.16}$$

Applying Lemma 5.1, we have $-\frac{\vartheta^2 \xi_0^2}{\sqrt{\vartheta^2 \xi_0^2 + \varepsilon_0^2}} \leq -|\vartheta \xi_0| + \varepsilon_0 \leq -\vartheta \xi_0 + \varepsilon_0$. Noting

Lemma 5.2 becomes $-\lambda_0\vartheta\tanh(\frac{\vartheta}{\iota_0}) \leq -\lambda_0|\vartheta| + \lambda_0\kappa\iota_0$, then (5.16) becomes

$$\begin{aligned}\dot{V}_0 \leq & -\frac{\Gamma_{10}\pi\vartheta^{2-\gamma_0}}{\gamma_0 T_d \Lambda_{10}} - \frac{\Gamma_{20}\pi\vartheta^{2+\gamma_0}}{\gamma_0 T_d \Lambda_{20}} - (\lambda_0 - |D|)|\vartheta| \\ & + \varepsilon_0 + \lambda_0\kappa\iota_0 \\ & \leq -\frac{\pi}{\gamma_0 T_d}\big((\frac{1}{2}M\vartheta_0^2)^{1-\frac{\gamma_0}{2}} + (\frac{1}{2}M\vartheta_0^2)^{1+\frac{\gamma_0}{2}}\big) \\ & + \varepsilon_0 + \lambda_0\kappa\iota_0 \\ & \leq -\frac{\pi}{\gamma_0 T_d}(V_0^{1-\frac{\gamma_0}{2}} + V_0^{1+\frac{\gamma_0}{2}}) + \Xi_0\end{aligned} \tag{5.17}$$

where λ_0 is selected $\lambda_0 \geq \bar{D}$ and $\Xi_0 = \varepsilon_0 + \lambda_0\kappa\iota_0$.

According to Lemma 5.4, V_0 is GPPTS with a small region

$$\Big\{\lim_{t\to T_{p1}} \vartheta \Big| V_0 \leq \min\Big\{\Big(\frac{2\gamma_0 T_d \Xi_0}{\pi}\Big)^{\frac{2}{2-\gamma_0}}, \Big(\frac{2\gamma_0 T_d \Xi_0}{\pi}\Big)^{\frac{2}{2+\gamma_0}}\Big\}\Big\} \tag{5.18}$$

and $T_{p1} = \sqrt{2}T_d$ is the settling time. Thus, ϑ is bounded which leads to $\lim_{t\to\infty}\dot{\vartheta} = 0$. The estimation error can be obtained by $\tilde{D} = \hat{D} - D = \dot{\vartheta}$. Therefore, for $\forall t \geq T_{p1}$, there exists a small constant $\delta_p > 0$ with $|\tilde{D}| \leq \delta_p$. According to (5.15), there also exists a positive constant $\delta_d > 0$ for the lumped disturbance estimation $\hat{D}$ with $|\hat{D}| \leq \delta_d$. Then the proof of Theorem 5.1 is completed. ■

Remark 5.3. Compared with nonlinear disturbance observers, the estimation error of the proposed disturbance observer can converge to a small region within a predefined time T_{p1}. Besides, the singularity issue of existing PTDOs [155] can be avoided and the chattering phenomenon [149] can be alleviated due to the continuity of the proposed PTDO.

5.3.3 Design of the CDC method

The lumped disturbance is further evaluated by considering the amplitude and directionality from the viewpoint of disturbance characteristics. In conventional AVSS controllers, the lumped disturbance is always canceled directly to ensure the system stability using the norm-based boundedness technique while its directionality is seldom

involved. However, the disturbance direction reveals how the lumped disturbance affects the tracking performance. For example, if the direction of the lumped disturbance is consistent with that of the expected motion, the tracking performance could be fostered by the lumped disturbance. Thus, the connection between the disturbance characteristics and the system stability deserves further investigation. Unlike the methods in [35, 156], a novel CDC is designed in this manuscript to make full use of the beneficial disturbances and to attenuate the chattering phenomenon simultaneously.

The coordinate transformation is considered

$$\begin{aligned} z_1 &= x_1 - y_d \\ z_2 &= x_2 - \hat{\alpha}_1 \end{aligned} \tag{5.19}$$

where y_d is the desired suspension space, and $\hat{\alpha}_1$ is the filtered virtual input signal, which will be defined later.

The CDC method mainly consists of the estimated disturbance $\hat{D}$ obtained from the PTDO, the revised DCI, and the novel SLF.

Definition 5.1. *For the AVSSs (5.5), a revised DCI is constructed as follows*

$$P = \frac{z_1 \hat{D}}{\sqrt{z_1^2+\varepsilon_1^2}\sqrt{\hat{D}^2+\varepsilon_2^2}} \tag{5.20}$$

where ε_1 and ε_2 are small positive constants.

From the DCI, one can obtain that $P > 0$ if $z_1\hat{D} > 0$, and vice versa. Thus, the direction consistency of the state z_1 and the disturbance estimation $\hat{D}$ can be reflected by the DCI (5.20). Therefore, we can conclude that $P < 0$ denotes the disturbance characteristic is beneficial, $P > 0$ means the disturbance characteristic is detrimental, and $P = 0$ indicates the disturbance characteristic is nil.

The lumped disturbance for the AVSSs can be classified into beneficial/nil/detrimental disturbance characteristics in the directional evaluation method DCI (5.20) using Definition 5.1. When the beneficial disturbance occurs, the tracking performance could be benefited from the lumped disturbance which can be kept in the controller to save en-

ergy. Thus, it is natural to incorporate the following SLF to decide whether the lumped disturbance is canceled or retained in the control process.

Furthermore, a novel SLF is designed as

$$H(P) = \begin{cases} \tanh(\frac{P}{\iota_1}), & \text{if} \quad P \geq 0 \\ 0, & \text{if} \quad P < 0 \end{cases} \tag{5.21}$$

where $\iota_1 > 0$ is a small constant.

The beneficial stiffness/damping nonlinearities and beneficial lumped disturbance are retained in the proposed control method by using the reference X-dynamics and the CDC method, respectively. Thus, less control efforts are needed to achieve satisfactory anti-vibration performance which leads to energy-efficient performance.

Remark 5.4. The estimation of the lumped disturbance $\hat{D}$ rather than D is employed in the DCI (5.20) since the actual lumped disturbance is difficult to be obtained directly. Even if the direction of the lumped disturbance is wrongly estimated during some periods, the stability of the closed-loop control scheme can remain.

Remark 5.5. Traditional CDC methods [35, 141, 156], where the DCI is given as $P = \text{sign}(z_1)\text{sign}(\hat{D})$ and the SLF is denoted as $H(P) = 1$ for $P \geq 0$ and $H(P) = 0$ for $P < 0$, will lead to a severe chattering problem. To attack this issue, a novel CDC method is proposed in this manuscript with the revised continuous DCI (5.20) and the continuous SLF (5.21) to alleviate the chattering phenomenon. Actually, the gains ε_1, ε_2, and ι_1 are used as a trade-off between achieving the ideal beneficial disturbance utilization and mitigating the chattering effects.

5.3.4 Predefined-time fault-tolerant control

A predefined-time fault-tolerant control is further proposed for AVSSs based on the PTDO, reference X-dynamics, and CDC technique.

The predefined-time filter is given as

$$\dot{\hat{\alpha}}_1 = -\frac{\eta\xi_f^2}{\sqrt{\eta^2\xi_f^2+\varepsilon_3^2}} - \frac{c+2}{2}\eta, \quad \hat{\alpha}_1(0) = \alpha_1(0) \tag{5.22}$$

with

$$\xi_f = \frac{k_1\pi\eta^{1-\gamma}}{\gamma T_c\Lambda_1\sqrt{k_1k_2}} + \frac{k_2\pi\eta^{1+\gamma}}{\gamma T_c\Lambda_2\sqrt{k_1k_2}} \tag{5.23}$$

where $c > 0$, $k_1 > 0$, $k_2 > 0$, $\gamma = p/q$ with $0 < p < q$, p and q denote positive odd integers, $\varepsilon_3 > 0$ is a small constant, $T_c > 0$, $\Lambda_1 = 2^{1-\gamma/2}$ and $\Lambda_2 = 2^{1+\gamma/2}\cdot 3^{-\gamma/2}$, α_1 is the virtual control signal which will be defined later, and $\eta = \hat{\alpha}_1 - \alpha_1$ denotes the filter error.

Remark 5.6. The filtering error η in existing control methods can only converge to the region near the equilibrium when the time approaches infinity, which is not suitable for the predefined-time controllers [150]. Thus, a predefined-time filter is developed in this chapter such that the convergence time of the filtering error η can be arbitrarily user-defined, which can further improve the control performance.

Remark 5.7. Compared with traditional filters, both the singularity and discontinuity problems can be simultaneously avoided by the utilization of the quadratic fraction inequality. Hence, the chattering phenomenon can be reduced.

According to the coordinate transformation (5.19) and the filter error definition, the time derivative of the tracking error becomes

$$\dot{z}_1 = \dot{x}_1 - \dot{y}_d = z_2 + \alpha_1 + \eta - \dot{y}_d. \tag{5.24}$$

Here, the virtual control signal is designed as

$$\begin{aligned} \alpha_1 &= \dot{y}_d - \frac{c+2}{2}z_1 - \frac{z_1\xi_1^2}{\sqrt{z_1^2\xi_1^2+\varepsilon_4^2}} \\ \xi_1 &= \frac{k_1\pi\zeta}{\gamma T_c\Lambda_1\sqrt{k_1k_2}} + \frac{k_2\pi z_1^{1+\gamma}}{\gamma T_c\Lambda_2\sqrt{k_1k_2}} \end{aligned} \tag{5.25}$$

where $\varepsilon_4 > 0$ is a small constant, and ζ is the continuous piecewise function

$$\zeta = \begin{cases} z_1^{1-\gamma}, & \text{if} \quad |z_1| > \epsilon_1 \\ \mu_1 z_1 + \mu_2 z_1^3, & \text{if} \quad |z_1| \leq \epsilon_1 \end{cases} \tag{5.26}$$

with $\mu_1 = (2+\gamma)\epsilon_1^{-\gamma}$, $\mu_2 = -(1+\gamma)\epsilon_1^{-2-\gamma}$.

Remark 5.8. From the design of the continuous virtual control signal (5.25), one can observe that the time derivative of the virtual control signal (5.25) still exists when the tracking error z_1 approaches zero due to the continuous piecewise function. Furthermore, it is easy to verify that for the AVSSs (5.5) with bounded initial states, $\dot{\alpha}_1$ is bounded by $|\dot{\alpha}_1| \leq \bar{\alpha}_1$ with unknown constant $\bar{\alpha}_1 > 0$.

Define the following Lyapunov function candidate as

$$V_1 = \frac{1}{2} z_1^2 + \frac{1}{2} \eta^2. \tag{5.27}$$

Differentiating (5.27) yields

$$\begin{aligned} \dot{V}_1 &= z_1(z_2 + \alpha_1 + \eta - \dot{y}_d) + \eta\dot{\eta} \\ &= z_1 z_2 - \frac{c+2}{2} z_1^2 - \frac{z_1^2 \xi_1^2}{\sqrt{z_1^2 \xi_1^2 + \varepsilon_4^2}} + z_1 \eta + \eta\dot{\eta}. \end{aligned} \tag{5.28}$$

Applying Lemma 5.1 and Young's inequality, one can obtain

$$\begin{aligned} -\frac{z_1^2 \xi_1^2}{\sqrt{z_1^2 \xi_1^2 + \varepsilon_4^2}} \leq -|z_1 \xi_1| + \varepsilon_4 \leq -z_1 \xi_1 + \varepsilon_4 \\ z_1 \eta \leq \frac{1}{2} z_1^2 + \frac{1}{2} \eta^2. \end{aligned} \tag{5.29}$$

Considering the predefined-time filter (5.22) and $|\dot{\alpha}_1| \leq \bar{\alpha}_1$, we have

$$\begin{aligned}\eta\dot{\eta} &= \eta\dot{\hat{\alpha}}_1 - \eta\dot{\alpha}_1 \\ &\leq -\frac{\eta^2\xi_f^2}{\sqrt{\eta^2\xi_f^2+\varepsilon_3^2}} - \frac{c+2}{2}\eta^2 + \frac{1}{2}\eta^2 + \frac{1}{2}\bar{\alpha}_1^2 \\ &\leq -\eta\xi_f - \frac{c+1}{2}\eta^2 + \frac{1}{2}\bar{\alpha}_1^2 + \varepsilon_3 \\ &\leq -\frac{k_1\pi\eta^{2-\gamma}}{\gamma T_c\Lambda_1\sqrt{k_1k_2}} - \frac{k_2\pi\eta^{2+\gamma}}{\gamma T_c\Lambda_2\sqrt{k_1k_2}} - \frac{c+1}{2}\eta^2 \\ &+ \frac{1}{2}\bar{\alpha}_1^2 + \varepsilon_3.\end{aligned} \tag{5.30}$$

Combining (5.28)-(5.30) yields

$$\begin{aligned}\dot{V}_1 \leq\ & z_1z_2 - \frac{c+1}{2}z_1^2 - z_1\xi_1 - \frac{k_1\pi\eta^{2-\gamma}}{\gamma T_c\Lambda_1\sqrt{k_1k_2}} \\ & - \frac{k_2\pi\eta^{2+\gamma}}{\gamma T_c\Lambda_2\sqrt{k_1k_2}} - \frac{c}{2}\eta^2 + \frac{1}{2}\bar{\alpha}_1^2 + \sum_{i=3}^{4}\varepsilon_i.\end{aligned} \tag{5.31}$$

Substitute ξ_1 into (5.31), then $\dot{V}_1$ needs to be further discussed.

If $|z_1| > \epsilon_1$, we have

$$\begin{aligned}\dot{V}_1 \leq\ & z_1z_2 - \frac{k_1\pi}{\gamma T_c\Lambda_1\sqrt{k_1k_2}}(z_1^{2-\gamma} + \eta^{2-\gamma}) \\ & - \frac{k_2\pi}{\gamma T_c\Lambda_2\sqrt{k_1k_2}}(z_1^{2+\gamma} + \eta^{2+\gamma}) \\ & - \frac{c+1}{2}z_1^2 - \frac{c}{2}\eta^2 + \frac{1}{2}\bar{\alpha}_1^2 + \sum_{i=3}^{4}\varepsilon_i.\end{aligned} \tag{5.32}$$

If $|z_1| \leq \epsilon_1$, then the control task has been completed. That is to say, the tracking error can converge to the predefined bound which is arbitrarily selected.

Combining (5.5) and (5.19) leads to

$$M\dot{z}_2 = M\dot{x}_2 - M\dot{\hat{\alpha}}_1 = G(\bar{x}) + u + D - M\dot{\hat{\alpha}}_1. \tag{5.33}$$

Here, the actual control is constructed as

$$u = -G(\bar{x}) + M\dot{\hat{\alpha}}_1 - \frac{c+2}{2}z_2 - \frac{z_2\xi_2^2}{\sqrt{z_2^2\xi_2^2+\varepsilon_5^2}} - H(P)\hat{D} \tag{5.34}$$

with

$$\xi_2 = \frac{k_1\Gamma_1\pi z_2^{1-\gamma}}{\gamma T_c\Lambda_1\sqrt{k_1k_2}} + \frac{k_2\Gamma_2\pi z_2^{1+\gamma}}{\gamma T_c\Lambda_2\sqrt{k_1k_2}} + |z_1|\tanh(\frac{z_2}{\iota_2}) \tag{5.35}$$

where $\Gamma_1 = M^{1-\gamma/2}$, $\Gamma_2 = M^{1+\gamma/2}$, $\iota_2 > 0$ is a small constant.

Theorem 5.2. *Consider the AVSS dynamics (5.5) with unknown actuator faults and external disturbances. If the PTDO is designed as (5.15), the predefined-time filter is constructed as (5.22), the virtual control signal is (5.25), and the predefined-time fault-tolerant control is proposed as (5.34), then we can conclude that the whole closed-loop system is SGPPTS, in the sense that, for the predefined time $T_p = T_c$ and the predefined bound ϵ_1, the tracking error $|z_1| \leq \epsilon_1$ holds for $\forall t \geq T_p$.*

Proof: Construct the following positive definite Lyapunov function V_2 as

$$V_2 = V_1 + \frac{1}{2}Mz_2^2. \tag{5.36}$$

The time derivative of (5.36) becomes

$$\begin{aligned}\dot{V}_2 &= \dot{V}_1 + z_2(G(\bar{x}) + u + D - M\dot{\hat{\alpha}}_1)\\ &= \dot{V}_1 - \frac{c+2}{2}z_2^2 - \frac{z_2^2\xi_2^2}{\sqrt{z_2^2\xi_2^2+\varepsilon_5^2}} - z_2(H\hat{D} - D).\end{aligned} \tag{5.37}$$

According to Lemmas 5.1 and 5.2, and Young's inequality, we have

$$\begin{aligned}-\frac{z_2^2\xi_2^2}{\sqrt{z_2^2\xi_2^2+\varepsilon_5^2}} &\leq -|z_2\xi_2| + \varepsilon_5 \leq -z_2\xi_2 + \varepsilon_5\\ -|z_1|z_2\tanh(\frac{z_2}{\iota_2}) &\leq -|z_1||z_2| + \frac{1}{2}z_1^2 + \frac{1}{2}\kappa^2\iota_2^2.\end{aligned} \tag{5.38}$$

Besides, considering the inequality $|H(P)| < 1$ holds and using Young's inequality,

the last item of (5.37) can be further revised as

$$-z_2(H\hat{D}-D) \leq |z_2||\hat{D}| + |z_2||D| \leq z_2^2 + \frac{1}{2}\delta_d^2 + \frac{1}{2}\bar{D}^2. \tag{5.39}$$

Inserting (5.38)-(5.39) into (5.37) and considering (5.35) yield

$$\begin{aligned}
\dot{V}_2 \leq \dot{V}_1 &- \frac{c}{2}z_2^2 - \frac{k_1\Gamma_1\pi z_2^{2-\gamma}}{\gamma T_c\Lambda_1\sqrt{k_1k_2}} - \frac{k_2\Gamma_2\pi z_2^{2+\gamma}}{\gamma T_c\Lambda_2\sqrt{k_1k_2}} \\
&- |z_1|z_2\tanh(\frac{z_2}{\iota_2}) + \varepsilon_5 + \frac{1}{2}\delta_d^2 + \frac{1}{2}\bar{D}^2 \\
&\leq -\frac{k_1\pi}{\gamma T_c\Lambda_1\sqrt{k_1k_2}}(z_1^{2-\gamma} + \eta^{2-\gamma} + \Gamma_1 z_2^{2-\gamma}) \\
&- \frac{k_2\pi}{\gamma T_c\Lambda_2\sqrt{k_1k_2}}(z_1^{2+\gamma} + \eta^{2+\gamma} + \Gamma_2 z_2^{2+\gamma}) + \frac{1}{2}\kappa^2\iota_2^2 \\
&- \frac{c}{2}(z_1^2 + \eta^2 + z_2^2) + \frac{1}{2}\bar{\alpha}_1^2 + \sum_{i=3}^{5}\varepsilon_i + \frac{1}{2}\delta_d^2 + \frac{1}{2}\bar{D}^2.
\end{aligned} \tag{5.40}$$

According to Lemma 5.3 and noting $\Gamma_1 = M^{1-\gamma/2}$, $\Gamma_2 = M^{1+\gamma/2}$, $\Lambda_1 = 2^{1-\gamma/2}$ and $\Lambda_2 = 2^{1+\gamma/2}\cdot 3^{-\gamma/2}$, the first two terms of (5.40) become

$$\begin{aligned}
&- \frac{k_1\pi}{\gamma T_c\Lambda_1\sqrt{k_1k_2}}(z_1^{2-\gamma} + \eta^{2-\gamma} + \Gamma_1 z_2^{2-\gamma}) \\
&\leq -\frac{k_1\pi}{\gamma T_c\sqrt{k_1k_2}}\big(\frac{1}{2}z_1^2 + \frac{1}{2}\eta^2 + \frac{1}{2}Mz_2^2\big)^{1-\frac{\gamma}{2}} \\
&\leq -\frac{k_1\pi}{\gamma T_c\sqrt{k_1k_2}}V_2^{1-\frac{\gamma}{2}}
\end{aligned} \tag{5.41}$$

$$\begin{aligned}
&- \frac{k_2\pi}{\gamma T_c\Lambda_2\sqrt{k_1k_2}}(z_1^{2+\gamma} + \eta^{2+\gamma} + \Gamma_2 z_2^{2+\gamma}) \\
&\leq -\frac{k_2\pi}{\gamma T_c\sqrt{k_1k_2}}\big(\frac{1}{2}z_1^2 + \frac{1}{2}\eta^2 + \frac{1}{2}Mz_2^2\big)^{1+\frac{\gamma}{2}} \\
&\leq -\frac{k_2\pi}{\gamma T_c\sqrt{k_1k_2}}V_2^{1+\frac{\gamma}{2}}.
\end{aligned} \tag{5.42}$$

Then the time derivative of V_2 can be written as

$$\begin{aligned}\dot{V}_2 \leq & -\frac{k_1\pi}{\gamma T_c\sqrt{k_1k_2}}V_2^{1-\frac{\gamma}{2}} - \frac{k_2\pi}{\gamma T_c\sqrt{k_1k_2}}V_2^{1+\frac{\gamma}{2}} \\ & - \frac{c}{2}(z_1^2+\eta^2+z_2^2) + \frac{1}{2}\kappa^2\iota_2^2 + \frac{1}{2}\bar{\alpha}_1^2 \\ & + \sum_{i=3}^{5}\varepsilon_i + \frac{1}{2}\delta_d^2 + \frac{1}{2}\bar{D}^2 \\ \leq & -\frac{\pi}{\gamma T_c\sqrt{k_1k_2}}(k_1V_2^{1-\frac{\gamma}{2}} + k_2V_2^{1+\frac{\gamma}{2}}) - cV_2 + \Xi\end{aligned} \tag{5.43}$$

where $\Xi = \frac{1}{2}\kappa^2\iota_2^2 + \frac{1}{2}\bar{\alpha}_1^2 + \sum_{i=3}^{5}\varepsilon_i + \frac{1}{2}\delta_d^2 + \frac{1}{2}\bar{D}^2$.

According to Lemma 5.5, the equilibrium point of AVSSs under the proposed predefined-time fault-tolerant control is SGPPTS, while the error z_1 would converge to an arbitrary prior-known bound $|z_1| \leq \epsilon_1$ within an arbitrary user-selected time $T_p = T_c$. Thus, the proof of Theorem 5.2 is completed. ■

Remark 5.9. The predefined-time stability has been applied in different mechanical systems [35, 145, 146, 149–151]. It should be pointed out that the controllers in [145, 146] encounter the singularity issues and the utilization of the sign functions in [35, 149–151] may lead to severe chattering problems. However, by using the piecewise function, quadratic fraction inequality, and hyperbolic tangent function in the PTDO (5.15), CDC method (5.20)-(5.21), and virtual control signal (5.25), then the actual control design (5.34)-(5.35) is nonsingular and continuous while the error signal z_1 would converge to the predefined bound ϵ_1 during the predefined time period T_p. Besides, one should note that the predefined settling time T_p and the predefined bound ϵ_1 in the proposed control scheme can be arbitrarily chosen independently since they depend on different parameters.

Remark 5.10. The parameter tuning of reference X-dynamics has little effect on system stability since the reference X-dynamics are always considered stable with positive damping effect [69]. During the tuning process of control parameters, the predefined settling time T_c and predefined residual bound ϵ_1 can be directly selected according to system requirements. ε_i for $i = 0...5$ and ι_j for $j = 0...2$ should be small positive

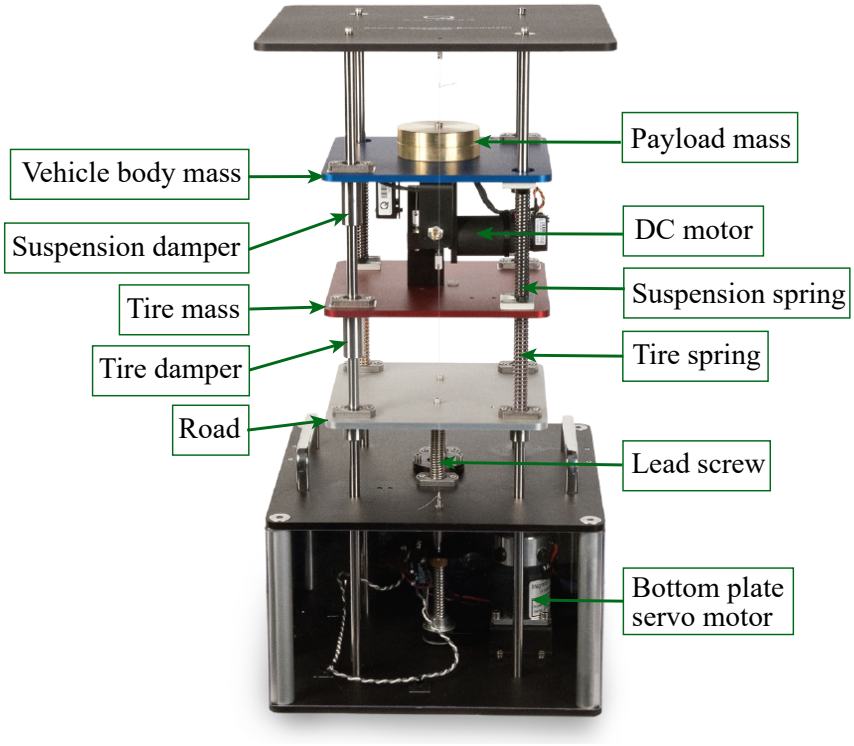

Fig. 5.3: The experimental AVSS platform

constants to enhance the control performance but too small gains will lead to higher chattering. p_0, q_0, p and q are positive odd integers with $0 < p_0 < q_0$ and $0 < p < q$ to ensure the predefined-time stability. Then k_1 and k_2 are selected to adjust the transient performance during the convergence process. The settling time of the PTDO T_{p1} should be chosen smaller than that of the controller design such that $T_{p1} < T_c$. Hence, the anti-vibration performance and the chattering problem should be carefully balanced during the tuning process.

5.4 Comparative experiments

Some comparative experiments are presented in this section to further illustrate the superior control performance of the proposed control design on an experimental quarter-car AVSS platform (refer to Fig. 5.3) [136]. Table 5.1 presents the nominal values of the AVSS model. The structure of the AVSS platform predominantly includes three distinct levels, linked together through various springs and dampers. The uppermost level, sus-

Table 5.1: Nominal values of the AVSS

Symbols	Values	Symbols	Values
m_s	2.45 kg	m_u	1 kg
w_{s1}	900 N/m	w_{s2}	10 N/m^3
w_d	8 Ns/m	w_t	1250 N/m
w_b	5 Ns/m		

Table 5.2: Parameters of the reference X-dynamics

Symbols	Values	Symbols	Values
m_r	22 kg	ϱ_1	5 Ns/m
ϕ_1	π/6 rad	ϱ_2	0.15 Ns/m
ℓ_1	0.1 m	σ_h	500 N/m
ℓ_2	0.2 m	σ_v	350 N/m
ϖ_1	-1 m/s^2	ϖ_2	1 m/s^2

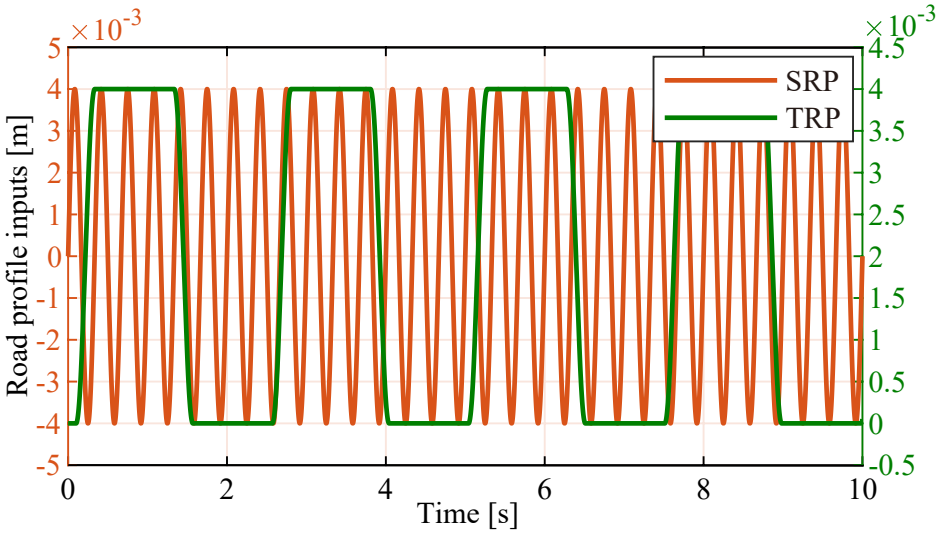

Fig. 5.4: The road profile input z_r

tained by the suspension damper/spring, is constituted by the payload and vehicle body. A direct current motor is employed as the actuator for the vibration suppression of the AVSS and the enhancement of passenger ride comfort. Energy dissipation and supply can be conducted by the actuator to reject the rough road effects. The spring damping system connects the middle and bottom levels. Furthermore, utilizing the servo motor and lead screw, rough road profiles can be generated by the bottom level. Additional details regarding the experimental platform and procedures are outlined in [87].

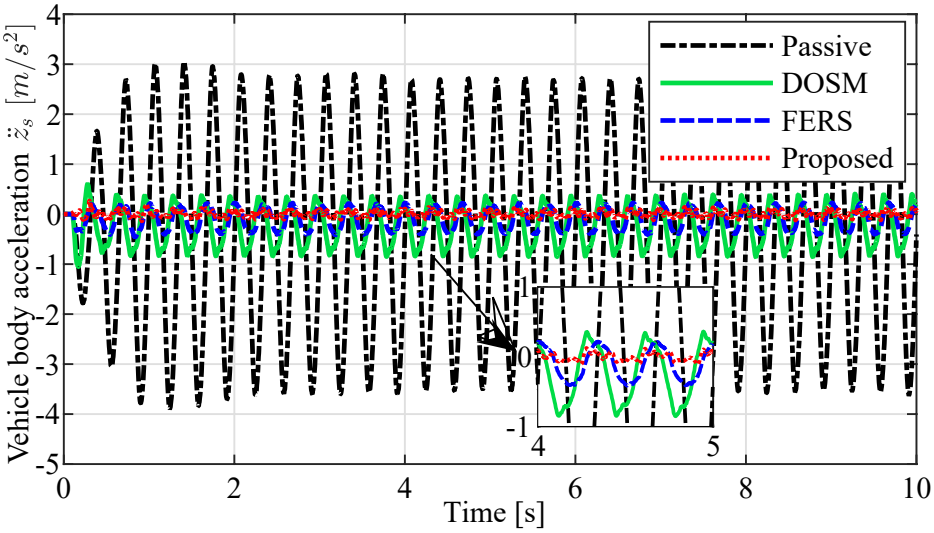

Fig. 5.5: The time-domain vehicle body acceleration $\ddot{z}_s$ under SRP

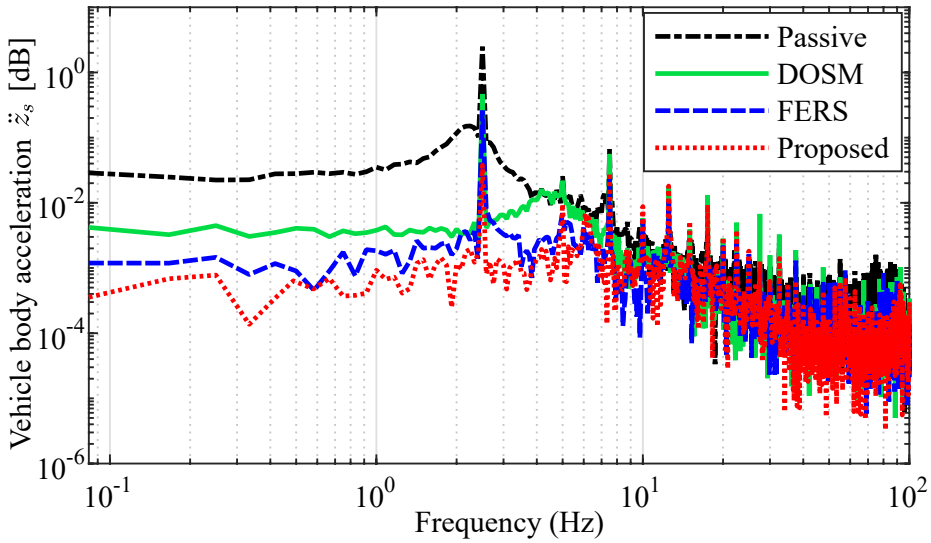

Fig. 5.6: The frequency-domain vehicle body acceleration $\ddot{z}_s$ under SRP

Two different cases of rough road profiles are considered to better evaluate the control performance including the sinusoidal road profile (SRP) and trapezoidal road profile (TRP) shown in Fig. 5.4. Using the harmonic balance technique and analyzing the displacement transmissibility [69], the parameters of the reference X-dynamics are selected in Table 5.2.

Four different suspension systems are evaluated.

1) Passive: This abbreviation is the passive suspension;

2) DOSM: This abbreviation denotes the disturbance observer-based sliding mode

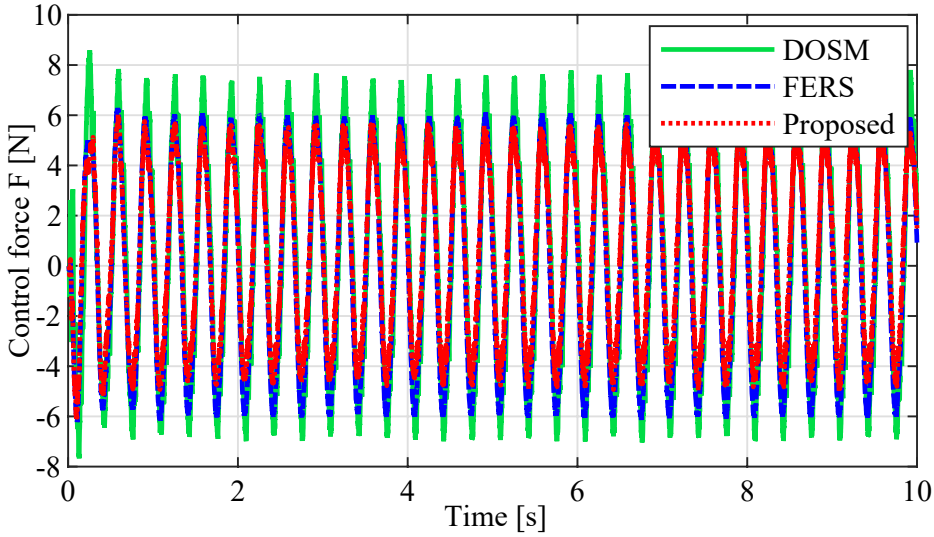

Fig. 5.7: The control input F under SRP

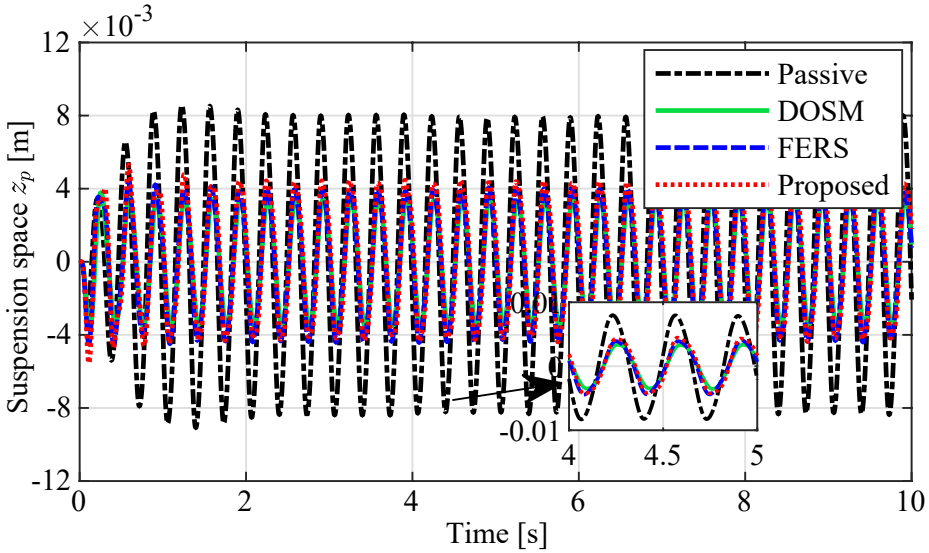

Fig. 5.8: The suspension space z_p under SRP

control [65];

3) FERS: This abbreviation means the finite-time estimator-based robust saturated control [98];

4) Proposed: This abbreviation indicates the proposed predefined-time fault-tolerant control.

The actuator faults are defined as $\rho = 0.85$ and $u_0 = 0.02\sin(3t)$. The initial states are set as zero for simplicity. The control values for DOSM method are $\chi = 500$, $l = 100$, $\alpha = 0.8$, $\alpha_1 = 9/7$, $\alpha_2 = 2.5$, $\alpha_3 = 7/9$, $\lambda_1 = 0.01$, $\lambda_2 = 0.02$, $k_1 = 20$, $k_2 = 160$. The

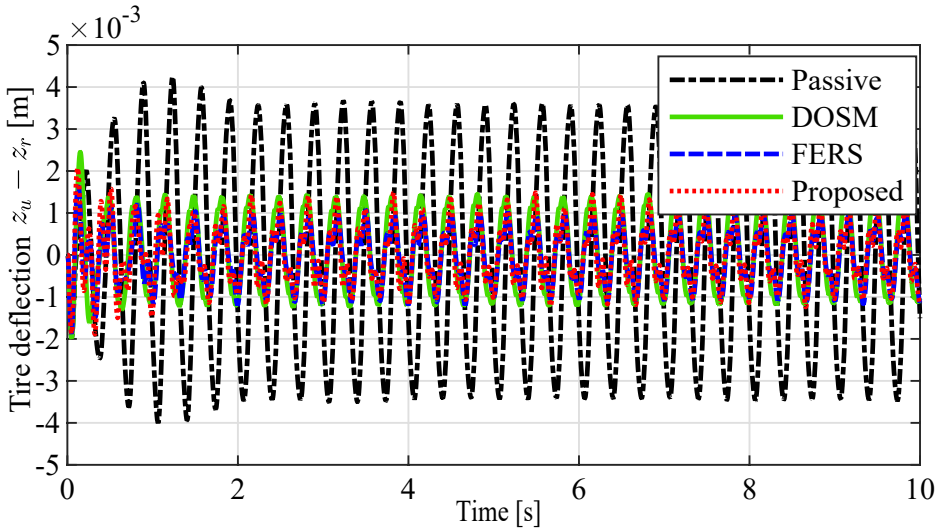

Fig. 5.9: The tire deflection $z_u - z_r$ under SRP

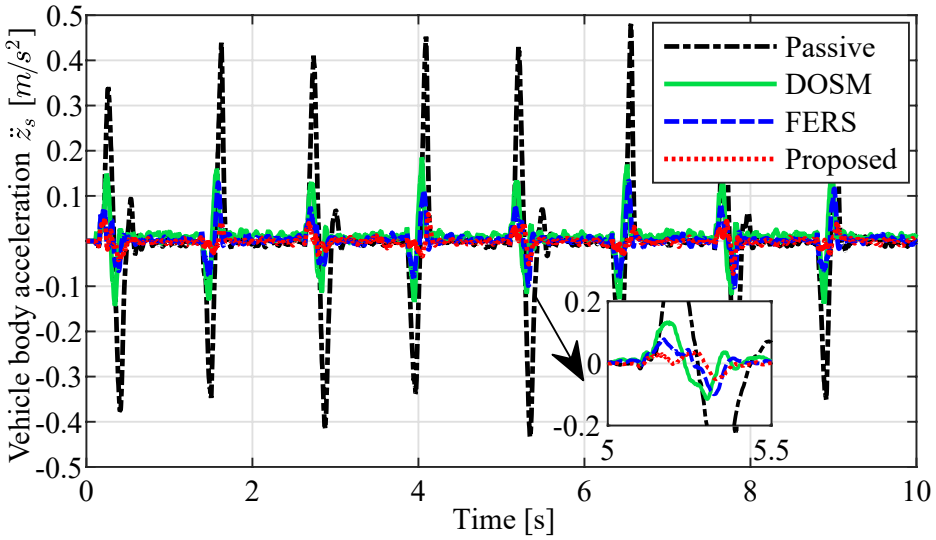

Fig. 5.10: The time-domain vehicle body acceleration $\ddot{z}_s$ under TRP

FERS control parameters are selected as $k_1 = 20, k_2 = 15, \lambda_0 = 2.8, \lambda_1 = 1.4, \lambda_2 = 0.9, \lambda_3 = 1.6, \lambda_4 = 1.2, L_1 = 149, L_2 = 21, \eta_1 = 9, \eta_2 = 11$. The control gains for the proposed control are given as $T_c = 0.5, k_1 = 1, k_2 = 5, c = 1, p = 7, q = 9, \epsilon_1 = 3 \times 10^{-4}$, $\varepsilon_i = 0.01$ for $i = 1...5$, $\iota_1 = \iota_2 = 0.1$. Furthermore, the gains for the predefined-time observer are $T_d = 0.1, p_0 = 7, q_0 = 9, \varepsilon_0 = 0.5, \iota_0 = 0.2$, and $\lambda_0 = 1$.

The comparative experimental results for four suspensions are provided in Figs. 5.5–5.9 and Figs. 5.10–5.14 for the SRP and TRP cases, respectively. The control performance evaluation of the ride comfort and energy consumption is presented in Table 5.3.

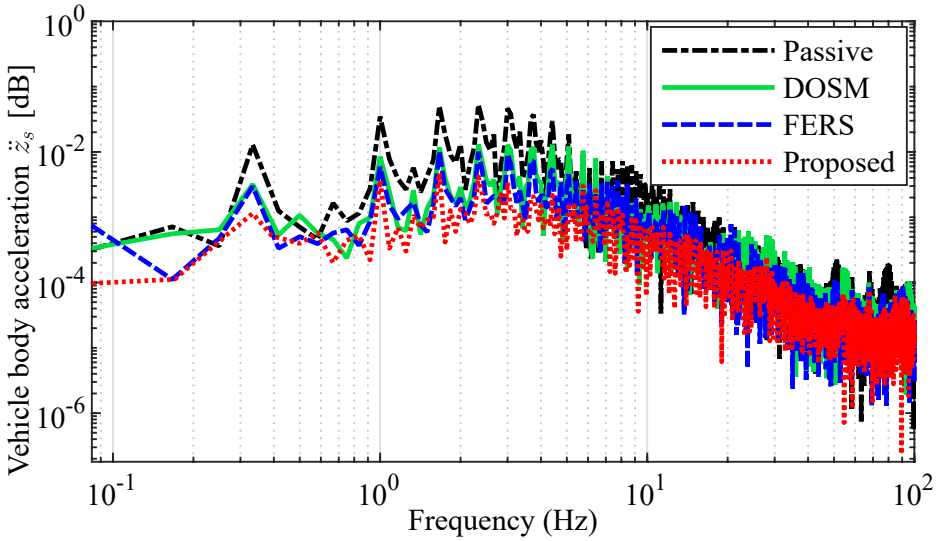

Fig. 5.11: The frequency-domain vehicle body acceleration $\ddot{z}_s$ under TRP

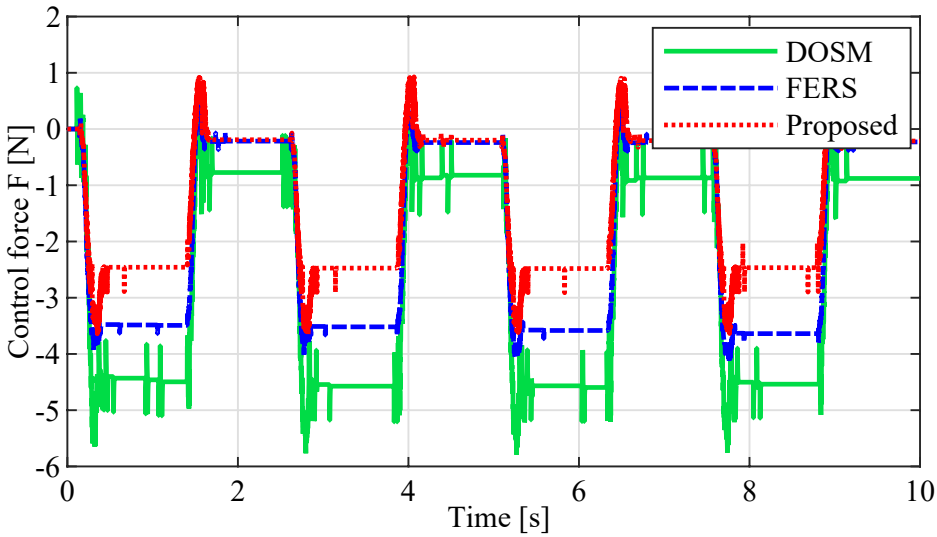

Fig. 5.12: The control input F under TRP

Vehicle body acceleration is always considered an important factor of ride comfort. Figs. 5.5 and 5.10 present the time-domain vehicle body acceleration of the passive suspension, DOSM control, FERS control, and proposed control under the SRP case and TRP case. Compared with the passive suspension, the amplitudes of the vehicle body acceleration of three AVSSs can be significantly mitigated. Meanwhile, the proposed control design shows the smallest amplitude of vehicle body acceleration among three AVSSs, which further indicates better ride comfort in isolating perturbations under rough road profiles, actuator faults, and external disturbances.

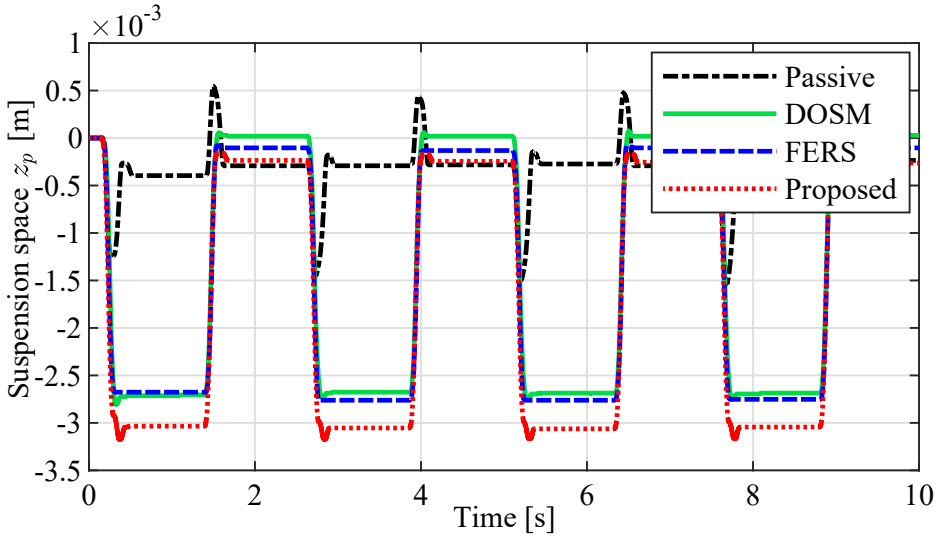

Fig. 5.13: The suspension space z_p under TRP

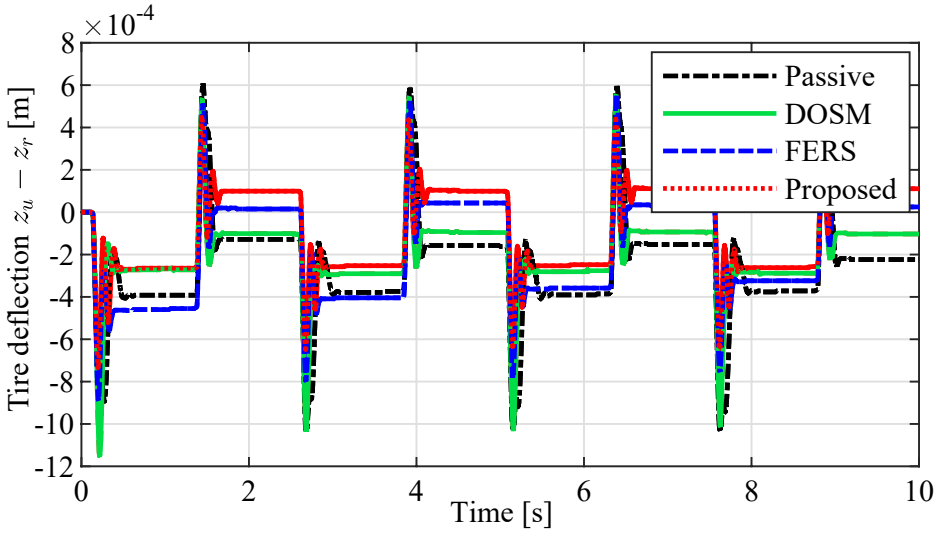

Fig. 5.14: The tire deflection $z_u - z_r$ under TRP

The corresponding frequency-domain results are given in Figs. 5.6 and 5.11. According to the International Organization of Standardization, humans exhibit particular sensitivity to oscillations within the frequency spectrum of 4 to 12.5 Hz [107]. The frequency-domain vehicle body acceleration of the proposed control is lower than the passive suspension, DOSM control, and FERS control, showing similar ride comfort enhancement in Figs. 5.6 and 5.11.

The control input signals for the AVSSs under two road profiles are given in Figs. 5.7 and 5.12. Compared with DOSM control and FERS control, the proposed control design

Table 5.3: Performance of Ride Comfort and Energy Consumption

Cases	Controllers	RMS_r	RMS_e
Case 1	Passive	2.1859	/
	DOSM	0.4658(↓78.7%)	0.1499
	FERS	0.2457(↓88.8%)	0.1392(↓7.1%)
	Proposed	0.0587(↓97.3%)	0.1048(↓30.1%)
Case 2	Passive	0.1186	/
	DOSM	0.0392(↓66.9%)	0.0201
	FERS	0.0254(↓78.6%)	0.0136(↓32.3%)
	Proposed	0.0211(↓82.2%)	0.0085(↓57.7%)

generates smaller control inputs under both SRP and TRP cases. This means that less energy consumption is required while better ride comfort can be obtained. Meanwhile, the chattering phenomenon can be slightly alleviated with no discontinuous terms in the proposed control design.

To quantitatively evaluate the ride comfort performance, the root-mean-square (RMS) indexes of the vehicle body acceleration RMS_r and energy consumption RMS_e are respectively denoted as $\text{RMS}_\text{r}(\ddot{z}_s) = \sqrt{\frac{1}{T}\int_0^T \ddot{z}_s^2 dt}$ and $\text{RMS}_\text{e}(P^*) = \sqrt{\frac{1}{T}\int_0^T (P^*(\tau))^2 d\tau}$ where $P^* = u(t)\dot{z}_p$ for $u(t)\dot{z}_p > 0$, $P^* = 0$ for else, and T is the total experimental period. The evaluation results of ride comfort index RMS_r and energy consumption index RMS_e are provided in Table 5.3. Compared with the passive suspension, the ride comfort indexes of the proposed control can be reduced significantly with a great RMS_r reduction of 97.3% and 82.2% under SRP and TRP cases, respectively. Moreover, the energy consumption indexes RMS_e of the proposed control decrease by 30.1% and 57.7% compared with the DOSM control method under SRP and TRP cases, respectively, where those of FERS control reduce only 7.1% and 32.3%, respectively. Therefore, both better ride comfort and energy consumption can be guaranteed using the proposed control design, which indicates the superior control performance.

To ensure the safety of the AVSS with physical constraints, the suspension space z_p and tire deflection $z_u - z_r$ should be restricted in permitted ranges under different road profiles. According to [121, 136], the maximum z_p of the AVSS platform is $z_{p\text{max}} = 0.038\text{m}$. From the curves in Figs. 5.8 and 5.13, the peaks of z_p of the passive suspension, DOSM control, FERS control, and proposed control all stay within the per-

mitted constraint. From the results in Figs. 5.9 and 5.14, the tire deflection constraint can be satisfied all the time where g denotes the gravity acceleration, indicating the road holding ability under different road profiles. Hence, the suspension space constraint and road holding ability can be ensured simultaneously.

5.5 Conclusion

In this chapter, a novel predefined-time fault-tolerant control is designed for the AVSSs with actuator faults and external disturbances. By employing the designed control scheme, the tracking errors can converge to the predefined residual bound within the predefined time interval, which can both be independent of initial states and control gains. Besides, a newly designed CDC method is integrated with the reference X-dynamics to reduce the energy cost (up to 57.7% compared to existing ones) while satisfactory ride comfort performance (up to 97.3% improvement) can be achieved. The continuous piecewise function and the quadratic fraction inequality are investigated to avoid the singularity issue and alleviate the chattering problem. Finally, various experimental results under SRP and TRP are carried out to demonstrate the superior capabilities of the proposed control design.

6 Predefined-Time Output Feedback Control for AVSSs

The exploration of energy-efficient active suspension control strategies for high-performance vibration suppression remains a critical challenge, particularly under partial-state measurements, uncertain dynamics, and external disturbances. This article proposes an innovative predefined-time output feedback control scheme for active vehicle suspension systems that achieves superior vibration mitigation with reduced energy consumption. By employing the time-varying scaling function technique, a predetermined-time extended state observer is developed to estimate unmeasurable velocities and lumped disturbance, while a second-order predefined-time filter is designed to avoid the explosion of computational complexity. Furthermore, using the effect characterization method and the X-mechanism reference dynamics, beneficial couplings/disturbances and nonlinearities can be reserved instead of direct cancellation, which leads to significant energy conservation up to 58% compared to other methods. Then the predefined-time output feedback control is proposed to ensure that settling time can be arbitrarily user-specified using only one parameter, which is independent of initial conditions and control gains. Comparative experiments are performed to present the effectiveness and robustness of the proposed control method.

6.1 Introduction

Recent developments in vehicle suspension systems have attracted significant attention for their abilities in vehicle stability and ride comfort improvement [39]. Unlike passive and semi-active suspensions, active vehicle suspension systems (AVSSs) exhibit a markedly increased capacity to improve ride comfort on uneven roadways in

Nomenclature			
m_s, m_u	Sprung and unsprung masses	W_s, W_d	Spring and damper forces
r_s, r_u, r_d	Displacements of sprung, unsprung masses and road	W_t, W_b	Elasticity and damping forces of tire
$\dot{r}_s, \dot{r}_u, \dot{r}_d$	Velocities of the sprung, unsprung masses and road	$\bar{l}_s, \bar{l}_d$	Suspension stiffness and damping coefficients
d_1, d_2	External disturbances	$\bar{l}_t, \bar{l}_b$	Tire stiffness and damping coefficients
F	Control input		

which actuators are integrated to exert appropriate forces to achieve absorption or mitigation of energy [157]. The last decade has witnessed extensive studies on active suspension controllers including adaptive control [147], robust control [158], sliding mode control [64], H-infinity control [1], and so on. Therefore, it is of great importance to enhance the active suspension performance by designing appropriate control techniques.

Most existing active suspension controllers are developed with asymptotic stability where control objectives can be realized only when the time approaches infinity [36]. The finite-time control strategies become more important due to their advantages in more rapid convergence speed, better disturbance rejection, and higher tracking accuracy [35, 159]. Traditional finite-time control methods for AVSSs include the terminal sliding mode control [65], extra power integrator design [134], and the homogeneous approach [3, 121]. However, the convergence time of the finite-time control is dependent on initial states, which leads to the development of the fixed-time control method [160]. An adaptive fuzzy control was designed for AVSSs with fixed-time stability to deal with the time-varying displacement constraints [113]. A fixed-time safe-by-design control was proposed for AVSSs such that the convergence time was irrelevant to initial conditions [136]. However, the settling time of fixed-time stability is a function of control gains, which is usually overestimated and difficult for parameter tuning. Recently, the predefined-time control has been constructed to guarantee the user-selected convergence time which is completely independent of initial conditions and control parameters [148, 161, 162]. The prescribed performance function-based predefined-time control was developed for AVSSs using time-delay estimation [37]. However, the initial value of the performance function was designed to be infinity, which is not practical in actual applications. Hence, more efforts should be devoted to the predefined-time active

suspension control field to enhance the anti-vibration performance.

We should also note that not all states can be easily obtained due to limited installation space, sensor failures, and high device cost [163]. However, few researchers are involved in the predefined-time output feedback control for AVSSs in the absence of velocity measurements. A fuzzy state observer was constructed for active suspensions to measure the velocity states in the fault-tolerant output feedback control scheme [9]. Furthermore, practical AVSSs may suffer from severe external disturbances including varying environmental conditions and changing passenger loads [119]. As an effective method to deal with unknown states and external disturbances, the extended state observer (ESO) method has captured considerable attention, which exerts disturbances as an extended state [164, 165]. A finite-time ESO was designed in the robust saturated control for AVSSs to obtain the velocities and lumped disturbance [98]. A finite-time output feedback control was proposed for half-car active suspensions using the nonlinear finite-time ESO [4]. Moreover, a fixed-time generalized ESO was constructed for motor servo systems [166]. However, the convergence time in traditional ESO designs is related to initial states and control gains, which is difficult to compute. Therefore, existing ESO designs with ambiguous settling time are not suitable for predefined-time active suspension control schemes [167, 168]. Further studies on predefined-time ESO for AVSSs are still required both in theory and practical applications considering partial-state measurements and unknown external disturbances.

To deal with the high energy consumption issue, various research attempts have been made in the control field [87, 140]. One typical method is to preserve the beneficial couplings and disturbances, which has been widely applied in hypersonic vehicles [169], unmanned aerial vehicles [170], and manned submersibles [171]. Coupling/disturbance terms in traditional active suspension controllers were directly canceled to guarantee system stability and control performance [172]. However, when the directions of couplings/disturbances are in the desired ones of the motions, these coupling/disturbance magnitudes should be considered beneficial, which can be reserved in the control system to save energy [173]. The integration of beneficial couplings/distur-

bances in former AVSS control designs was established on the assumption that all states needed to be measurable, which requires further discussion in the output feedback control scheme. Furthermore, another useful method for AVSS energy reservation is the employment of beneficial nonlinearities including damping and stiffness introduced by the X-mechanism reference dynamics [73, 174]. A single-layer reference model was constructed in the AVSS control system to present the promising energy-saving performance, which however neglected the damping effect [69]. Then more common reference model designs were designed with two layers to include both stiffness and damping nonlinearities in the active suspension controllers to enhance energy conservation [130, 175]. Therefore, considering beneficial couplings, disturbances, and nonlinearities, further studies of the energy-saving performance in the predefined-time output feedback control scheme for AVSSs should be investigated.

Motivated by the analysis above, this article focuses on a predefined-time output feedback control scheme for AVSSs with partial-state measurements, uncertain dynamics, and external disturbances. More precisely, utilizing the time-varying scaling function design, an innovative predefined-time ESO is designed to estimate velocities and disturbances while a new second-order predefined-time (SOPT) filter is constructed to avoid computational explosion. The characteristics of state couplings and disturbances are assessed respectively such that only detrimental ones are canceled. Furthermore, the advantageous nonlinearities in the X-mechanism reference are inherited. Thus, excellent vibration suppression results can be obtained with the energy conservation performance. Based on the predefined-time ESO, SOPT filter, effect characterization method, and X-mechanism reference, a pioneering predefined-time output feedback control is proposed for AVSSs. The main contributions are summarized as follows.

1) This should be the *first* predefined-time output feedback control for AVSSs to achieve predefined-time convergence, maintain energy conservation, overcome partial-state measurements, address uncertain dynamics, and reject external disturbances. Compared with existing finite-time AVSS controllers [134, 136], the settling time of the proposed control design is independent of initial states and

control gains, which can be adjusted by only one parameter.

2) A novel predefined-time ESO and a new SOPT filter are proposed for AVSSs to estimate velocities/disturbances and avoid the explosion of computational complexity, respectively, by introducing the time-varying scaling function technique. Different from existing AVSS control methods [5], the velocity measurements are not required while observation errors can converge to the neighborhood near zero within a prearranged time.

3) Distinguished from AVSS controllers suffering from high energy consumption [121, 133], beneficial couplings, disturbances, and nonlinearities are inherited in the proposed control scheme to achieve energy conservation. Specifically, beneficial stiffness/damping nonlinearities are reserved by introducing the X-mechanism reference dynamics. Then the coupling/disturbance effect characterization method is established to preserve beneficial couplings and disturbances of AVSSs instead of the direct cancellation, thereby enhancing energy-saving performance.

The rest of this article is outlined as follows. Section 6.2 presents the model transformation and problem formulation. The main results including the X-mechanism reference design, predefined-time ESO design, coupling and disturbance characterization, and predefined-time output feedback control are provided in Section 6.3. Then the comparative experimental results are presented in Section 6.4. Finally, Section 6.5 concludes the whole article.

6.2 Model transformation and problem formulation

The quarter-car AVSS dynamics can be described as [176]

$$\begin{cases} m_s\ddot{r}_s = -W_s(r_s, r_u) - W_d(\dot{r}_s, \dot{r}_u) + F + d_1 \\ m_u\ddot{r}_u = W_s(r_s, r_u) + W_d(\dot{r}_s, \dot{r}_u) - W_t(r_u, r_d) \\ \qquad\quad - W_b(\dot{r}_u, \dot{r}_d) - F + d_2 \end{cases} \tag{6.1}$$

with

$$\begin{aligned} W_s(r_s, r_u) &= \bar{l}_s(r_s - r_u) \\ W_d(\dot{r}_s, \dot{r}_u) &= \bar{l}_d(\dot{r}_s - \dot{r}_u) \\ W_t(r_u, r_d) &= \bar{l}_t(r_u - r_d) \\ W_b(\dot{r}_u, \dot{r}_d) &= \bar{l}_b(\dot{r}_u - \dot{r}_d). \end{aligned} \tag{6.2}$$

Consider the uncertain dynamic coefficient $\bar{l}_i$ to satisfy $\bar{l}_i = l_i(1+\gamma_i)$ where l_i is the nominal value of $\bar{l}_i$ with the perturbation range coefficient γ_i for $i = \{s, d, t, b\}$.

The dynamic model can be written as

$$\begin{aligned} &\frac{m_s m_u}{m_s + m_u}\ddot{r}_p = -l_s r_p - l_d\dot{r}_p - l_s\gamma_s r_p - l_d\gamma_d\dot{r}_p + F \\ &+ \frac{m_s m_u}{m_s + m_u}(\bar{l}_t r_t + \bar{l}_b\dot{r}_t) + \frac{m_u}{m_s + m_u}d_1 - \frac{m_s}{m_s + m_u}d_2 \end{aligned} \tag{6.3}$$

where $r_p = r_s - r_u$ is the suspension space, $r_t = r_u - r_d$ stands for the tire deflection.

Using the coordinate transformation $x_1 = r_p$ and $x_2 = \dot{r}_p$, the system dynamics can be obtained as

$$\begin{cases} \dot{x}_1 = x_2 \\ m_0\dot{x}_2 = -l_s x_1 - l_d x_2 + D + F \end{cases} \tag{6.4}$$

where $m_0 = m_s m_u/(m_s+m_u)$, $D = -l_s\gamma_s r_p - l_d\gamma_d\dot{r}_p + \frac{m_s m_u}{m_s+m_u}(\bar{l}_t r_t + \bar{l}_b\dot{r}_t) + \frac{m_u}{m_s+m_u}d_1 - \frac{m_s}{m_s+m_u}d_2$.

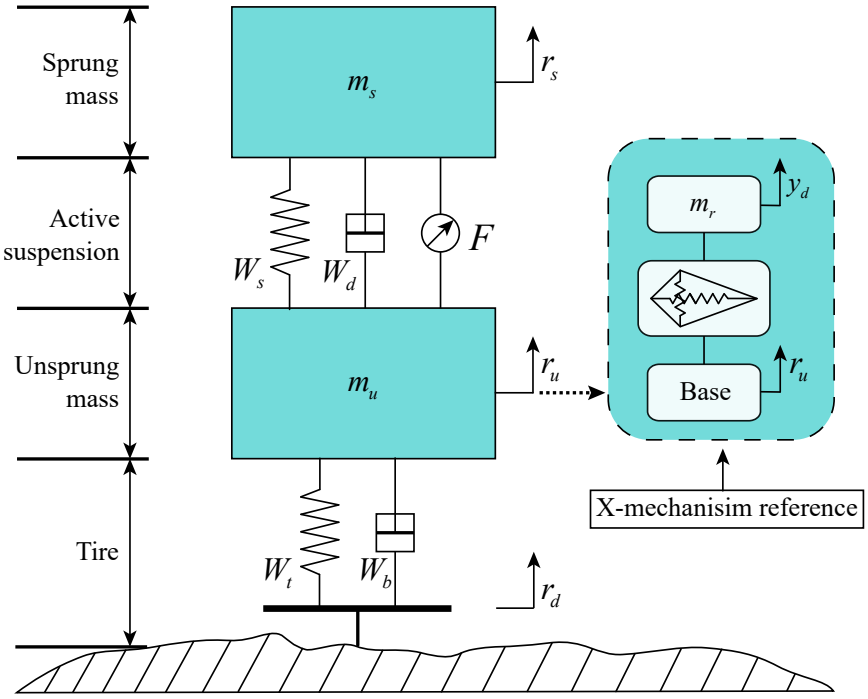

Fig. 6.1: A quarter-car AVSS structure

Assumption 6.1 ([98]). *The time-varying lumped disturbance D and its first-order derivative are bounded by $|D| \leq \delta_{D1}$ and $|\dot{D}| \leq \delta_{D2}$.*

Assumption 6.2 ([87]). *To guarantee the boundedness of system outputs, $\ddot{y}_d$ and $\dddot{y}_d$ are assumed bounded in which $\varpi_1 \leq \ddot{y}_d \leq \varpi_2$ with known constants ϖ_1 and ϖ_2.*

The bounded lumped disturbance assumption arises from practical physical constrains in real-world systems, which is widely adopted in existing AVSS control designs [98]. Besides, Assumption 6.2 is also commonly utilized in existing AVSS controllers [87], since y_d is considered as the system reference signal.

A time-varying function is defined as

$$\bar{\mu}(t, t_c) = \begin{cases} 1 + 10(\frac{t}{t_c})^6 - 36(\frac{t}{t_c})^5 + 45(\frac{t}{t_c})^4 \\ -20(\frac{t}{t_c})^3, \text{ if } t \in [0, t_c], \\ 0, \text{ if } t \in (t_c, \infty) \end{cases} \tag{6.5}$$

where $t_c > 0$ is a predefined time constant.

Next a time-varying scaling function $\mu(t, t_c, \iota)$ can be constructed as [167]

$$\mu(t, t_c, \iota) = \frac{1}{\bar{\mu}(t,t_c)+\iota} \tag{6.6}$$

where $0 < \iota \ll 1$. The following characteristics hold for the time-varying scaling function $\mu(t, t_c, \iota)$.

1) $\mu(t, t_c, \iota)$ is at least C^3 on $(0, \infty)$.

2) $t = 0$, $\mu(t, t_c, \iota) = \frac{1}{1+\iota}$; $t \geq t_c$, $\mu(t, t_c, \iota) = \frac{1}{\iota}$.

3) $\mu(t, t_c, \iota)$ is monotonically increasing on $(0, t_c)$.

Lemma 6.1 ([177]). *If a Lyapunov function $V(t)$ is designed to satisfy*

$$\dot{V}(t) \leq -\Big(\varsigma + \frac{\dot{\mu}(t,t_c,\iota)}{\mu(t,t_c,\iota)}\Big)V(t), \quad V_0 = V(0), \tag{6.7}$$

with $\varsigma > 0$ and $\mu(t, t_c, \iota)$ is defined in (6.6), then $V(t)$ can approach to $V(t) \leq \iota V_0$ within predefined time t_c and then converge to zero asymptotically.

Lemma 6.2. *If a Lyapunov function $V(t)$ is constructed to satisfy*

$$\dot{V}(t) \leq -\Big(\varsigma + \frac{\dot{\mu}(t,t_c,\iota)}{\mu(t,t_c,\iota)}\Big)V(t) + \epsilon, \quad V_0 = V(0), \tag{6.8}$$

with $\varsigma > 0$, $\epsilon > 0$ is a small constant and $\mu(t, t_c, \iota)$ is defined in (6.6), then $V(t)$ can approach to $V(t) \leq \iota V_0 + \epsilon/\varsigma$ within predefined time t_c and then converge to $V(t) \leq \epsilon/\varsigma$ asymptotically.

Proof: The proof of Lemma 6.2 is presented in Appendix A.

Remark 6.1. If $\iota = 0$ such that $\mu(t, t_c, \iota) = 1/\bar{\mu}(t, t_c)$, one can obtain that $V(t)$ approaches to zero when $t \to t_c$ while $\dot{\mu}/\mu$ will grow unbounded. However, by integrating a positive small constant $\iota > 0$ in $\mu(t, t_c, \iota)$, the term $\dot{\mu}/\mu$ remains bounded for $\forall t \geq 0$.

Remark 6.2. If the parameter ι is selected as $\iota = \iota_a/\iota_b$ with $\iota_a > 0$ and $\iota_b > V_0$, then $V(t)$ can converge to a user-defined region $V(t) \leq \iota_a$ within the predefined time t_c.

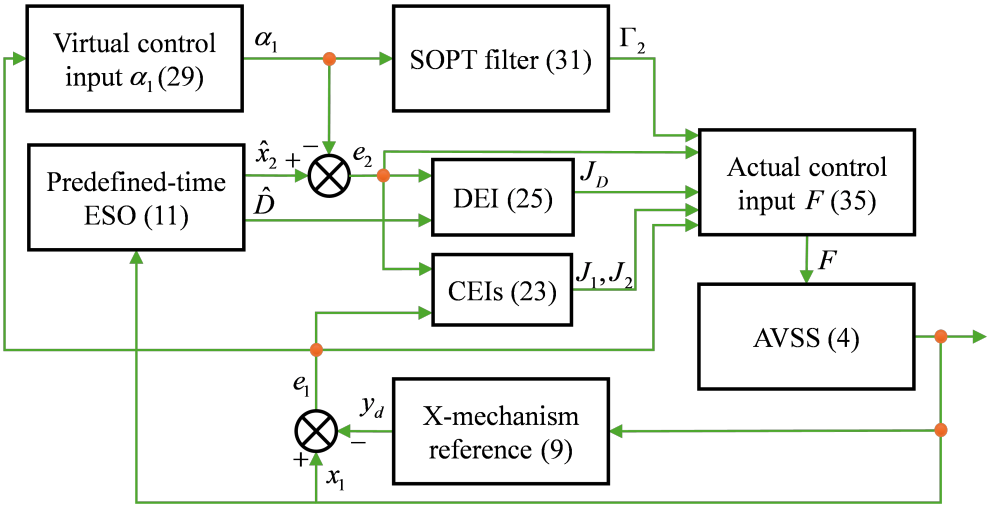

Fig. 6.2: Block diagram of the control scheme

6.3 Main results

In this section, the output feedback control problem for AVSSs with uncertain dynamics and external disturbances will be tackled. The overall block diagram of the proposed control scheme is illustrated in Fig. 6.2. First, the X-mechanism reference is introduced such that beneficial nonlinearities can be reserved. Then a predefined-time ESO is proposed to approximate the unknown velocity and lumped disturbance, which can ensure the preassigned-time convergence of the estimation errors. Furthermore, beneficial couplings and disturbances are retained based on the characterization analysis to achieve energy conservation performance. Finally, a novel predefined-time output feedback control is proposed for AVSSs, while the corresponding system stability and predefined-time convergence analyses are provided.

6.3.1 X-mechanism reference design

The X-mechanism reference model is established based on a two-layer structure [39], including the object mass M, road length L_1 and L_2, initial angles θ_1 and θ_2. A geometric connection exists $L_1 \sin\theta_1 = L_2 \sin\theta_2$. Then the output of the X-mechanism reference model can be regarded as the desired suspension space y_d, in which beneficial nonlinearities including stiffness and damping effects can be reserved in the control

system for satisfactory anti-vibration results and energy conservation performance [73]. The X-mechanism reference model is constructed as [35]

$$M\ddot{y}_d + \chi_1 + l_v y_d/n^2 + l_a\dot{y}_d + l_r n_x \chi_2 \dot{y}_d = -M\ddot{r}_u \tag{6.9}$$

where

$$\begin{aligned}
\chi_1 &= \frac{l_h\Omega}{2n}\Big(L_1\cos\theta_1 - \sqrt{L_1^2-\Omega^2} + L_2\cos\theta_2 \\
&\quad - \sqrt{L_2^2-\Omega^2}\Big)\Big(1/\sqrt{L_1^2-\Omega^2} - 1/\sqrt{L_2^2-\Omega^2}\Big) \\
\chi_2 &= \Big(L_1/\big(2n\sqrt{L_1^2-\Omega^2}\big) - L_2/\big(2n\sqrt{L_2^2-\Omega^2}\big)\Big)^2 \\
\Omega &= L_1\sin\theta_1 + y_d/(2n) = L_2\sin\theta_2 + y_d/(2n)
\end{aligned} \tag{6.10}$$

and $n = 2$ denoting the layer, $n_x = 3n - 1$ representing the joint number, l_v and l_h being the vertical/horizontal spring stiffness, l_a and l_r meaning the air resistance/rotating friction coefficients. According to Assumption 6.2, an allowable range $\varpi_1 \leq \ddot{y}_d \leq \varpi_2$ is defined to constrain the output of y_d with known constant ϖ_1 and ϖ_2.

6.3.2 Predefined-time ESO design

Consider $\hat{x}_1$, $\hat{x}_2$, $\hat{x}_3$ as the estimations of x_1, x_2, x_3, respectively, where $x_3 = D$, $\hat{x}_3 = \hat{D}$ represent the real and estimated lumped disturbance. The estimation errors are defined as $\tilde{x}_i = x_i - \hat{x}_i$ for $i = 1, 2, 3$. A predefined-time ESO is proposed as

$$\begin{cases}
\dot{\hat{x}}_1 = \hat{x}_2 + \pi_1\xi\tilde{x}_1 + 2\dfrac{\dot{\xi}}{\xi}\tilde{x}_1 \\
m_0\dot{\hat{x}}_2 = \hat{x}_3 - l_s x_1 - l_d\hat{x}_2 + F + \pi_2 m_0\xi^2\tilde{x}_1 \\
\dot{\hat{x}}_3 = \pi_3\xi^3\tilde{x}_1
\end{cases} \tag{6.11}$$

where $\xi = \pi_4(\pi_5 + \dot{\mu}_0/\mu_0)$, $\mu_0 = \mu(t, t_{c0}, \iota_0)$, with $t_{c0} > 0, \iota_0 > 0, \pi_i > 0$ for $i = 1, ..., 5$ are positive constants.

The observer error dynamics can be obtained as

$$\begin{cases} \dot{\tilde{x}}_1 = \tilde{x}_2 - \pi_1 \xi \tilde{x}_1 - 2\dfrac{\hat{\xi}}{\xi}\tilde{x}_1 \\ \dot{\tilde{x}}_2 = m_0^{-1}\tilde{x}_3 - \pi_2 \xi^2 \tilde{x}_1 - m_0^{-1} l_d \tilde{x}_2 \\ \dot{\tilde{x}}_3 = \dot{D} - \pi_3 \xi^2 \tilde{x}_1. \end{cases} \tag{6.12}$$

Using the coordinate transformation $\zeta_1 = \xi^2 \tilde{x}_1, \zeta_2 = \xi \tilde{x}_2, \zeta_3 = \tilde{x}_3$, (6.12) can be written as

$$\begin{cases} \dot{\zeta}_1 = \xi^2 \tilde{x}_2 - \pi_1 \xi^3 \tilde{x}_1 = \xi(\zeta_2 - \pi_1 \zeta_1) \\ \dot{\zeta}_2 = \dot{\xi}\tilde{x}_2 + \xi(m_0^{-1}\tilde{x}_3 - \pi_2 \xi^2 \tilde{x}_1 - m_0^{-1} l_d \tilde{x}_2) \\ \quad = \xi(m_0^{-1}\zeta_3 - \pi_2 \zeta_1) + (\dot{\xi} - m_0^{-1} l_d \xi)\tilde{x}_2 \\ \dot{\zeta}_3 = -\pi_3 \xi \zeta_1 + \dot{D}. \end{cases} \tag{6.13}$$

Define the vector $\zeta = [\zeta_1, \zeta_2, \zeta_3]^T$. One can obtain

$$\dot{\zeta} = \xi H_0 \zeta + B_0 \tag{6.14}$$

with

$$H_0 = \begin{bmatrix} -\pi_1 & 1 & 0 \\ -\pi_2 & 0 & m_0^{-1} \\ -\pi_3 & 0 & 0 \end{bmatrix}, \quad B_0 = \begin{bmatrix} 0 \\ (\dot{\xi} - m_0^{-1} l_d \xi)\tilde{x}_2 \\ \dot{D} \end{bmatrix}.$$

If the constants π_1, π_2, π_3 are carefully selected such that H_0 is Hurwitz, there exists $P_0^T = P_0 > 0$ such that $H_0^T P_0 + P_0 H_0 = -I_3$ where I_3 is the 3×3 identity matrix.

Theorem 6.1. *Consider the AVSSs (6.4) with Assumption 6.1. If a predefined-time ESO is defined as (6.11), π_4 and π_5 are selected to satisfy $\xi > 1$ such that $\pi_4 \geq \lambda_{\min}(P_0)$ and $\pi_5 > \frac{2c_1\lambda_{\max}(P_0)}{\lambda_{\min}(P_0)} + \frac{(\lambda_{\max}(P_0))^2}{\lambda_{\min}(P_0)}$, the observer error $\tilde{x}$ can converge to $\|\tilde{x}\| \leq \delta_\zeta$ within the predefined time t_{c0} where $\delta_\zeta > 0$ will be established subsequently.*

Proof: The Lyapunov function is constructed as

$$V_e = \zeta^T P_0 \zeta. \tag{6.15}$$

The time derivative of V_e becomes

$$\begin{aligned}
\dot{V}_e &= \xi\zeta^T(H_0^T P_0 + P_0 H_0)\zeta + 2\zeta^T P_0 B_0 \\
&= -\xi\zeta^T\zeta + 2\zeta^T P_0 B_0 \\
&\leq -\pi_4(\pi_5 + \frac{\dot{\mu}_0}{\mu_0})\zeta^T\zeta + 2\lambda_{\max}(P_0)\|\zeta\||\dot{D}| \\
&+ 2\lambda_{\max}(P_0)\|\zeta\|\|(\dot{\xi} - m_0^{-1} l_d \xi)\tilde{x}_2\|.
\end{aligned} \tag{6.16}$$

Consider that π_4 is selected as $\pi_4 \geq \lambda_{\min}(P_0)$ while following inequalities hold

$$\begin{aligned}
&2\lambda_{\max}(P_0)\|\zeta\|\|(\dot{\xi} - m_0^{-1} l_d \xi)\tilde{x}_2\| \\
&\leq 2\lambda_{\max}(P_0)\|\zeta\|\|(\dot{\xi}/\xi - m_0^{-1} l_d)\zeta_2\| \\
&\leq 2c_1\lambda_{\max}(P_0)\|\zeta\|^2 \leq \frac{2c_1\lambda_{\max}(P_0)}{\lambda_{\min}(P_0)} V_e \\
&2\|\zeta\|\lambda_{\max}(P_0)\|\dot{D}\| \\
&\leq (\lambda_{\max}(P_0))^2\|\zeta\|^2 + \|\dot{D}\|^2 \\
&\leq \frac{(\lambda_{\max}(P_0))^2}{\lambda_{\min}(P_0)} V_e + \delta_{D2}^2
\end{aligned} \tag{6.17}$$

where $|\dot{\xi}/\xi - m_0^{-1} l_d| \leq |\dot{\xi}/\xi| + |m_0^{-1} l_d| \leq c_1$ holds with $c_1 > 0$ due to constants m_0, l_d, and the boundedness of $\dot{\xi}/\xi$, and $\|\dot{D}\| \leq \delta_{D2}^2$ is used according to Assumption 6.1.

Considering the inequalities above, (6.16) can be written as

$$\begin{aligned}
\dot{V}_e &\leq -\Big(\pi_5 - \frac{2c_1\lambda_{\max}(P_0)}{\lambda_{\min}(P_0)} - \frac{(\lambda_{\max}(P_0))^2}{\lambda_{\min}(P_0)} + \frac{\dot{\mu}_0}{\mu_0}\Big) V_e + \delta_{D2}^2 \\
&\leq -(\varsigma_0 + \frac{\dot{\mu}_0}{\mu_0}) V_e + \epsilon_0
\end{aligned} \tag{6.18}$$

where π_5 is selected to satisfy $\varsigma_0 = \pi_5 - \frac{2c_1\lambda_{\max}(P_0)}{\lambda_{\min}(P_0)} - \frac{(\lambda_{\max}(P_0))^2}{\lambda_{\min}(P_0)} > 0$, and $\epsilon_0 = \delta_{D2}^2$. According to Lemma 6.2, V_e will converge to the region $V_e \leq \iota_0 V_e(0) + \epsilon_0/\varsigma_0$ within the prior-known time t_{c0}, i.e., ζ will converge to

$$\|\zeta\| \leq \sqrt{\frac{\iota_0 V_e(0)+\epsilon_0/\varsigma_0}{\lambda_{\min}(P_0)}} = \delta_\zeta \tag{6.19}$$

within the predefined time t_{c0}. Furthermore, if the parameters π_4 and π_5 are chosen to satisfy $\xi > 1$, then the observer error $\|\tilde{x}\| \leq \|\zeta\| \leq \delta_\zeta$ within the predefined time t_{c0}. ■

Remark 6.3. Different from existing ESO designs [98, 121, 178], the estimation errors of the proposed predefined-time ESO can converge to the neighborhood of zero within a user-defined time t_{c0}, which can greatly enhance the observation performance.

6.3.3 Characterization of couplings and disturbances

The coordinate transformation is constructed as

$$\begin{aligned} e_1 &= x_1 - y_d \\ e_2 &= \hat{x}_2 - \alpha_1 \end{aligned} \tag{6.20}$$

where y_d is the desired trajectory of suspension space, α_1 denotes the virtual control input which will be defined later.

The error dynamics of the system can be written as

$$\dot{e}_1 = \Phi_1(e_2) + \alpha_1 + \tilde{x}_2 - \dot{y}_d \tag{6.21}$$

$$\begin{aligned} \dot{e}_2 &= \Phi_2(e_1) + m_0^{-1}(\hat{D} - l_s y_d - l_d \hat{x}_2 + F) \\ &\quad + \pi_2 \xi^2 \tilde{x}_1 - \dot{\alpha}_1 \end{aligned} \tag{6.22}$$

where $\Phi_1(e_2) = e_2$ and $\Phi_2(e_1) = -m_0^{-1} l_s e_1$ are the functions of e_2 and e_1, respectively.

Therefore, $\Phi_1(e_2)$ in the subsystem (6.21) and $\Phi_2(e_1)$ in the subsystem (6.22) are the coupling terms, which may have a profound effect on system stability and control performance. Considering the highly nonlinear characteristics, these coupling terms were usually considered known terms and then canceled directly in conventional control designs where the state signals were assumed measurable [5]. However, most existing AVSS controllers suffer from the absence of explicit discussion on the coupling effects, which may lead to performance loss if beneficial couplings are not reserved. Therefore, the characterization analysis of coupling terms is necessary and significant in the AVSS control design.

Furthermore, the lumped disturbance D in the AVSS dynamics should be assessed in terms of the direction and amplitude. Traditional control designs canceled the lumped disturbance directly to ensure system stability using the norm-based boundedness method [98]. However, the direction, which was seldom considered, may reveal the disturbance influence on tracking capability. Therefore, the connection between the disturbance characterization and tracking performance should be discussed thoroughly.

Definition 6.1. *For the error dynamics (6.21)-(6.22), the coupling effect indexes (CEIs) are defined as*

$$J_1 = \text{sgn}(e_1)\text{sgn}(\Phi_1(e_2)), J_2 = \text{sgn}(e_2)\text{sgn}(\Phi_2(e_1)). \tag{6.23}$$

Based on the constructed CEIs, the coupling effect can be determined

$$\begin{cases} J_i \lesseqgtr 0: \text{ Coupling effect is beneficial/detrimental,} \\ J_i = 0: \text{ Coupling effect is nil,} \quad i = 1, 2. \end{cases} \tag{6.24}$$

Definition 6.2. *Consider the error dynamics (6.21)-(6.22), the disturbance effect index (DEI) is denoted by*

$$J_D = \text{sgn}(e_2)\text{sgn}(\hat{D}). \tag{6.25}$$

Then the disturbance effect is given as

$$\begin{cases} J_D \lessgtr 0: \text{ Disturbance effect is beneficial/detrimental}, \\ J_D = 0: \text{ Disturbance effect is nil}. \end{cases} \tag{6.26}$$

Definitions 6.1 and 6.2 provide a novel perspective to analyze the effects of state couplings and lumped disturbance. If the beneficial ones occur, direct cancellation is not necessary which should be reserved instead to enhance the control performance. Thus, less control input could be potentially needed, leading to energy conservation performance.

Remark 6.4. Different from existing AVSS controllers [5], the velocity state and lumped disturbance in this article are obtained from the predefined-time ESO since the actual signals are previously unknown. The system stability can be kept even if the directions of velocity and lumped disturbance are wrongly estimated during some periods. Moreover, the switching logic in the CEIs and DEI may lead to the chattering phenomenon, which needs more investigations in future work.

6.3.4 Predefined-time output feedback control design

A Lyapunov function is defined as

$$V_1 = \frac{1}{2}e_1^2 \tag{6.27}$$

and its time derivative becomes

$$\dot{V}_1 = e_1\dot{e}_1 = e_1(\Phi_1(e_2) + \alpha_1 + \tilde{x}_2 - \dot{y}_d). \tag{6.28}$$

The virtual control input α_1 is designed as

$$\alpha_1 = -\frac{k_1+1+\dot{\mu}_1/\mu_1}{2}e_1 + \dot{y}_d \tag{6.29}$$

where $k_1 > 0$, $\mu_1 = \mu(t, t_{c1}, \iota_1)$ with $t_{c1} > 0$, $\iota_1 > 0$.

Considering Young's inequality, (6.28) yields

$$\begin{aligned}\dot{V}_1 &= e_1(\Phi_1(e_2) - \frac{k_1 + 1 + \dot{\mu}_1/\mu_1}{2}e_1 + \dot{y}_d + \tilde{x}_2 - \dot{y}_d) \\ &\leq e_1\Phi_1(e_2) - \frac{k_1 + \dot{\mu}_1/\mu_1}{2}e_1^2 + \frac{1}{2}\delta_\zeta^2.\end{aligned} \tag{6.30}$$

It should be noted that the velocity signal is required in calculating $\dot{\alpha}_1$. Since only the displacement measurement is provided, a SOPT filter is proposed to estimate $\dot{\alpha}_1$. Denote Γ_1 and Γ_2 are the estimates of α_1 and $\dot{\alpha}_1$ with estimate errors $\tilde{\Gamma}_1 = \alpha_1 - \Gamma_1$, $\tilde{\Gamma}_2 = \dot{\alpha}_1 - \Gamma_2$. The novel SOPT filter is proposed as

$$\begin{cases}\dot{\Gamma}_1 = \Gamma_2 + \rho_1\varphi\tilde{\Gamma}_1 + \dfrac{\dot{\varphi}}{\varphi}\tilde{\Gamma}_1 \\ \dot{\Gamma}_2 = \rho_2\varphi^2\tilde{\Gamma}_1\end{cases} \tag{6.31}$$

where $\varphi = \rho_3(\rho_4 + \frac{\dot{\mu}_2}{\mu_2})$ with $\rho_i > 0$ for $i = 1, ..., 4$, $\mu_2 = \mu(t, t_{c2}, \iota_2)$ with $t_{c2} > 0$, $\iota_2 > 0$.

Consider the coordinate transformation $\eta = [\eta_1, \eta_2]^T$ with $\eta_1 = \varphi\tilde{\Gamma}_1$, $\eta_2 = \tilde{\Gamma}_2$. Then the error dynamics for the SOPT filter are

$$\begin{cases}\dot{\eta}_1 = \dot{\varphi}\tilde{\Gamma}_1 + \varphi(\tilde{\Gamma}_2 - \rho_1\varphi\tilde{\Gamma}_1 - \dfrac{\dot{\varphi}}{\varphi}\tilde{\Gamma}_1) = -\rho_1\varphi\eta_1 + \varphi\eta_2 \\ \dot{\eta}_2 = -\rho_2\varphi\eta_1 + \ddot{\alpha}_1\end{cases} \tag{6.32}$$

which can be written in the matrix form

$$\dot{\eta} = \varphi H_1\eta + B_1 \tag{6.33}$$

with

$$H_1 = \begin{bmatrix}-\rho_1 & 1 \\ -\rho_2 & 0\end{bmatrix}, \quad B_1 = \begin{bmatrix}0 \\ \ddot{\alpha}_1\end{bmatrix}. \tag{6.34}$$

Since H_1 is Hurwitz, there exists $P_1^T = P > 0$ such that $H_1^T P_1 + P_1 H_1 = -I_2$ with the 2×2 identity matrix I_2.

Lemma 6.3. *If the SOPT filter is proposed as (6.31), ρ_3 and ρ_4 are selected to satisfy*

$\phi > 1$ *such that* $\rho_3 > \lambda_{\min}(P_1)$, $\rho_4 > (\lambda_{\max}(P_1))^2/\lambda_{\min}(P_1)$, *then the filtering error* $\|\tilde{\Gamma}\|$ *can converge to* $\|\tilde{\Gamma}\| \leq \delta_\Gamma$ *within the predefined time* t_{c2} *where* $\delta_\Gamma > 0$ *will be specified subsequently.*

Proof: The proof of Lemma 6.3 is presented in Appendix B.

Remark 6.5. Unlike traditional predefined-time controllers using finite-time differentiators [179] or first-order command filters [180], a novel SOPT filter is proposed to avoid the phenomenon of "explosion of complexity" while the filtering error $||\tilde{\Gamma}||$ can converge to a small neighborhood near zero within the prior-known time t_{c2}.

The actual control input for the predefined-time output feedback control is proposed

$$\begin{aligned} F = &-G(J_1)e_1 - G(J_2)m_0\Phi_2(e_1) - G(J_D)\hat{D} + l_s y_d \\ &+ l_d\hat{x}_2 + m_0\Gamma_2 - \frac{k_2 + \dot{\mu}_1/\mu_1}{2}m_0 e_2 - k_3 \tanh(\frac{e_2}{\nu}) \end{aligned} \tag{6.35}$$

where $k_2 > 0$ and $k_3 > 0$ are positive design constants, $\nu > 0$ is a small sharpness gain, the function G is constructed as

$$G(y) = \begin{cases} 1, \text{ if } y \geq 0, \\ 0, \text{ if } y < 0. \end{cases} \tag{6.36}$$

Theorem 6.2. *For the AVSSs with external disturbances under Assumptions 6.1 and 6.2, if the predefined-time ESO (6.11), virtual control input* α_1 *(6.29), SOPT filter (6.31), actual control law (6.35) are proposed, then the tracking error* e_1 *will approach to* $|e_1| \leq \delta_e$ *within the preset time* t_{c1} *where* $\delta_e > 0$ *will be determined subsequently.*

Proof: The Lyapunov function is defined as

$$V_2 = V_1 + \frac{1}{2}m_0 e_2^2. \tag{6.37}$$

The time derivative of (6.37) can be obtained as

$$\begin{aligned}\dot{V}_2 &= \dot{V}_1 + e_2 m_0 \dot{e}_2 \\ &= \dot{V}_1 + e_2(m_0\Phi_2(e_1) + \hat{D} - l_s y_d - l_d \hat{x}_2 + F \\ &+ m_0\pi_2\xi^2\tilde{x}_1 - m_0\dot{\alpha}_1) \\ &\leq -\frac{k_1 + \dot{\mu}_1/\mu_1}{2}e_1^2 - \frac{k_2 + \dot{\mu}_1/\mu_1}{2}m_0 e_2^2 \\ &+ (1 - G(J_1))e_1\Phi_1(e_2) + (1 - G(J_2))m_0 e_2\Phi_2(e_1) \\ &+ (1 - G(J_D))\hat{D}e_2 + (m_0\pi_2\xi^2\tilde{x}_1 - m_0\tilde{\Gamma}_2)e_2 \\ &- k_3 e_2 \tanh(\frac{e_2}{\nu}) + \frac{1}{2}\delta_\zeta^2.\end{aligned} \tag{6.38}$$

The following terms should be further discussed.

$$\begin{aligned}R_1 &= (1 - G(J_1))e_1\Phi_1(e_2), \\ R_2 &= (1 - G(J_2))m_0 e_2\Phi_2(e_1), \\ R_3 &= (1 - G(J_D))\hat{D}e_2.\end{aligned} \tag{6.39}$$

The signs of R_1, R_2 and R_3 should be further discussed. Let us take R_1 as an example. If the coupling effect of $\Phi_1(e_2)$ is beneficial such that $J_1 < 0$, then we have $e_1\Phi_1(e_2) < 0$. One can obtain $G(J_1) = 0$ and $R_1 = (1 - G(J_1))e_1\Phi_1(e_2) < 0$. If the coupling effect of $\Phi_1(e_2)$ is detrimental such that $J_1 > 0$, then it leads to $e_1\Phi_1(e_2) > 0$. We have $G(J_1) = 1$ and $R_1 = (1 - G(J_1))e_1\Phi_1(e_2) = 0$. Furthermore, if the coupling effect of $\Phi_1(e_1)$ is nil, denoting $J_1 = 0$, it means $e_1\Phi_1(e_2) = 0$. Then one can have $G(J_1) = 0$ and $R_1 = (1 - G(J_1))e_1\Phi_1(e_2) = 0$. Therefore, the inequality $R_1 = (1 - G(J_1))e_1\Phi_1(e_2) \leq 0$ always holds. Similarly, the inequalities R_2 and R_3 can be demonstrated. Then the beneficial couplings and lumped disturbance can remain in the control design for enhanced control performance and potentially less energy consumption.

Note that if k_3 is selected such that $|m_0\pi_2\xi^2\tilde{x}_1 - m_0\tilde{\Gamma}_2| \leq k_3$, then one has

$$\begin{aligned}&(m_0\pi_2\xi^2\tilde{x}_1 - m_0\tilde{\Gamma}_2)e_2 - k_3e_2\text{tanh}(\frac{e_2}{\nu})\\&\leq k_3|e_2| - k_3e_2\text{tanh}(\frac{e_2}{\nu}) \leq 0.2785k_3\nu.\end{aligned} \tag{6.40}$$

Then one can obtain

$$\begin{aligned}\dot{V}_2 &\leq -\frac{k_1 + \dot{\mu}_1/\mu_1}{2}e_1^2 - \frac{k_2 + \dot{\mu}_1/\mu_1}{2}m_0e_2^2\\&+ \frac{1}{2}\delta_\zeta^2 + 0.2785k_3\nu\\&\leq -(\varsigma_2 + \dot{\mu}_1/\mu_1)V_2 + \epsilon_2\end{aligned} \tag{6.41}$$

where $\varsigma_2 = \min\{k_1, k_2\}$, $\epsilon_2 = \frac{1}{2}\delta_\zeta^2 + 0.2785k_3\nu$.

Then we have V_2 will converge to the region $V_2(t) \leq \iota_1V_2(0)+\epsilon_2/\varsigma_2$ within the predefined time t_{c1}, which suggests that e_1 will converge to $|e_1| \leq \sqrt{2\iota_1V_2(0) + 2\epsilon_2/\varsigma_2} = \delta_e$ within the preset time t_{c1}. ■

Remark 6.6. Compared with existing finite-time/fixed-time active suspension controllers [65, 134, 136], the maximum allowable settling time t_{c1} can be arbitrarily selected which is independent of initial conditions and control gains.

Remark 6.7. The parameter determination process for the proposed control scheme is mainly driven by control performance specifications and stability requirements. The predefined convergence time t_{c1} should satisfy $t_{c1} \geq t_{c0}$ and $t_{c1} \geq t_{c2}$ to prioritize the convergence rates of the predefined-time ESO and SOPT filter over the controller. Then $0 < \iota_i \ll 1$ for $i = 0, 1, 2$ are selected to regulate the scaling function performance. Furthermore, $\pi_i > 0$ for $i = 1, ..., 5$ are tuned for the predefined-time ESO with stability conditions $\pi_4 \geq \lambda_{\text{min}}(P_0)$ and $\pi_5 > \frac{2c_1\lambda_{\text{max}}(P_0)}{\lambda_{\text{min}}(P_0)} + \frac{(\lambda_{\text{max}}(P_0))^2}{\lambda_{\text{min}}(P_0)}$. Similarly, the performance of the SOPT filter is adjusted using $\rho_i > 0$ for $i = 1, ..., 4$ with stability constraints $\rho_3 > \lambda_{\text{min}}(P_1)$ and $\rho_4 > (\lambda_{\text{max}}(P_1))^2/\lambda_{\text{min}}(P_1)$. Besides, transient performance is enhanced by adopting relatively larger k_1 and k_2, whereas the control gain k_3 and the sharpness gain ν should be jointly tuned to balance system robustness against chattering mitigation.

Table 6.1: AVSS nominal parameters

Symbols	Values	Symbols	Values
m_s	2.45 kg	m_u	1 kg
l_s	900 N/m	l_d	8 Ns/m
l_t	1250 N/m	l_b	5 Ns/m

Table 6.2: X-mechanism reference parameters

Symbols	Values	Symbols	Values
M	22 kg	l_a	5 Ns/m
θ_1	π/6 rad	l_r	0.15 Ns/m
L_1	0.1 m	l_h	500 N/m
L_2	0.2 m	l_v	350 N/m
ϖ_1	-1 m/s^2	ϖ_2	1 m/s^2

6.4 Experimental validation

This section presents comparative experiments conducted on a quarter-car bench-scale AVSS to verify the anti-vibration performance of the proposed control methodology in stabilizing the vehicle body and attenuating disturbances. The hardware experimental platform comprises three vertically aligned plates, which is depicted in Fig. 6.3 with the parameters given in Table 6.1. The uppermost plate is described as the vehicle's body, supported by the suspension structure using dampers and springs. Positioned between the top and middle plates, a premium DC motor is used to generate the required active control force. The lower plate is coupled with a brushed servo motor, designed to provide various road profiles through the lead screw. The sprung mass displacement, suspension space, and road excitation are measured using high-resolution optical encoders, while the acceleration of the vehicle body is obtained via a dual-axis accelerometer. More detailed information on this AVSS setup and experiment procedures can be referred to [96]. The sampling time is set to 1 ms based on the physical platform and computer software.

In this section, two different road inputs are provided to validate the control performance of the proposed control method including the sinusoidal road input (SRI) and

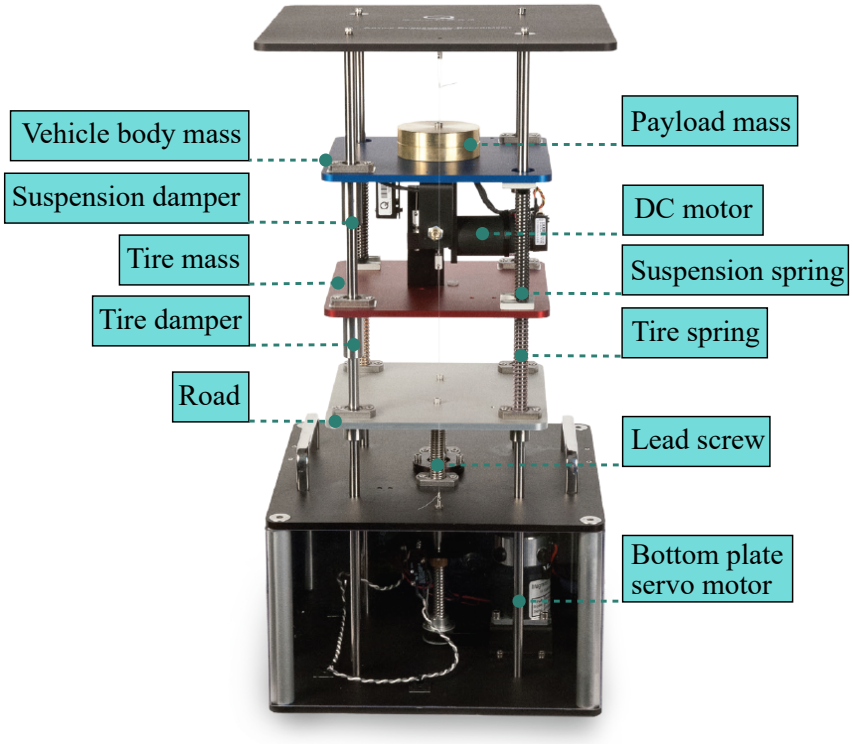

Fig. 6.3: AVSS experimental platform setup

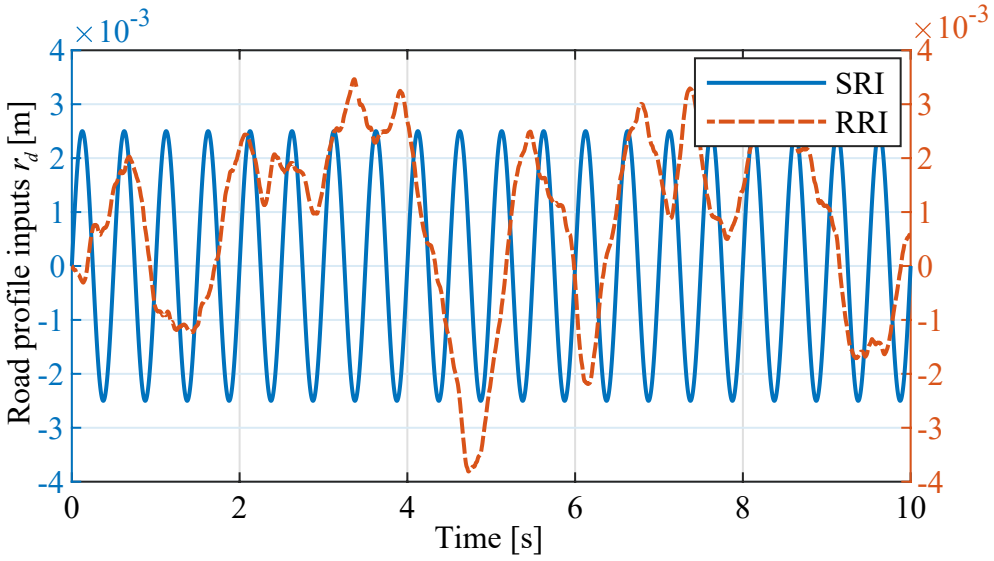

Fig. 6.4: The road profiles r_d

random road input (RRI) presented in Fig. 6.4. Utilizing the harmonic balance technique and examining the displacement transmissibility [69], the parameters for the X-mechanism reference dynamics are presented in Table 6.2. Initial values are set to zero for simplicity. Additionally, the uncertain dynamic coefficients present $\gamma_i = 10\%$ per-

turbations from their nominal values.

Five suspension systems are considered.

1) Passive: This abbreviation means the passive suspension system.

2) NTSM: This abbreviation stands for the nonsingular terminal sliding mode control [65].

3) PMRC: This abbreviation is the partial measurement-based robust control [98].

4) OFFT: This abbreviation presents the output feedback finite-time control [121].

5) Proposed: This abbreviation denotes the proposed predefined-time output-feedback control.

The values for the NTSM design are selected as $\chi = 500$, $l = 100$, $\lambda_1 = \lambda_2 = 0.01$, $k_1 = 1$, $k_2 = 10$, $\alpha = 0.9$, $\alpha_1 = 9/7$, $\alpha_2 = 3$, $\alpha_3 = 0.5$. Furthermore, the parameters for the PMRC method are given as $L_1 = 10$, $L_2 = 20$, $\lambda_0 = 4$, $\lambda_1 = 2$, $\lambda_2 = 1$, $\lambda_3 = 2$, $\lambda_4 = 1$, $k_1 = 40$, $k_2 = 10$, $\eta_1 = 12$, $\eta_2 = 12$. The values for the OFFT control are $p = 1.5$, $q = 1$, $\alpha_1 = 0.25$, $c_1 = c_2 = c_3 = 1.5$, $c_4 = c_5 = 0.5$, $c_6 = 8$, $c_7 = 3$. Moreover, the gains of the proposed control method are set as $t_{c1} = t_{c2} = t_{c3} = 1$s for the predefined time, $\iota_1 = \iota_2 = \iota_3 = 0.1, \pi_1 = \pi_2 = 10, \pi_3 = 2, \pi_4 = \pi_5 = 5, \rho_1 = \rho_2 = 20$, $\rho_3 = \rho_4 = 5$, $k_1 = 220$, $k_2 = 120$, $k_3 = 5$, and $\nu = 0.1$. The initial states are selected as zero for simplicity.

The comparative experimental outcomes for the five suspension systems are illustrated in Figs. 6.5–6.9 for the SRI case and Figs. 6.10–6.14 for the RRI case.

Vehicle body acceleration is consistently regarded as a crucial factor for ride comfort. The time-domain vehicle body accelerations of the passive suspension, NTSM, PMRC, OFFT, and proposed control are depicted in Figs. 6.5 and 6.10, while the corresponding frequency-domain accelerations are provided in Figs. 6.6 and 6.11, respectively. According to Figs. 6.5 and 6.10, vehicle body acceleration amplitudes of four active suspensions can be obviously reduced in comparison with those of the passive suspension. Furthermore, the proposed design can achieve the lowest vehicle body acceleration

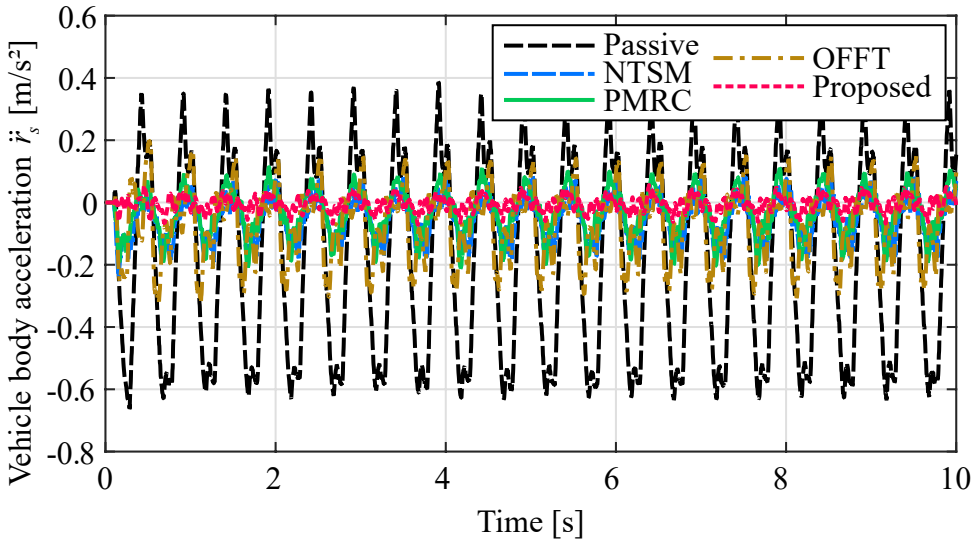

Fig. 6.5: Case SRI: The time-domain vehicle body acceleration $\ddot{r}_s$

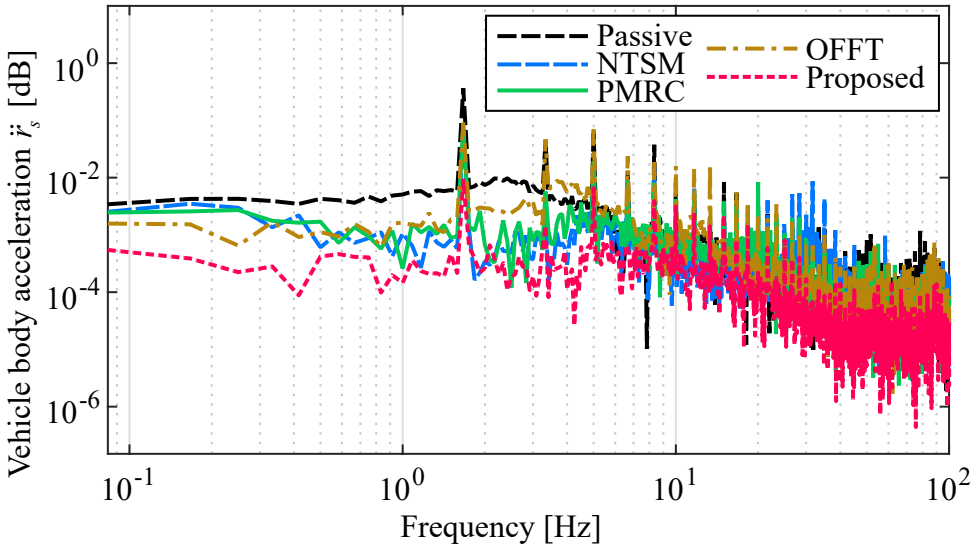

Fig. 6.6: Case SRI: The frequency-domain vehicle body acceleration $\ddot{r}_s$

among four AVSS controllers which presents higher ride comfort under different rough roads. The sensitive frequency spectrum for humans lies within 4Hz to 12.5Hz according to the International Organization of Standardization [107]. From the corresponding frequency-domain vehicle body accelerations in Figs. 6.6 and 6.11, a similar conclusion can be made since the acceleration level of the proposed control is smaller than those of the passive suspension, NTSM control, PMRC design, and OFFT method.

The control input signals under the SRI case and RRI case are given in Figs. 6.7 and 6.12. In comparison with the NTSM, PMRC, and OFFT methods, the proposed control

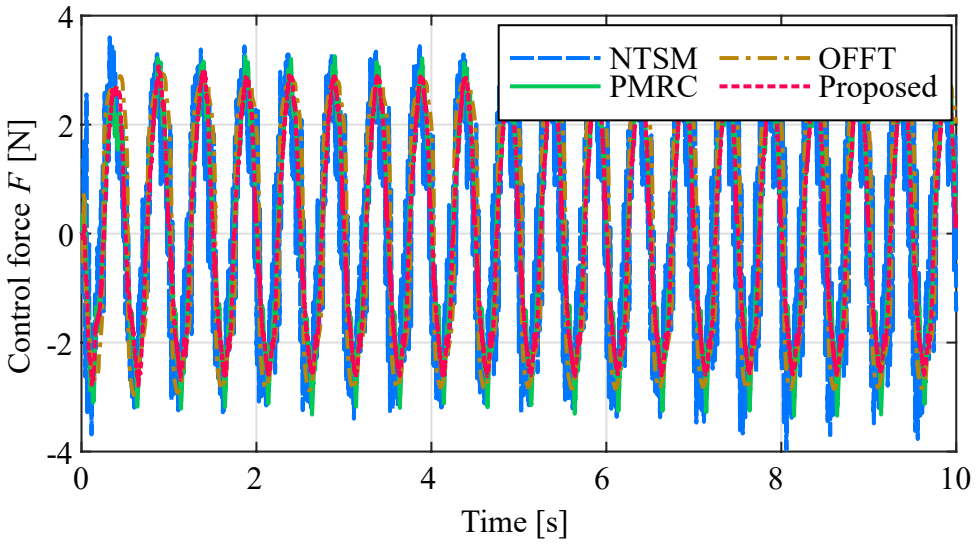

Fig. 6.7: Case SRI: The control force F

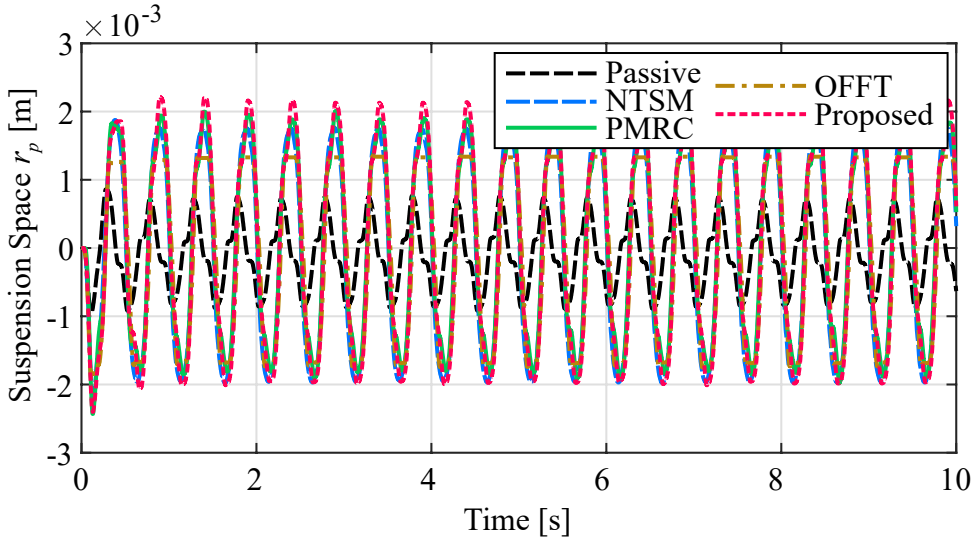

Fig. 6.8: Case SRI: The suspension space $\ddot{r}_p$

exhibits smaller control inputs in both cases. Thus, less control efforts are needed while more satisfactory ride comfort can be achieved. Moreover, the chattering phenomenon in traditional NTSM and PMRC methods are more conspicuous which may degrade the control performance.

To quantitatively evaluate the control performance, two indexes, $\mathrm{RMS_R}(\ddot{z}_s)$ and $\mathrm{RMS_E}(\Psi)$ are employed to compare the ride comfort and energy consumption, respectively, which are described as $\mathrm{RMS_R}(\ddot{z}_s) = \sqrt{\frac{1}{T}\int_0^T \ddot{z}_s^2 dt}$ and $\mathrm{RMS_E}(\Psi) = \sqrt{\frac{1}{T}\int_0^T (\Psi(\tau))^2 d\tau}$ where $\Psi = F\dot{r}_p$ for $F\dot{r}_p > 0$, $\Psi = 0$ for else, and T is the experiment period. The assessment

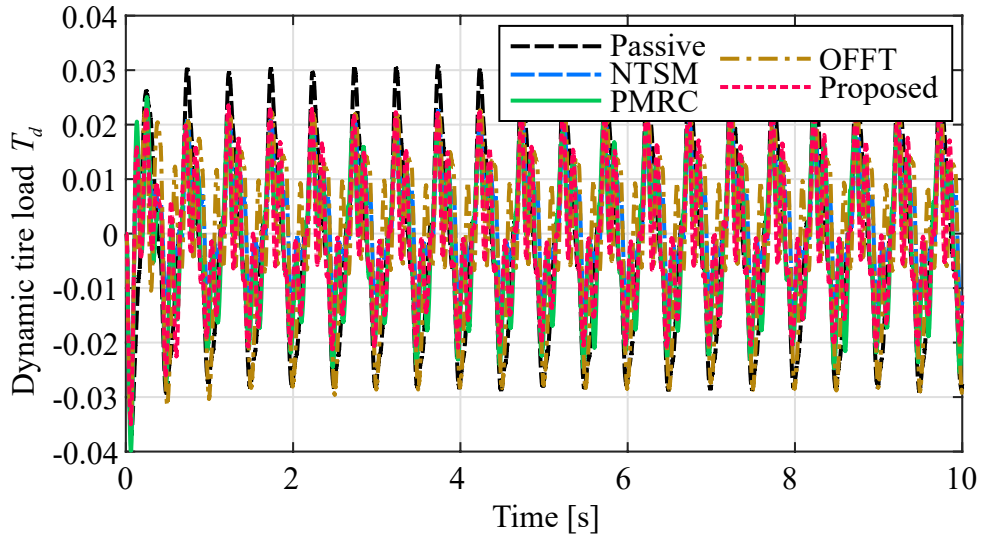

Fig. 6.9: Case SRI: The dynamic tire load T_d

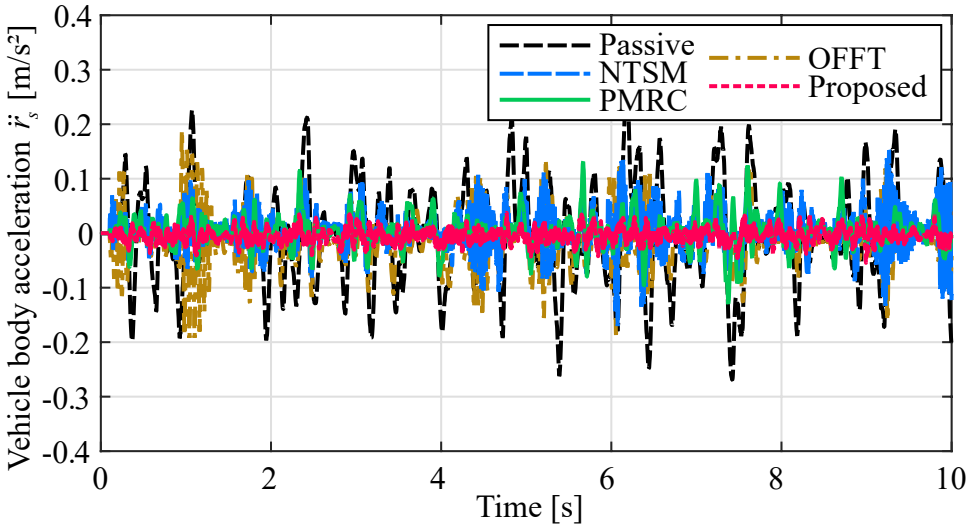

Fig. 6.10: Case RRI: The time-domain vehicle body acceleration $\ddot{r}_s$

of control performance regarding ride comfort and energy consumption is detailed in Table 6.3. When contrasted with the passive suspension, the ride comfort RMS_R of the proposed control witnesses a significant reduction of 93.5% and 81.7% under SRI and RRI cases, respectively. Furthermore, the energy consumption indexes of the PMRC design (14.2% and 9.8% reduction) and OFFT method (11.8% and 43.3% reduction) under SRI and RRI cases are presented to show the energy-saving performance compared with those of the NTSM method. However, the RMS_E of the proposed control can drop by 31.5% and 58.1% compared with the NTSM method, respectively. Hence,

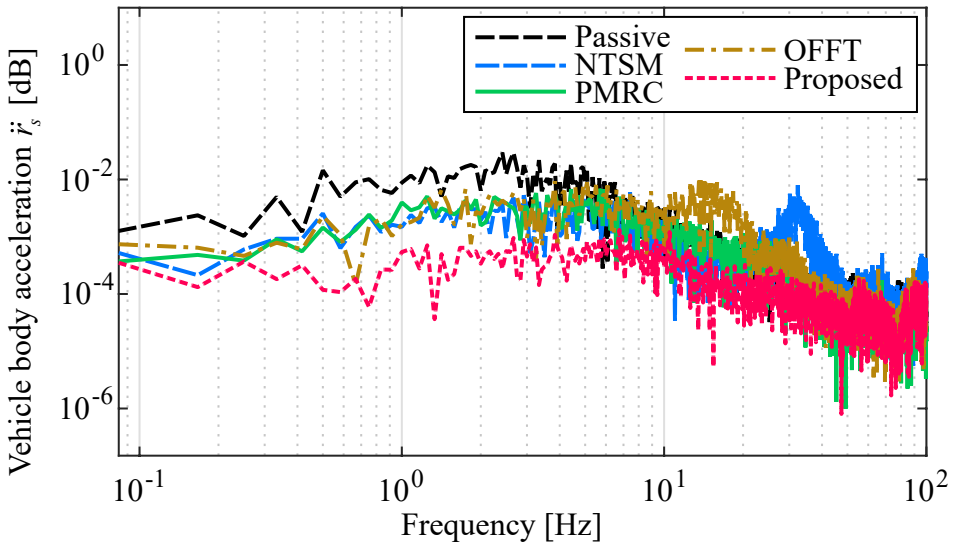

Fig. 6.11: Case RRI: The frequency-domain vehicle body acceleration $\ddot{r}_s$

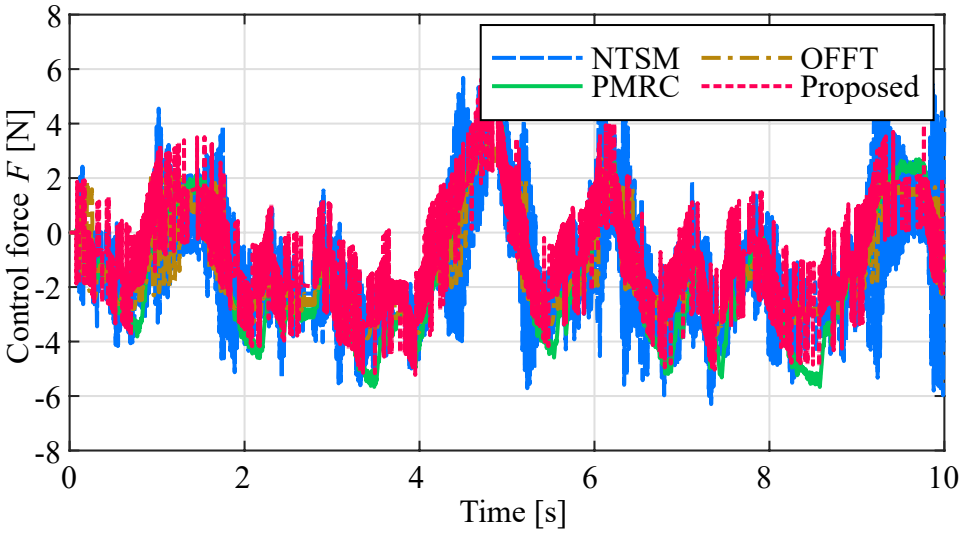

Fig. 6.12: Case RRI: The control force F

less energy consumption is used with the proposed control method while satisfactory ride comfort is guaranteed, which further indicates superior control performance.

Moreover, the maximum suspension space should not exceed a certain permissible extent, which is 3.8 cm for the experimental AVSS setup. From Figs. 6.8 and 6.13, the suspension space performance for five suspensions are all kept within reasonable limits. Furthermore, the requirements for dynamic tire load under SRI and RRI cases can be obeyed within the acceptable range such that $T_d = |W_t + W_b|/((m_s + m_u)g) \leq 1$. Therefore, driving safety and road-holding ability can be guaranteed simultaneously.

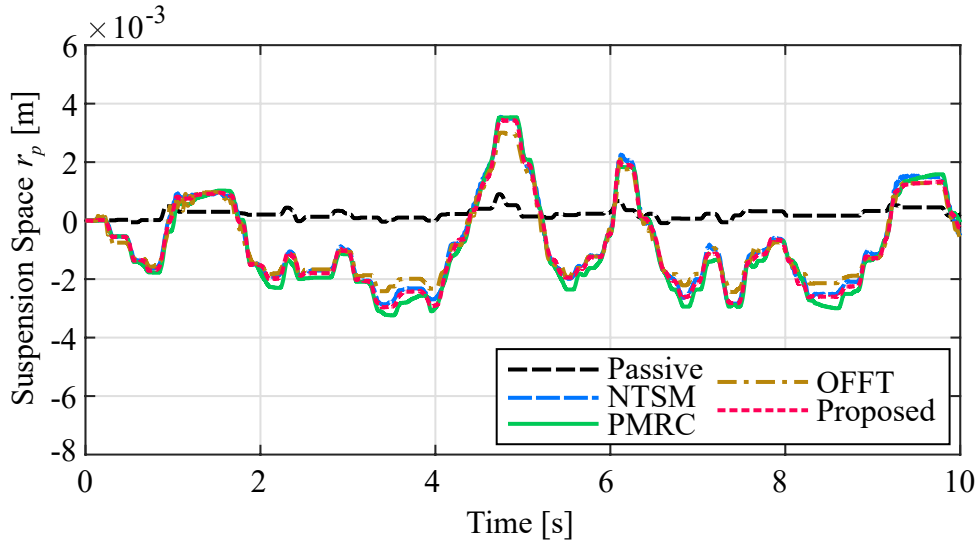

Fig. 6.13: Case RRI: The suspension space $\ddot{r}_p$

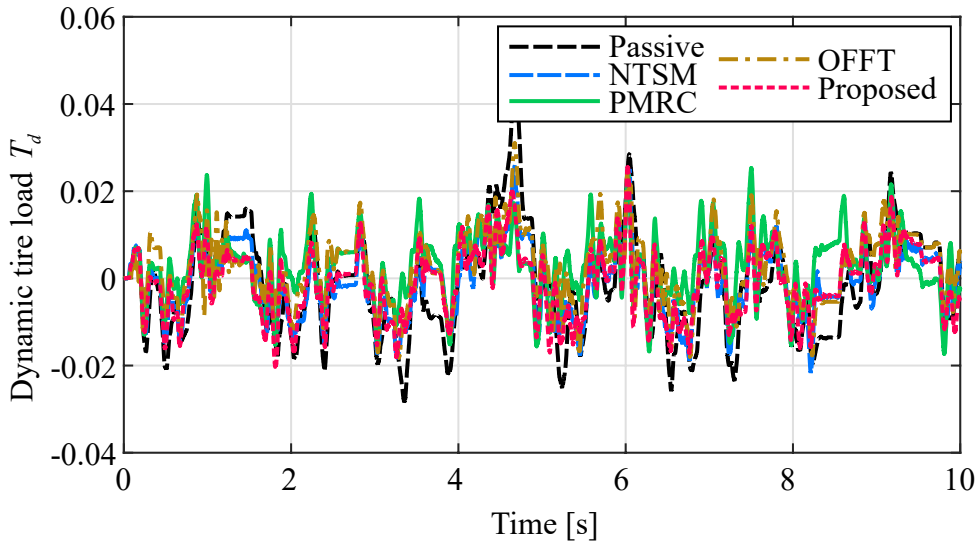

Fig. 6.14: Case RRI: The dynamic tire load T_d

6.5 Conclusion

In this paper, a novel energy-efficient predefined-time output feedback control is proposed for AVSSs with partial-state measurements, uncertain dynamics, and external disturbances. The X-mechanism reference dynamics are introduced to retain the beneficial stiffness/damping nonlinearities; the control performance can be enhanced utilizing the effect characterization method which reserves beneficial couplings/disturbances instead of direct cancellation, which leads to the potential energy conservation performance. By

Table 6.3: Performance Evaluation of Ride Comfort and Energy Consumption

Cases	Controllers	RMS_R	RMS_E
Case 1	Passive	0.3677	/
	NTSM	0.1036(↓ 71.6%)	0.0289
	PMRC	0.0928(↓ 74.7%)	0.0248(↓ 14.2%)
	OFFT	0.1340(↓ 63.6%)	0.0255(↓ 11.8%)
	Proposed	0.0239(↓ 93.5%)	0.0198(↓ 31.5%)
Case 2	Passive	0.0900	/
	NTSM	0.0355(↓ 60.6%)	0.0215
	PMRC	0.0303(↓ 66.3%)	0.0194(↓ 9.8%)
	OFFT	0.0588(↓ 34.7%)	0.0122(↓ 43.3%)
	Proposed	0.0165(↓ 81.7%)	0.0090(↓ 58.1%)

using the time-varying scaling function technique, a novel predefined-time ESO is proposed to estimate the velocities and disturbances. Together with the predefined-time ESO and SOPT filter, tracking errors can converge to a small region within the user-selected time, which is independent of initial states and control parameters. Comparative experiments are provided to demonstrate that the proposed predefined-time output feedback control can obtain better ride comfort with significant energy conservation up to 58% compared to other methods. Future studies will focus on advanced smoothing techniques to mitigate chattering while preserving the effect characterization method, alongside real-car verification to optimize the vibration isolation performance.

Appendix A Proof of Lemma 6.2

Consider $\bar{V}(t) = \mu V(t)$ and then its time derivative becomes

$$\begin{aligned}\dot{\bar{V}}(t) &= \dot{\mu}V(t) + \mu\dot{V}(t) = -\varsigma\bar{V}(t) + \mu\epsilon \\ &\leq -\varsigma\bar{V}(t) + \epsilon/\iota\end{aligned} \tag{6.42}$$

which leads to

$$\begin{aligned}\bar{V}(t) &\leq \frac{\epsilon}{\varsigma\iota} + (\bar{V}(0) - \frac{\epsilon}{\varsigma\iota})e^{-\varsigma t} \leq \frac{\epsilon}{\varsigma\iota} + \mu(0, t_c, \iota)V_0 e^{-\varsigma t} \\ &\leq \frac{\epsilon}{\varsigma\iota} + \frac{1}{1+\iota}V_0 e^{-\varsigma t}.\end{aligned} \tag{6.43}$$

One can obtain

$$V(t) \leq \tfrac{\epsilon}{\varsigma\iota\mu} + \tfrac{1}{(1+\iota)\mu}V_0 e^{-\varsigma t} \tag{6.44}$$

then $V(t)$ will approach to the region $V(t) \leq \iota V_0 + \epsilon/\varsigma$ within predefined time t_c and then converge to $V(t) \leq \epsilon/\varsigma$ asymptotically. ■

Appendix B Proof of Lemma 6.3

For the Lyapunov function $V_\eta = \eta P_1 \eta$, its time derivative becomes

$$\begin{aligned}\dot{V}_\eta &= -\varphi\eta^T\eta + 2\eta^T P_1 B_1 \\ &= -\rho_3(\rho_4 + \frac{\dot{\mu}_2}{\mu_2})\eta^T\eta + 2\lambda_{\max}(P_1)\|\eta\|\|\ddot{\alpha}_1\|.\end{aligned} \tag{6.45}$$

Since μ_1 is at least C^3, one can obtain that $\dot{\alpha}_1$, $\ddot{\alpha}_1$ exit. For AVSSs (6.4) with bounded initial states and bounded $\ddot{y}_d$ and $\dddot{y}_d$ in Assumption 6.2, there might exist a positive constant δ_α such that $|\ddot{\alpha}_1| \leq \delta_\alpha$. By selecting $\rho_3 > \lambda_{\min}(P_1)$, (6.45) yields

$$\begin{aligned}\dot{V}_\eta &\leq -(\rho_4 + \frac{\dot{\mu}_2}{\mu_2})V_\eta + 2\lambda_{\max}(P_1)\|\eta\|\|\ddot{\alpha}_1\| \\ &\leq -(\rho_4 - \frac{(\lambda_{\max}(P_1))^2}{\lambda_{\min}(P_1)} + \frac{\dot{\mu}_2}{\mu_2})V_\eta + \delta_\alpha^2 \\ &\leq -(\varsigma_1 + \frac{\dot{\mu}_2}{\mu_2})V_\eta + \epsilon_1\end{aligned} \tag{6.46}$$

with $\varsigma_1 = \rho_4 - (\lambda_{\max}(P_1))^2/\lambda_{\min}(P_1)$, $\epsilon_1 = \delta_\alpha^2$.

If ρ_4 is selected to satisfy $\varsigma_1 > 0$, then we have V_η will converge to the region $V_\eta \leq$

$\iota_2 V_\eta(0) + \epsilon_1/\varsigma_1$ within the predefined time t_{c2}. Therefore, η will converge to

$$\|\eta\| \leq \sqrt{\frac{\iota_2 V_\eta(0)+\epsilon_1/\varsigma_1}{\lambda_{\min}(P_1)}} = \delta_\Gamma. \tag{6.47}$$

Furthermore, if ρ_3 and ρ_4 are chosen to satisfy $\varphi > 1$, then the filtering error $\|\tilde{\Gamma}\|$ can converge to $\|\tilde{\Gamma}\| \leq \|\eta\| \leq \delta_\Gamma$ within the predefined time t_{c2}. ■

7 Conclusions and Future Works

7.1 Conclusions

The main objective of this thesis is systematically investigate finite-time energy-saving control for AVSSs with system uncertainties and external disturbances. Various active suspension control designs are presented to enhance driving performance under critical road conditions. Hence, promising improvements in ride comfort, driving safety, and energy conservation can be achieved under physical suspension limitations. The contributions of this thesis can be enumerated as follows.

To effectively handle uncertain dynamics and external disturbances, a novel finite-time saturated control is proposed for AVSSs to strengthen the suspension performance including ride comfort and driving maneuverability. The whole control structure is model-free to enhance the robustness under changing road conditions. Moreover, the control signal is designed to be naturally constrained within a predesignate range hyperbolic function and the bound-based adaptive method to avoid possible input saturations. Therefore, an enhanced version of model-free active suspension control is proposed such that the finite-time stability can be derived with the naturally control input.

To address the inherent challenge of excessive energy consumption, a new fixed-time safe-by-design control scheme is proposed for AVSSs employing a bioinspired X-shaped reference. By introducing and analyzing beneficial stiffness and damping effects, potential energy conservation can be achieved since low control inputs are required. Furthermore, to restrain displacement and velocity within safety boundaries, asymmetric time-varying barrier Lyapunov functions are integrated, together with input saturations, to ensure safe-by-design properties. The fixed-time control theory is an advanced extension of existing finite-time stability, where the convergence time is free from initial state conditions. The transient response characteristics and better disturbance-rejection

ability can be enhanced to improve ride comfort and driving safety.

To better address actuator faults, reduce energy consumption, and improve transient performance, a predefined-time fault-tolerant control is developed for uncertain AVSSs with external disturbances. Apart from the reference X-dynamics with beneficial nonlinearities, beneficial disturbance effects are analyzed and reserved utilizing the conditional disturbance cancellation scheme, thus enriching the energy conservation performance. As an upgrade to fixed-time stability, the proposed controller can achieve predefined-time convergence, making the settling time independent of both initial states and control gains, while also allowing for arbitrary specification of the residual bound. Furthermore, by utilizing the continuous piece-wise function and the quadratic fraction inequality, the singularity problem can be avoided and the chattering phenomenon can be alleviated.

Despite the partial state measurement which is usually neglected in most existing active suspension controllers, a predefined-time output feedback control is established for AVSSs with uncertain dynamics and external disturbances. A predefined-time extended state observer is first proposed based on the time-varying scaling function, which can be used to estimate velocities and disturbances. To further improve energy efficiency, alongside the X-mechanism reference dynamics with beneficial nonlinearities, both advantageous disturbances and couplings are assessed and retained by using the effect characterization method. The settling time of the closed-loop control system can be prior-specified using only one constant, which is irrelevant to initial states and control gains.

7.2 Future works

This thesis presents an in-depth and detailed investigation into the finite-time control for AVSSs to achieve ride comfort and driving safety. However, there remain numerous aspects in both theory and applications of active suspension control designs that merit further exploration. The following areas may be considered.

1) The actuator bandwidth limitations may restrict the vibration suppression abil-

ity under high-frequency road conditions. Different bandwidth-aware controllers should be explored to improve control performance.

2) Considering that only quarter-car AVSSs are investigated in this thesis, the theoretical analysis should be extended to half-car and full-car systems to incorporate critical roll/pitch coupling effects, stochastic disturbances, and varying payloads.

3) The proposed control algorithms need to be implemented on practical platforms rather than laboratory setups to verify their suspension performance compared with existing controller designs. In addition to the simulations on the full-car model, hardware-in-the-loop validations and prototype field trials will be conducted.

4) With the development of sensing technology, rough road profiles could potentially be predicted in advance. This would enable AVSSs to utilize known road surface data for planning and control designs under extreme road conditions, ensuring driving safety without significantly compromising ride comfort.

Bibliography

[1] G. Chen, G. Du, J. Xia, X. Xie, and Z. Wang, "Aperiodic sampled-data H_∞ control of vehicle active suspension system: An uncertain discrete-time model approach," *IEEE Trans. Ind. Inf.*, vol. 20, no. 4, pp. 6739 – 6750, 2024.

[2] H. Pan, W. Sun, X. Jing, H. Gao, and J. Yao, "Adaptive tracking control for active suspension systems with non-ideal actuators," *J. Sound Vib.*, vol. 399, pp. 2–20, 2017.

[3] H. Pan, W. Sun, H. Gao, and J. Yu, "Finite-time stabilization for vehicle active suspension systems with hard constraints," *IEEE Trans. Intell. Transp. Syst.*, vol. 16, no. 5, pp. 2663–2672, 2015.

[4] M. Du, D. Zhao, M. Yang, and H. Chen, "Nonlinear extended state observer-based output feedback stabilization control for uncertain nonlinear half-car active suspension systems," *Nonlinear Dyn.*, vol. 100, no. 3, pp. 2483–2503, 2020.

[5] Q. Zeng and J. Zhao, "Event-triggered controller design for active suspension systems: An adaptive backstepping method with error-dependent gain," *Control Eng. Pract.*, vol. 136, p. 105547, 2023.

[6] J. Wu, H. Zhou, Z. Liu, and M. Gu, "Ride comfort optimization via speed planning and preview semi-active suspension control for autonomous vehicles on uneven roads," *IEEE Trans. Veh. Technol.*, vol. 69, no. 8, pp. 8343–8355, 2020.

[7] W. Sun, H. Gao, and O. Kaynak, "Vibration isolation for active suspensions with performance constraints and actuator saturation," *IEEE/ASME Trans. Mechatron.*, vol. 20, no. 2, pp. 675–683, 2015.

[8] U. S. Pusadkar, S. D. Chaudhari, P. D. Shendge, and S. B. Phadke, “Linear disturbance observer based sliding mode control for active suspension systems with non-ideal actuator,” *J. Sound Vib.*, vol. 442, pp. 428–444, 2019.

[9] Y. Li, S. Ma, K. Li, and S. Tong, “Adaptive fuzzy output feedback fault-tolerant control for active suspension systems,” *IEEE Trans. Intell. Veh.*, vol. 9, no. 1, pp. 2469–2478, 2024.

[10] Y. Chai, J. Bian, and M. Li, “A novel quasi-zero-stiffness isolation platform via tunable positive and negative stiffness compensation mechanism,” *Nonlinear Dyn.*, vol. 112, no. 1, pp. 101–123, 2024.

[11] X. Yin, L. Zhang, Y. Zhu, C. Wang, and Z. Li, “Robust control of networked systems with variable communication capabilities and application to a semi-active suspension system,” *IEEE/ASME Trans. Mechatron.*, vol. 21, no. 4, pp. 2097–2107, 2016.

[12] Y. Liao, P. Liu, J. Zhao, P. Kin Wong, D. Ning, and H. Du, “A novel closed-loop current control unit for decoupling vibration control of semi-active electrically interconnected suspension,” *Mech. Syst. Signal Process.*, vol. 212, p. 111308, 2024.

[13] J. Zhao, P. K. Wong, W. Li, M. A. Ghadikolaeia, and Z. Xie, “Reliable fuzzy sampled-data control for nonlinear suspension systems against actuator faults,” *IEEE/ASME Trans. Mechatron.*, vol. 27, no. 6, pp. 5518–5528, 2022.

[14] J. Bian and X. Jing, “Superior nonlinear passive damping characteristics of the bio-inspired limb-like or X-shaped structure,” *Mech. Syst. Signal Process.*, vol. 125, pp. 21–51, 2019.

[15] K. Ke, M. C. H. Yam, P. Zhang, Y. Shi, Y. Li, and S. Liu, “Self-centring damper with multi-energy-dissipation mechanisms: Insights and structural seismic demand perspective,” *J. Constr. Steel Res.*, vol. 204, p. 107837, 2023.

[16] K. Ye, J. C. Ji, and T. Brown, "Design of a quasi-zero stiffness isolation system for supporting different loads," *J. Sound Vib.*, vol. 471, p. 115198, 2020.

[17] J. Bian and X. Jing, "Analysis and design of a novel and compact X-structured vibration isolation mount (X-mount) with wider quasi-zero-stiffness range," *Nonlinear Dyn.*, vol. 101, no. 4, pp. 2195–2222, 2020.

[18] N. Su, J. Bian, S. Peng, and Y. Xia, "Generic optimal design approach for inerter-based tuned mass systems," *Int. J. Mech. Sci.*, vol. 233, p. 107654, 2022.

[19] W. Sun, H. Gao, and B. Yao, "Adaptive robust vibration control of full-car active suspensions with electrohydraulic actuators," *IEEE Trans. Control Syst. Technol.*, vol. 21, no. 6, pp. 2417–2422, 2013.

[20] X. Wang, D. Huang, N. Qin, C. Chen, and K. Zhang, "Modeling and second-order sliding mode control for lateral vibration of high-speed train with mr dampers," *IEEE Trans. Intell. Transp. Syst.*, vol. 23, no. 8, pp. 10 299–10 308, 2022.

[21] X. Tang, D. Ning, H. Du, W. Li, and W. Wen, "Takagi-sugeno fuzzy model-based semi-active control for the seat suspension with an electrorheological damper," *IEEE Access*, vol. 8, pp. 98 027–98 037, 2020.

[22] D. Lee, S. Jin, and C. Lee, "Deep reinforcement learning of semi-active suspension controller for vehicle ride comfort," *IEEE Trans. Veh. Technol.*, vol. 72, no. 1, pp. 327–339, 2023.

[23] D. Karnopp, M. J. Crosby, and R. A. Harwood, "Vibration control using semi-active force generators," *Journal of Engineering for Industry*, vol. 96, no. 2, pp. 619–626, 1974.

[24] S. Savaresi and C. Spelta, "Mixed sky-hook and add: Approaching the filtering limits of a semi-active suspension," *J. Dyn. Syst. Meas. Contr.*, vol. 129, no. 4, pp. 382–392, 2006.

[25] M. M. Morato, M. Q. Nguyen, O. Sename, and L. Dugard, "Design of a fast real-time LPV model predictive control system for semi-active suspension control of a full vehicle," *J. Franklin Inst.*, vol. 356, no. 3, pp. 1196–1224, 2019.

[26] M. S. Fallah, R. B. Bhat, and W. F. Xie, "Optimized control of semiactive suspension systems using H_∞ robust control theory and current signal estimation," *IEEE/ASME Trans. Mechatron.*, vol. 17, no. 4, pp. 767–778, 2012.

[27] M. Zhu, G. Lv, C. Zhang, J. Jiang, and H. Wang, "Delay-dependent sliding mode variable structure control of vehicle magneto-rheological semi-active suspension," *IEEE Access*, vol. 10, pp. 51 128–51 141, 2022.

[28] X. Tang, H. Du, S. Sun, D. Ning, Z. Xing, and W. Li, "Takagi–Sugeno fuzzy control for semi-active vehicle suspension with a magnetorheological damper and experimental validation," *IEEE/ASME Trans. Mechatron.*, vol. 22, no. 1, pp. 291–300, 2017.

[29] L. H. Cseko, M. Kvasnica, and B. Lantos, "Explicit MPC-based RBF neural network controller design with discrete-time actual kalman filter for semiactive suspension," *IEEE Trans. Control Syst. Technol.*, vol. 23, no. 5, pp. 1736–1753, 2015.

[30] M. Zhang, X. Jing, and G. Wang, "Bioinspired nonlinear dynamics-based adaptive neural network control for vehicle suspension systems with uncertain/unknown dynamics and input delay," *IEEE Trans. Ind. Electron.*, vol. 68, no. 12, pp. 12 646–12 656, 2021.

[31] W. Sun, H. Pan, and H. Gao, "Filter-based adaptive vibration control for active vehicle suspensions with electrohydraulic actuators," *IEEE Trans. Veh. Technol.*, vol. 65, no. 6, pp. 4619–4626, 2016.

[32] K. Arumugam and B. S. Chen, "Finite-time based fault-tolerant control for half-car active suspension system with cyber-attacks: A memory event-triggered approach," *IEEE Trans. Veh. Technol.*, vol. 73, no. 9, pp. 12 704–12 717, 2024.

[33] C. M. Ho, D. T. Tran, and K. K. Ahn, "Adaptive sliding mode control based nonlinear disturbance observer for active suspension with pneumatic spring," *J. Sound Vib.*, vol. 509, p. 116241, 2021.

[34] Z. Zhou, M. Zhang, D. Navarro-Alarcon, and X. Jing, "Predefined-time fault-tolerant control for active vehicle suspension systems with reference X-dynamics and conditional disturbance cancellation," *IEEE Trans. Intell. Transp. Syst.*, vol. 25, no. 11, pp. 18 661 – 18 672, 2024.

[35] M. Zhang, X. Jing, L. Zhang, W. Huang, and S. Li, "Toward a finite-time energy-saving robust control method for active suspension systems: Exploiting beneficial state-coupling, disturbance, and nonlinearities," *IEEE Trans. Syst. Man Cybern.: Syst.*, vol. 53, no. 9, pp. 5885–5896, 2023.

[36] Q. Zeng and J. Zhao, "Adaptive switching event-triggered control for active suspension systems with acceleration performance constraint," *IEEE Trans. Intell. Transp. Syst.*, vol. 24, no. 8, pp. 8028–8037, 2023.

[37] T. Huang, J. Wang, and H. Pan, "Approximation-free prespecified time bionic reliable control for vehicle suspension," *IEEE Trans. Autom. Sci. Eng.*, vol. 21, no. 4, pp. 5333–5343, 2024.

[38] T. O. Terefe and H. G. Lemu, "Solution approaches to differential equations of mechanical system dynamics: A case study of car suspension system," *Adv. Sci. Technol.-Res.*, vol. 12, no. 2, pp. 266–273, 2018.

[39] X. Jing, "The X-structure/mechanism approach to beneficial nonlinear design in engineering," *Appl. Math. Mech.*, vol. 43, no. 7, pp. 979–1000, 2022.

[40] L. Liu, C. Zhu, Y. J. Liu, and S. Tong, "Intelligent motion tracking control of vehicle suspension systems with constraints via neural performance analysis," *IEEE Trans. Intell. Transp. Syst.*, vol. 23, no. 8, pp. 13 896–13 903, 2022.

[41] Y. Sun, J. Liu, Y. Gao, Z. Liu, and Y. Zhao, "Adaptive neural tracking control for manipulators with prescribed performance under input saturation," *IEEE/ASME Trans. Mechatron.*, vol. 28, no. 2, pp. 1037–1046, 2023.

[42] Q. Shen, P. Shi, Y. Shi, and J. Zhang, "Adaptive output consensus with saturation and dead-zone and its application," *IEEE Trans. Ind. Electron.*, vol. 64, no. 6, pp. 5025–5034, 2017.

[43] P. Li, X. Yu, Y. Zhang, and X. Peng, "Adaptive multivariable integral tsmc of a hypersonic gliding vehicle with actuator faults and model uncertainties," *IEEE/ASME Trans. Mechatron.*, vol. 22, no. 6, pp. 2723–2735, 2017.

[44] F. Tyan, Y.-F. Hong, S.-H. Tu, and W. S. Jeng, "Generation of random road profiles," *Journal of Advanced Engineering*, vol. 4, no. 2, pp. 1373–1378, 2009.

[45] P. K. Wong, W. Li, X. Ma, Z. Yang, X. Wang, and J. Zhao, "Adaptive event-triggered dynamic output feedback control for nonlinear active suspension systems based on interval type-2 fuzzy method," *Mech. Syst. Signal Process.*, vol. 212, p. 111280, 2024.

[46] G. Koch, O. Fritsch, and B. Lohmann, "Potential of low bandwidth active suspension control with continuously variable damper," *Control Eng. Pract.*, vol. 18, no. 11, pp. 1251–1262, 2010.

[47] R. Azmi, M. Mirzaei, and A. Habibzadeh-Sharif, "A novel optimal control strategy for regenerative active suspension system to enhance energy harvesting," *Energy Convers. Manage.*, vol. 291, p. 117277, 2023.

[48] G. Prassad and M. Mohan, "A contemporary adaptive air suspension using LQR control for passenger vehicles," *ISA Trans.*, vol. 93, pp. 244–254, 2019.

[49] C. Chen, R. Ma, and W. Ma, "GA-LQR for vehicle semi-active suspension with bilstm inverse model of magnetic rheological damper," *Trans. Can. Soc. Mech. Eng.*, vol. 47, no. 3, pp. 423–435, 2023.

[50] Y. Lu, A. Khajepour, A. Soltani, R. Li, R. Zhen, Y. Liu, and M. Wang, "Gain-adaptive skyhook-LQR: a coordinated controller for improving truck cabin dynamics," *Control Eng. Pract.*, vol. 130, p. 105365, 2023.

[51] G. Koch, K. J. Diepold, and B. Lohmann, "Multi-objective road adaptive control of an active suspension system," in *Motion and Vibration Control*, H. Ulbrich and L. Ginzinger, Eds., Conference Proceedings, pp. 189–200. Springer Netherlands, 2009.

[52] L. V. V. Gopala Rao and S. Narayanan, "Sky-hook control of nonlinear quarter car model traversing rough road matching performance of LQR control," *J. Sound Vib.*, vol. 323, no. 3, pp. 515–529, 2009.

[53] H. Gao, W. Sun, and P. Shi, "Robust sampled-data H_∞ control for vehicle active suspension systems," *IEEE Trans. Control Syst. Technol.*, vol. 18, no. 1, pp. 238–245, 2010.

[54] W. Sun, H. Gao, and O. Kaynak, "Finite frequency H_∞ control for vehicle active suspension systems," *IEEE Trans. Control Syst. Technol.*, vol. 19, no. 2, pp. 416–422, 2011.

[55] H. Li, X. Jing, and H. R. Karimi, "Output-feedback-based H_∞ control for vehicle suspension systems with control delay," *IEEE Trans. Ind. Electron.*, vol. 61, no. 1, pp. 436–446, 2014.

[56] H. Li, X. Jing, H. K. Lam, and P. Shi, "Fuzzy sampled-data control for uncertain vehicle suspension systems," *IEEE Trans. Cybern.*, vol. 44, no. 7, pp. 1111–1126, 2014.

[57] H. Jing, R. Wang, C. Li, and J. Bao, "Robust finite-frequency H_∞ control of full-car active suspension," *J. Sound Vib.*, vol. 441, pp. 221–239, 2019.

[58] H. Zhang, X. Zheng, H. Li, Z. Wang, and H. Yan, "Active suspension system control with decentralized event-triggered scheme," *IEEE Trans. Ind. Electron.*, vol. 67, no. 12, pp. 10 798–10 808, 2020.

[59] Z. Zhang, A. Qin, J. Zhang, B. Zhang, Q. Fan, and N. Zhang, "Fuzzy sampled-data H_∞ sliding-mode control for active hysteretic suspension of commercial vehicles with unknown actuator-disturbance," *Control Eng. Pract.*, vol. 117, p. 104940, 2021.

[60] C. Kim and P. I. Ro, "A sliding mode controller for vehicle active suspension systems with non-linearities," *Proc. Inst. Mech. Eng., Part D: J. Automob. Eng.*, vol. 212, no. 2, pp. 79–92, 1998.

[61] J. Na, Y. Huang, X. Wu, S. F. Su, and G. Li, "Adaptive finite-time fuzzy control of nonlinear active suspension systems with input delay," *IEEE Trans. Cybern.*, vol. 50, no. 6, pp. 2639–2650, 2020.

[62] J. J. Rath, M. Defoort, H. R. Karimi, and K. C. Veluvolu, "Output feedback active suspension control with higher order terminal sliding mode," *IEEE Trans. Ind. Electron.*, vol. 64, no. 2, pp. 1392–1403, 2017.

[63] J. J. Rath, M. Defoort, C. Sentouh, H. R. Karimi, and K. C. Veluvolu, "Output-constrained robust sliding mode based nonlinear active suspension control," *IEEE Trans. Ind. Electron.*, vol. 67, no. 12, pp. 10 652–10 662, 2020.

[64] Z. Liu and H. Pan, "Barrier function-based adaptive sliding mode control for application to vehicle suspensions," *IEEE Trans. Transp. Electrif.*, vol. 7, no. 3, pp. 2023–2033, 2021.

[65] G. Wang, M. Chadli, and M. V. Basin, "Practical terminal sliding mode control of nonlinear uncertain active suspension systems with adaptive disturbance observer," *IEEE/ASME Trans. Mechatron.*, vol. 26, no. 2, pp. 789–797, 2021.

[66] H. Chen, Y. J. Liu, L. Liu, S. Tong, and Z. Gao, "Anti-saturation-based adaptive sliding-mode control for active suspension systems with time-varying vertical displacement and speed constraints," *IEEE Trans. Cybern.*, vol. 52, no. 7, pp. 6244–6254, 2022.

[67] W. Sun, Z. Zhao, and H. Gao, "Saturated adaptive robust control for active suspension systems," *IEEE Trans. Ind. Electron.*, vol. 60, no. 9, pp. 3889–3896, 2013.

[68] C. Hua, J. Chen, Y. Li, and L. Li, "Adaptive prescribed performance control of half-car active suspension system with unknown dead-zone input," *Mech. Syst. Signal Process.*, vol. 111, pp. 135–148, 2018.

[69] H. Pan, X. Jing, W. Sun, and H. Gao, "A bioinspired dynamics-based adaptive tracking control for nonlinear suspension systems," *IEEE Trans. Control Syst. Technol.*, vol. 26, no. 3, pp. 903–914, 2018.

[70] A. Alleyne and J. K. Hedrick, "Nonlinear adaptive control of active suspensions," *IEEE Trans. Control Syst. Technol.*, vol. 3, no. 1, pp. 94–101, 1995.

[71] B. Liu, M. Saif, and H. Fan, "Adaptive fault tolerant control of a half-car active suspension systems subject to random actuator failures," *IEEE/ASME Trans. Mechatron.*, vol. 21, no. 6, pp. 2847–2857, 2016.

[72] H. Li, Z. Zhang, H. Yan, and X. Xie, "Adaptive event-triggered fuzzy control for uncertain active suspension systems," *IEEE Trans. Cybern.*, vol. 49, no. 12, pp. 4388–4397, 2019.

[73] J. Li, X. Jing, Z. Li, and X. Huang, "Fuzzy adaptive control for nonlinear suspension systems based on a bioinspired reference model with deliberately designed nonlinear damping," *IEEE Trans. Ind. Electron.*, vol. 66, no. 11, pp. 8713–8723, 2019.

[74] Y. J. Liu, S. Lu, D. Li, and S. Tong, "Adaptive controller design-based ABLF for a class of nonlinear time-varying state constraint systems," *IEEE Trans. Syst. Man Cybern.: Syst.*, vol. 47, no. 7, pp. 1546–1553, 2017.

[75] Y. J. Liu, Q. Zeng, S. Tong, C. L. P. Chen, and L. Liu, "Adaptive neural network control for active suspension systems with time-varying vertical displace-

ment and speed constraints," *IEEE Trans. Ind. Electron.*, vol. 66, no. 12, pp. 9458–9466, 2019.

[76] N. Yagiz and Y. Hacioglu, "Backstepping control of a vehicle with active suspensions," *Control Eng. Pract.*, vol. 16, no. 12, pp. 1457–1467, 2008.

[77] H. Pang, X. Zhang, J. Yang, and Y. Shang, "Adaptive backstepping-based control design for uncertain nonlinear active suspension system with input delay," *Int. J. Robust Nonlinear Control*, vol. 29, no. 16, pp. 5781–5800, 2019.

[78] W. Sun, H. Gao, and O. Kaynak, "Adaptive backstepping control for active suspension systems with hard constraints," *IEEE/ASME Trans. Mechatron.*, vol. 18, no. 3, pp. 1072–1079, 2013.

[79] X. Zheng, H. Zhang, H. Yan, F. Yang, Z. Wang, and L. Vlacic, "Active full-vehicle suspension control via cloud-aided adaptive backstepping approach," *IEEE Trans. Cybern.*, vol. 50, no. 7, pp. 3113–3124, 2020.

[80] S. Liu, L. Zhang, M. Chen, C. Yang, J. Zhang, and J. Wang, "Multiple suspensions coordinated control for corner module architecture intelligent electric vehicles on stepped roads," *IEEE Trans. Intell. Veh.*, early access, Mar. 2024, doi: 10.1109/TIV.2024.3375389.

[81] C. M. Ho and K. K. Ahn, "Observer based adaptive neural networks fault-tolerant control for pneumatic active suspension with vertical constraint and sensor fault," *IEEE Trans. Veh. Technol.*, vol. 72, no. 5, pp. 5862–5876, 2023.

[82] D. Fischer and R. Isermann, "Mechatronic semi-active and active vehicle suspensions," *Control Eng. Pract.*, vol. 12, no. 11, pp. 1353–1367, 2004.

[83] S. Zhou, Z. Liu, H. Gao, M. Zhao, L. Wang, and G. Jiang, "Turn-on/off control with dynamic significance of active suspension based on energy dissipation principle for manned lunar rover under low gravity and rough terrain conditions," *Mech. Syst. Signal Process.*, vol. 209, p. 111071, 2024.

[84] D. Guida and C. M. Pappalardo, “Control design of an active suspension system for a quarter-car model with hysteresis,” *J. Vib. Eng. Technol.*, vol. 3, no. 3, pp. 277–299, 2015.

[85] Z. Chu, X. Xiang, D. Zhu, C. Luo, and D. Xie, “Adaptive trajectory tracking control for remotely operated vehicles considering thruster dynamics and saturation constraints,” *ISA Trans.*, vol. 100, pp. 28–37, 2020.

[86] Y. Ren, L. Zhang, Y. Ying, S. Li, and Y. Tang, “Model-parameter-free prescribed time trajectory tracking control for under-actuated unmanned surface vehicles with saturation constraints and external disturbances,” *J. Mar. Sci. Eng.*, vol. 11, no. 9, p. 1717, 2023.

[87] M. H. Zhang and X. J. Jing, “Energy-saving robust saturated control for active suspension systems via employing beneficial nonlinearity and disturbance,” *IEEE Trans. Cybern.*, vol. 52, no. 10, pp. 10 089–10 100, 2022.

[88] L. Kong, W. He, Y. Dong, L. Cheng, C. Yang, and Z. Li, “Asymmetric bounded neural control for an uncertain robot by state feedback and output feedback,” *IEEE Trans. Syst. Man Cybern.: Syst.*, vol. 51, no. 3, pp. 1735–1746, 2021.

[89] J. Pliego-Jiménez, M. A. Arteaga-Pérez, and M. López-Rodríguez, “Finite-time control for rigid robots with bounded input torques,” *Control Eng. Pract.*, vol. 102, p. 104556, 2020.

[90] D. Song, D. Yang, X. Zeng, and X. Zhang, “Adaptive robust finite-time control for active suspension systems via disturbance observation,” *Proc. Inst. Mech. Eng., Part D: J. Automob. Eng.*, vol. 237, no. 8, pp. 2049–2061, 2023.

[91] B. Huang, S. Zhang, Y. He, B. Wang, and Z. Deng, “Finite-time anti-saturation control for Euler-Lagrange systems with actuator failures,” *ISA Trans.*, vol. 124, pp. 468–477, 2022.

[92] B. Tian, Z. Li, and Q. Zong, "A continuous multivariable finite-time control scheme for double integrator systems with bounded control input," *IEEE Trans. Autom. Control*, vol. 67, no. 11, pp. 6068–6073, 2022.

[93] S. Lian, W. Meng, Z. Lin, K. Shao, J. Zheng, H. Li, and R. Lu, "Adaptive attitude control of a quadrotor using fast nonsingular terminal sliding mode," *IEEE Trans. Ind. Electron.*, vol. 69, no. 2, pp. 1597–1607, 2022.

[94] A. A. Wijaya, F. Yakub, S. S. Abdullah, R. Akmeliawati, S. Aljazzar, and I. Makoto, "Neuroadaptive natural logarithm sliding mode control for nonlinear active suspension systems," *IEEE Trans. Intell. Veh.*, pp. 1–15, 2024.

[95] H. Pang, X. Zhang, and Z. Xu, "Adaptive backstepping-based tracking control design for nonlinear active suspension system with parameter uncertainties and safety constraints," *ISA Trans.*, vol. 88, pp. 23–36, 2019.

[96] M. Zhang, X. Jing, W. Huang, and P. Li, "Saturated PD-SMC method for suspension systems by exploiting beneficial nonlinearities for improved vibration reduction and energy-saving performance," *Mech. Syst. Signal Process.*, vol. 179, p. 109376, 2022.

[97] Z. Zhou, X. Jing, and M. Zhang, "A novel robust finite-time control for active suspension systems with naturally bounded inputs," in *The International Conference on Applied Nonlinear Dynamics, Vibration and Control*, Conference Paper, pp. 431–443, 2023.

[98] X. Guo, J. Zhang, and W. Sun, "Robust saturated fault-tolerant control for active suspension system via partial measurement information," *Mech. Syst. Signal Process.*, vol. 191, p. 110116, 2023.

[99] Y. Hong, J. Huang, and Y. Xu, "On an output feedback finite-time stabilization problem," *IEEE Trans. Autom. Control*, vol. 46, no. 2, pp. 305–309, 2001.

[100] S. P. Bhat and D. S. Bernstein, "Finite-time stability of homogeneous systems," in *Proceedings of the 1997 American Control Conference*, vol. 4, pp. 2513–2514, 1997.

[101] H. Wang, P. X. Liu, X. Zhao, and X. Liu, "Adaptive fuzzy finite-time control of nonlinear systems with actuator faults," *IEEE Trans. Cybern.*, vol. 50, no. 5, pp. 1786–1797, 2020.

[102] Q. Hu and B. Jiang, "Continuous finite-time attitude control for rigid spacecraft based on angular velocity observer," *IEEE Trans. Aerosp. Electron. Syst.*, vol. 54, no. 3, pp. 1082–1092, 2018.

[103] Y. Su, C. Zheng, and P. Mercorelli, "Nonlinear PD fault-tolerant control for dynamic positioning of ships with actuator constraints," *IEEE/ASME Trans. Mechatron.*, vol. 22, no. 3, pp. 1132–1142, 2017.

[104] H. Pan, X. Jing, W. Sun, and Z. Li, "Analysis and design of a bioinspired vibration sensor system in noisy environment," *IEEE/ASME Trans. Mechatron.*, vol. 23, no. 2, pp. 845–855, 2018.

[105] *Active suspension experiment set up and configuration*, Quanser Innovate Educate, 2012.

[106] Z. Liu, Y. Si, and W. Sun, "Ride comfort oriented integrated design of preview active suspension control and longitudinal velocity planning," *Mech. Syst. Signal Process.*, vol. 208, p. 110992, 2024.

[107] *Mechanical Vibration and Shock–Evaluation of Human Exposure to Whole Body Vibration–Part 1: General Requirements*, International Organization for Standardization, Standard ISO 2631–1:1997, 1997.

[108] H. Pang, Y. Shang, and J. Yang, "An adaptive sliding mode–based fault-tolerant control design for half-vehicle active suspensions using T–S fuzzy approach," *J. Vib. Control*, vol. 26, no. 17-18, pp. 1411–1424, 2020.

[109] J. Na, Y. Huang, X. Wu, Y. J. Liu, Y. Li, and G. Li, "Active suspension control of quarter-car system with experimental validation," *IEEE Trans. Syst. Man Cybern.: Syst.*, vol. 52, no. 8, pp. 4714–4726, 2022.

[110] H. Taghavifar and S. Rakheja, "Multi-objective optimal robust seat suspension control of off-road vehicles in the presence of disturbance and parametric uncertainty using metaheuristics," *IEEE Trans. Intell. Veh.*, vol. 5, no. 3, pp. 372–384, 2020.

[111] W. S. Cortez and D. V. Dimarogonas, "Safe-by-design control for Euler–Lagrange systems," *Automatica*, vol. 146, p. 110620, 2022.

[112] K. Shao, J. Zheng, R. Tang, X. Li, Z. Man, and B. Liang, "Barrier function based adaptive sliding mode control for uncertain systems with input saturation," *IEEE/ASME Trans. Mechatron.*, vol. 27, no. 6, pp. 4258–4268, 2022.

[113] T. Jia, Y. Pan, H. Liang, and H. K. Lam, "Event-based adaptive fixed-time fuzzy control for active vehicle suspension systems with time-varying displacement constraint," *IEEE Trans. Fuzzy Syst.*, vol. 30, no. 8, pp. 2813–2821, 2022.

[114] W. Qin, W. B. Shangguan, H. Yin, Y. H. Chen, and J. Huang, "Constraint-following control design for active suspension systems," *Mech. Syst. Signal Process.*, vol. 154, p. 107578, 2021.

[115] W. He, H. Huang, and S. S. Ge, "Adaptive neural network control of a robotic manipulator with time-varying output constraints," *IEEE Trans. Cybern.*, vol. 47, no. 10, pp. 3136–3147, 2017.

[116] Z. Feng, R. B. Li, and X. Jing, "Neuroadaptive control for active suspension systems with time-varying motion constraints: A feasibility-condition-free method," *IEEE Trans. Cybern.*, vol. 54, no. 1, pp. 287–297, 2024.

[117] G. Zhu and J. Du, "Global robust adaptive trajectory tracking control for surface ships under input saturation," *IEEE J. Oceanic Eng.*, vol. 45, no. 2, pp. 442–450, 2020.

[118] L. Liu, T. Gao, Y. J. Liu, and S. Tong, "Time-varying asymmetrical BLFs based adaptive finite-time neural control of nonlinear systems with full state constraints," *IEEE/CAA J. Autom. Sin.*, vol. 7, no. 5, pp. 1335–1343, 2020.

[119] H. Pan, X. Jing, and W. Sun, "Robust finite-time tracking control for nonlinear suspension systems via disturbance compensation," *Mech. Syst. Signal Process.*, vol. 88, pp. 49–61, 2017.

[120] J. Sun, J. Yi, and Z. Pu, "Fixed-time adaptive fuzzy control for uncertain nonstrict-feedback systems with time-varying constraints and input saturations," *IEEE Trans. Fuzzy Syst.*, vol. 30, no. 4, pp. 1114–1128, 2022.

[121] H. Pan and W. Sun, "Nonlinear output feedback finite-time control for vehicle active suspension systems," *IEEE Trans. Ind. Inf.*, vol. 15, no. 4, pp. 2073–2082, 2019.

[122] Y. Zhang, Y. Liu, and L. Liu, "Adaptive finite-time NN control for 3-DOF active suspension systems with displacement constraints," *IEEE Access*, vol. 7, pp. 13 577–13 588, 2019.

[123] F. Zhao, S. S. Ge, F. Tu, Y. Qin, and M. Dong, "Adaptive neural network control for active suspension system with actuator saturation," *IET Control Theory Appl.*, vol. 10, no. 14, pp. 1696–1705, 2016.

[124] W. He, Y. Chen, and Z. Yin, "Adaptive neural network control of an uncertain robot with full-state constraints," *IEEE Trans. Cybern.*, vol. 46, no. 3, pp. 620–629, 2016.

[125] P. Ning, C. Hua, K. Li, and R. Meng, "Adaptive fixed-time control for uncertain nonlinear cascade systems by dynamic feedback," *IEEE Trans. Syst. Man Cybern.: Syst.*, vol. 53, no. 5, pp. 2961–2970, 2023.

[126] T. Yang, X. Zhang, Y. Fang, N. Sun, and M. Iwasaki, "Observer-based adaptive fuzzy event-triggered control for mechatronic systems with inaccurate signal

transmission and motion constraints," *IEEE/ASME Trans. Mechatron.*, vol. 27, no. 6, pp. 5208–5221, 2022.

[127] H. Yang and D. Ye, "Adaptive fixed-time bipartite tracking consensus control for unknown nonlinear multi-agent systems: An information classification mechanism," *Inf. Sci.*, vol. 459, pp. 238–254, 2018.

[128] K. Liu and R. Wang, "Antisaturation adaptive fixed-time sliding mode controller design to achieve faster convergence rate and its application," *IEEE Trans. Circuits Syst. II Express Briefs*, vol. 69, no. 8, pp. 3555–3559, 2022.

[129] D. Ba, Y. X. Li, and S. Tong, "Fixed-time adaptive neural tracking control for a class of uncertain nonstrict nonlinear systems," *Neurocomputing*, vol. 363, pp. 273–280, 2019.

[130] M. Zhang and X. Jing, "A bioinspired dynamics-based adaptive fuzzy SMC method for half-car active suspension systems with input dead zones and saturations." *IEEE Trans. Cybern.*, vol. 51, no. 4, pp. 1743–1755, 2020.

[131] Z. Wu, X. Jing, J. Bian, F. Li, and R. Allen, "Vibration isolation by exploring bio-inspired structural nonlinearity," *Bioinspir. Biomim.*, vol. 10, no. 5, p. 056015, 2015.

[132] Y. Huang, J. Na, X. Wu, and G. Gao, "Approximation-free control for vehicle active suspensions with hydraulic actuator," *IEEE Trans. Ind. Electron.*, vol. 65, no. 9, pp. 7258–7267, 2018.

[133] T. Wang and Y. Li, "Neural-network adaptive output-feedback saturation control for uncertain active suspension systems," *IEEE Trans. Cybern.*, vol. 52, no. 3, pp. 1881–1890, 2022.

[134] Y. Liu, Y. Zhang, L. Liu, S. Tong, and C. Chen, "Adaptive finite-time control for half-vehicle active suspension systems with uncertain dynamics," *IEEE/ASME Trans. Mechatron.*, vol. 26, no. 1, pp. 168–178, 2021.

[135] X. Zhang, B. Liu, Z. Liu, and D. Li, “Influence of temperature field on particle distribution in feeder pipeline with CFD simulation,” *China Powder Sci. Technol.*, vol. 27, no. 04, pp. 193–203, 2021.

[136] Z. Zhou, M. Zhang, H. Liu, and X. Jing, “Fixed-time safe-by-design control for uncertain active vehicle suspension systems with nonlinear reference dynamics,” *IEEE/ASME Trans. Mechatron.*, vol. 29, no. 5, pp. 3348–3359, 2024, doi: 10.1109/TMECH.2023.3342013.

[137] J. D. Sánchez-Torres, D. Gómez-Gutiérrez, E. López, and A. G. Loukianov, “A class of predefined-time stable dynamical systems,” *IMA J. Math. Control Inf.*, vol. 35, pp. i1–i29, 2018.

[138] E. Jiménez-Rodríguez, A. J. Muñoz-Vázquez, J. D. Sánchez-Torres, M. Defoort, and A. G. Loukianov, “A Lyapunov-like characterization of predefined-time stability,” *IEEE Trans. Autom. Control*, vol. 65, no. 11, pp. 4922–4927, 2020.

[139] S. Yan and W. Sun, “Self-powered suspension criterion and energy regeneration implementation scheme of motor-driven active suspension,” *Mech. Syst. Signal Process.*, vol. 94, pp. 297–311, 2017.

[140] S. Yan, W. Sun, and H. Gao, “Vibration suppression for motor-driven uncertain active suspensions with hard constraints and analysis of energy consumption,” *IEEE Trans. Syst. Man Cybern.: Syst.*, vol. 52, no. 1, pp. 618–630, 2022.

[141] M. Zhang and X. Jing, “Switching logic-based saturated tracking control for active suspension systems based on disturbance observer and bioinspired X-dynamics,” *Mech. Syst. Signal Process.*, vol. 155, p. 107611, 2021.

[142] Y. J. Liu, Q. Zeng, S. Tong, C. L. P. Chen, and L. Liu, “Actuator failure compensation-based adaptive control of active suspension systems with prescribed performance,” *IEEE Trans. Ind. Electron.*, vol. 67, no. 8, pp. 7044–7053, 2020.

[143] H. Pan, H. Li, W. Sun, and Z. Wang, "Adaptive fault-tolerant compensation control and its application to nonlinear suspension systems," *IEEE Trans. Syst. Man Cybern.: Syst.*, vol. 50, no. 5, pp. 1766–1776, 2020.

[144] M. Zhang, X. Jing, Z. Zhou, and W. Huang, "Transportation for 4-DOF tower cranes: A periodic sliding mode control approach," *IEEE Trans. Intell. Transp. Syst.*, vol. 25, no. 11, pp. 15 909–15 921, 2020.

[145] B. Huang, F. Zhang, M. Song, and P. Huang, "Event-based predefined-time deployment control for space triangular tethered satellite system with input quantization," *IEEE Trans. Aerosp. Electron. Syst.*, vol. 59, no. 5, pp. 4936–4946, 2023.

[146] C. Wu, J. Yan, J. Shen, X. Wu, and B. Xiao, "Predefined-time attitude stabilization of receiver aircraft in aerial refueling," *IEEE Trans. Circuits Syst. II Express Briefs*, vol. 68, no. 10, pp. 3321–3325, 2021.

[147] Q. Wang, J. Cao, and H. Liu, "Adaptive fuzzy control of nonlinear systems with predefined time and accuracy," *IEEE Trans. Fuzzy Syst.*, vol. 30, no. 12, pp. 5152–5165, 2022.

[148] B. Mao, X. Wu, J. Lü, and G. Chen, "Predefined-time bounded consensus of multiagent systems with unknown nonlinearity via distributed adaptive fuzzy control," *IEEE Trans. Cybern.*, vol. 53, no. 4, pp. 2622–2635, 2023.

[149] B. Xiao, S. Yin, and H. Gao, "Reconfigurable tolerant control of uncertain mechanical systems with actuator faults: A sliding mode observer-based approach," *IEEE Trans. Control Syst. Technol.*, vol. 26, no. 4, pp. 1249–1258, 2018.

[150] W. Wei and W. Zhang, "Command-filter-based adaptive fuzzy finite-time output feedback control for state-constrained nonlinear systems with input saturation," *IEEE Trans. Fuzzy Syst.*, vol. 30, no. 10, pp. 4044–4056, 2022.

[151] H. Sai, Z. Xu, and J. Cui, "Nonconservative adaptive practical predefined-time sliding mode tracking of uncertain robotic manipulators," *Int. J. Robust Nonlinear Control*, vol. 33, no. 18, pp. 11 036–11 061, 2023.

[152] Y. Zhang, M. Chadli, and Z. Xiang, "Predefined-time adaptive fuzzy control for a class of nonlinear systems with output hysteresis," *IEEE Trans. Fuzzy Syst.*, vol. 31, no. 8, pp. 2522–2531, 2023.

[153] Z. Zhou, G. Tang, H. Huang, L. Han, and R. Xu, "Adaptive nonsingular fast terminal sliding mode control for underwater manipulator robotics with asymmetric saturation actuators," *Control Theory Technol.*, vol. 18, pp. 81–91, 2020.

[154] S. Xie and Q. Chen, "Adaptive nonsingular predefined-time control for attitude stabilization of rigid spacecrafts," *IEEE Trans. Circuits Syst. II Express Briefs*, vol. 69, no. 1, pp. 189–193, 2022.

[155] J. Chen, Z. Chen, H. Zhang, B. Xiao, and L. Cao, "Predefined-time observer-based nonsingular sliding-mode control for spacecraft attitude stabilization," *IEEE Trans. Circuits Syst. II Express Briefs*, vol. 71, no. 3, pp. 1291–1295, 2024.

[156] Z. Guo, J. Guo, J. Zhou, and J. Chang, "Robust tracking for hypersonic reentry vehicles via disturbance estimation-triggered control," *IEEE Trans. Aerosp. Electron. Syst.*, vol. 56, no. 2, pp. 1279–1289, 2020.

[157] H. Pang, M. Wang, L. Wang, and J. Luo, "A composite vibration control strategy for active suspension system based on dynamic event triggering and long short-term memory neural network," *IEEE Trans. Transp. Electrif.*, vol. 10, no. 3, pp. 5355–5367, 2024.

[158] X. Jin, J. Wang, X. He, Z. Yan, L. Xu, C. Wei, and G. Yin, "Improving vibration performance of electric vehicles based on in-wheel motor-active suspension system via robust finite frequency control," *IEEE Trans. Intell. Transp. Syst.*, vol. 24, no. 2, pp. 1631–1643, 2023.

[159] Q. Zeng and J. Zhao, "Disturbance observer-based event-triggered control of vehicle suspension with finite-time prescribed performance," *IEEE Trans. Transp. Electrif.*, vol. 10, no. 1, pp. 277–287, 2024.

[160] T. Huang, J. Wang, H. Pan, and W. Sun, "Finite-time fault-tolerant integrated motion control for autonomous vehicles with prescribed performance," *IEEE Trans. Transp. Electrif.*, vol. 9, no. 3, pp. 4255–4265, 2023.

[161] S. Xie, Q. Chen, and X. He, "Predefined-time approximation-free attitude constraint control of rigid spacecraft," *IEEE Trans. Aerosp. Electron. Syst.*, vol. 59, no. 1, pp. 347–358, 2023.

[162] S. Sui, L. Zhao, and C. L. P. Chen, "Adaptive fuzzy predefined-time tracking control design for nonstrict-feedback high-order nonlinear systems with input quantization," *IEEE Trans. Fuzzy Syst.*, vol. 32, no. 10, pp. 5978–5990, 2024.

[163] H. Xu, D. Yu, and Y. J. Liu, "Observer-based fuzzy adaptive predefined time control for uncertain nonlinear systems with full-state error constraints," *IEEE Trans. Fuzzy Syst.*, vol. 32, no. 3, pp. 1370–1382, 2023.

[164] J. Chai, M. Wang, Z. Li, and Z. Xu, "Improved super-twisting sliding mode control for single-phase T-type three-level converters based on fixed-time extended state observer," *IEEE Trans. Transp. Electrif.*, vol. 10, no. 3, pp. 5307–5317, 2024.

[165] W. Liu, M. Gong, H. Chen, and D. Zhao, "Energy-saving tracking control and experiment of nonlinear active suspension for multi-axle vehicles considering road slope," *Mech. Syst. Signal Process.*, vol. 226, p. 112328, 2025.

[166] M. Piao, Y. Wang, M. Sun, X. Zhang, Z. Chen, and Y. Yan, "Fixed-time-convergent generalized extended state observer based motor control subject to multiple disturbances," *IEEE Trans. Ind. Inf.*, vol. 17, no. 12, pp. 8066–8079, 2021.

[167] D. Ye, A. M. Zou, S. Sun, and Y. Xiao, "A predefined-time extended-state observer-based approach for velocity-free attitude control of spacecraft," *IEEE Trans. Aerosp. Electron. Syst.*, vol. 59, no. 6, pp. 8051–8061, 2023.

[168] A. Zou, Y. Liu, Z. Hou, and Z. Hu, "Practical predefined-time output-feedback consensus tracking control for multiagent systems," *IEEE Trans. Cybern.*, vol. 53, no. 8, pp. 5311–5322, 2023.

[169] Z. Guo, J. Zhou, J. Guo, J. Cieslak, and J. Chang, "Coupling-characterization-based robust attitude control scheme for hypersonic vehicles," *IEEE Trans. Ind. Electron.*, vol. 64, no. 8, pp. 6350–6361, 2017.

[170] Z. Huang, M. Chen, and P. Shi, "Disturbance utilization-based tracking control for the fixed-wing UAV with disturbance estimation," *IEEE Trans. Circuits Syst. I Regul. Pap.*, vol. 70, no. 3, pp. 1337–1349, 2023.

[171] X. Fang and F. Liu, "Coupling and disturbance characterization based robust control for manned submersibles," *J. Franklin Inst.*, vol. 356, no. 15, pp. 8468–8483, 2019.

[172] Q. Zeng and J. Zhao, "Adaptive switching control of active suspension systems: A switched system point of view," *IEEE Trans. Control Syst. Technol.*, vol. 32, no. 2, pp. 663–671, 2024.

[173] Z. Guo, Q. Ma, J. Guo, B. Zhao, and J. Zhou, "Performance-involved coupling effect-triggered scheme for robust attitude control of HRV," *IEEE/ASME Trans. Mechatron.*, vol. 25, no. 3, pp. 1288–1298, 2020.

[174] H. Gao, L. Liu, and Y. Liu, "Adaptive tracking event-triggered control of quarter-car bioinspiration active suspension systems," *IEEE Trans. Syst. Man Cybern.: Syst.*, vol. 53, no. 1, pp. 475–484, 2023.

[175] Z. Zhang, J. Zhang, H. Yin, B. Zhang, and X. Jing, "Bio-inspired structure reference model oriented robust full vehicle active suspension system control via constraint-following," *Mech. Syst. Signal Process.*, vol. 179, p. 109368, 2022.

[176] Z. Zhang and J. Dong, "A new optimization control policy for fuzzy vehicle suspension systems under membership functions online learning," *IEEE Trans. Syst. Man Cybern.: Syst.*, vol. 53, no. 5, pp. 3255–3266, 2023.

[177] A.-M. Zou and Y. Liu, “Attitude tracking control of spacecraft with preset-time preset-bounded convergence,” *Int. J. Robust Nonlinear Control*, vol. 32, no. 18, pp. 10 162–10 179, 2022.

[178] Z. Xu, W. Deng, H. Shen, and J. Yao, “Extended-state-observer-based adaptive prescribed performance control for hydraulic systems with full-state constraints,” *IEEE/ASME Trans. Mechatron.*, vol. 27, no. 6, pp. 5615–5625, 2022.

[179] Y. Zhang, B. Niu, X. Zhao, P. Duan, H. Wang, and B. Gao, “Global predefined-time adaptive neural network control for disturbed pure-feedback nonlinear systems with zero tracking error,” *IEEE Trans. Neural Networks Learn. Syst.*, vol. 34, no. 9, pp. 6328–6338, 2023.

[180] S. Sui, C. L. P. Chen, and S. Tong, “Command filter-based predefined time adaptive control for nonlinear systems,” *IEEE Trans. Autom. Control*, vol. 69, no. 11, pp. 7863–7870, 2024.